NASA Technical Memorandum 2000–206892, Volume 10

SeaWiFS Postlaunch Technical Report Series

Stanford B. Hooker, Editor
NASA Goddard Space Flight Center
Greenbelt, Maryland

Elaine R. Firestone, Senior Technical Editor
SAIC General Sciences Corporation
Beltsville, Maryland

Volume 10, SeaWiFS Postlaunch Calibration and Validation Analyses, Part 2

Charles R. McClain
NASA Goddard Space Flight Center
Greenbelt, Maryland

Robert A. Barnes, Robert E. Eplee, Jr., Bryan A. Franz, N. Christina Hsu, Frederick S. Patt, Christophe M. Pietras, Wayne D. Robinson, Brian D. Schieber, and G. Michael Schmidt
SAIC General Sciences Corporation
Beltsville, Maryland

Menghua Wang
University of Maryland, Baltimore County
Baltimore, Maryland

Sean W. Bailey
Futuretech Corporation
Greenbelt, Maryland

P. Jeremy Werdell
Science Systems and Applications Incorporated
Lanham, Maryland

Table of Contents

Abstract

The effort to resolve data quality issues and improve on the initial data evaluation methodologies of the SeaWiFS Project was an extensive one. These evaluations have resulted, to date, in three major reprocessings of the entire data set where each reprocessing addressed the data quality issues that could be identified up to the time of the reprocessing. Three volumes of the *SeaWiFS Postlaunch Technical Report Series* (Volumes 9, 10, and 11) are needed to document the improvements implemented since launch. Volume 10 continues the sequential presentation of postlaunch data analysis and algorithm descriptions begun in Volume 9. Chapter 1 of Volume 10 describes an absorbing aerosol index, similar to that produced by the Total Ozone Mapping Spectrometer (TOMS) Project, which is used to flag pixels contaminated by absorbing aerosols, such as, dust and smoke. Chapter 2 discusses the algorithm being used to remove SeaWiFS out-of-band radiance from the water-leaving radiances. Chapter 3 provides an itemization of all significant changes in the processing algorithms for each of the first three reprocessings. Chapter 4 shows the time series of global clear water and deep-water (depths greater than 1,000 m) bio-optical and atmospheric properties (normalized water-leaving radiances, chlorophyll, atmospheric optical depth, etc.) based on the eight-day composites as a check on the sensor calibration stability. Chapter 5 examines the variation in the derived products with scan angle using high resolution data around Hawaii to test for residual scan modulation effects and atmospheric correction biases. Chapter 6 provides a methodology for evaluating the atmospheric correction algorithm and atmospheric derived products using ground-based observations. Similarly, Chapter 7 presents match-up comparisons of coincident satellite and *in situ* data to determine the accuracy of the water-leaving radiances, chlorophyll a, and $K(490)$ products.

PROLOGUE

The SeaWiFS Project Calibration and Validation Team (CVT) is responsible for the overall quality of the data products and for verifying the processing code. Volume 38 of the *SeaWiFS Technical Report Series* (Prelaunch) outlined the prelaunch quality control strategy. Since SeaWiFS began routine data processing in September 1997, the CVT has constantly worked to resolve data quality issues and improve on the initial data evaluation methodologies. These evaluations resulted in three major reprocessings of the entire data set (February 1998, August 1998, and May 2000). Each reprocessing addressed the data quality issues that could be identified up to the time of each reprocessing.

The number of chapters (21) needed to document this extensive work in the *SeaWiFS Postlaunch Technical Report Series* requires three volumes: Volumes 9, 10, and 11. Volume 10 continues the sequential presentation of postlaunch data analysis and algorithm descriptions begun in Volume 9. The chapters describe the various data quality issues, analyses, and algorithm improvements that were developed through the third reprocessing. The data evaluations after the third reprocessing indicate that the data products, in most situations including Case-2 waters, are within the prelaunch Case-1 water accuracy goals. Nonetheless, it is expected that other improvements and new geophysical data products will be developed in the future which will require additional reprocessings. The SeaWiFS Project Office will remain dedicated to providing better products and to the documentation of future analysis and algorithm improvement studies.

A short synopsis of each chapter in this volume is given below.

1. The Description of the SeaWiFS Absorbing Aerosol Index

The method of detecting absorbing aerosols from SeaWiFS is described in this chapter. This technique uses a term defined as the *absorbing aerosol index* which measures the wavelength-dependent change in Rayleigh scattered reflectance due to aerosol absorption relative to a pure Rayleigh atmosphere. The sensitivities of the SeaWiFS absorbing aerosol index to various types of absorbing and non-absorbing aerosols were shown using radiative transfer codes. Discussions of separating the signature of absorbing aerosols from that of phytoplankton on the spectral dependence of SeaWiFS reflectances are also included.

2. Analyses of the SeaWiFS Spectral Band-Pass Effects

This chapter describes an effort to study the effects of the SeaWiFS spectral band pass on the retrieved normalized water-leaving radiances and ocean near-surface chlorophyll concentrations. SeaWiFS routinely provides ocean near-surface optical and microphysical property data, however, these retrievals include the effects of the relatively wide SeaWiFS spectral band passes. Because the SeaWiFS bio-optical algorithm was derived using *in situ* measurements, which were acquired at the SeaWiFS nominal band center wavelengths, it was necessary to assess the effects of the SeaWiFS spectral band pass on the retrieved chlorophyll concentrations.

3. Changes Made in the Operational SeaWiFS Processing

This chapter discusses the major changes made in the SeaWiFS processing for the second reprocessing in August 1998 and the third reprocessing in May 2000. Each major change in the processing programs and tables is presented with a description of the effects of the change. For the second reprocessing, a review of the major changes to the data is presented using an eight-day period of data as an example. The effect of the changes for the third reprocessing are also examined and compared to the results of the second reprocessing using two eight-day periods of data. The changes have increased the usefulness of the data in both oceanographic and atmospheric applications.

4. SeaWiFS Global Clear-Water Analysis

The SeaWiFS CVT made a comparison of global clear-water radiances retrieved by SeaWiFS with normalized water-leaving radiances measured by the Marine Optical Buoy (MOBY) as a check on the accuracy and stability of the vicarious calibration of SeaWiFS. The procedures and results of this comparison are described in this chapter.

5. Along-Scan Effects in SeaWiFS Data

The SeaWiFS CVT has looked for along-scan effects in SeaWiFS data by examining mean radiances of local area coverage (LAC) scenes over MOBY and by analyzing the ratio of SeaWiFS-to-MOBY (S:M) match-up data. Analyses of the SeaWiFS along-scan data and S:M ratios show decreases in the water-leaving radiances retrieved by SeaWiFS as the scan angles or optical paths of the observations increase. These two analyses, which are independent of each other, both point to an overcorrection of the SeaWiFS data by the SeaWiFS atmospheric correction algorithm.

6. SeaWiFS Aerosol Optical Thickness Match-up Analyses

In this chapter, a match-up procedure is described which compares the retrieved SeaWiFS aerosol optical thicknesses with data from *in situ* measurements. The aerosol optical thickness at 865 nm is a by-product of the SeaWiFS atmospheric correction and is routinely retrieved from SeaWiFS measurements. This work is part of the SeaWiFS calibration and validation efforts in studying the aerosol optical properties over the ocean, thereby, validating aerosol models used in the atmospheric correction of ocean color sensors. The aerosol model is an integral part of the SeaWiFS atmospheric correction. The SeaWiFS aerosol retrieval algorithm, the data acquisitions from both SeaWiFS and the *in situ* measurements, and the match-up procedure are described. Finally, some preliminary comparison results are presented and discussed.

7. Normalized Water-Leaving Radiance and Chlorophyll a Match-up Analyses

Validation of SeaWiFS requires the use of *in situ* (field collected) data sets. The SeaWiFS and the Sensor Intercomparison and Merger for Biological and Interdisciplinary Oceanic Studies (SIMBIOS) Projects have sponsored numerous PIs to collect *in situ* optics and chlorophyll data for the purpose of comparing values to those derived from the SeaWiFS instrument. The match-up design described here uses field data stored in SeaWiFS Bio-optical Archive and Storage System (SeaBASS), match-up analysis software, and a plotting and statistics package to validate the primary SeaWiFS derived ocean products, i.e., normalized water-leaving radiance, chlorophyll *a* concentration, and the diffuse attenuation coefficient.

Chapter 1

The Description of the SeaWiFS Absorbing Aerosol Index

N. Christina Hsu and Wayne D. Robinson
SAIC General Sciences Corporation
Beltsville, Maryland

Sean W. Bailey
Futuretech Corporation
Greenbelt, Maryland

P. Jeremy Werdell
Science Systems and Applications, Incorporated
Lanham, Maryland

Abstract

The method of detecting absorbing aerosols from SeaWiFS is described in this chapter. This technique uses a term defined as the *absorbing aerosol index* which measures the wavelength-dependent change in Rayleigh scattered reflectance due to aerosol absorption relative to a pure Rayleigh atmosphere. The sensitivities of the SeaWiFS absorbing aerosol index to various types of absorbing and non-absorbing aerosols were shown using radiative transfer codes. Discussions of separating the signature of absorbing aerosols from that of phytoplankton on the spectral dependence of SeaWiFS reflectances are also included.

1.1 INTRODUCTION

The presence of absorbing aerosols leads to errors in determining water-leaving radiances and, therefore, retrieving chlorophyll *a* concentrations. In this chapter, a method is described to distinguish absorbing aerosols from nonabsorbing aerosols over the ocean, using an absorbing aerosol index (AI) similar to the one developed for the Total Ozone Mapping Spectrometer (TOMS) sensor (Hsu et al. 1996 and Herman et al. 1997).

1.2 AEROSOL INDEX

In the case of SeaWiFS, AI is determined from the 412 and 490 nm remote sensing reflectances, $R_{\rm rs}(\lambda)$, which have weak or negligible dependence on ozone and water vapor absorption. A compact notation for the reflectance ratio, $R^{\lambda_i}_{\lambda_j}$, is used to represent $R_{\rm rs}(\lambda_i)/R_{\rm rs}(\lambda_j)$ in the definition for AI:

$$I \;=\; -100\Big[\log_{10}\Big(\tilde{R}^{412}_{490}\Big) \;-\; \log_{10}\Big(\hat{R}^{412}_{490}\Big)\Big], \qquad (1)$$

where I is the aerosol index, $\tilde{R}^{412}_{490}$ is the top of the atmosphere (TOA) reflectance ratio measured by SeaWiFS, and $\hat{R}^{412}_{490}$ is the reflectance ratio calculated assuming an atmosphere containing only large nonabsorbing particles and Rayleigh scattering molecules. Essentially, I is a measure of the wavelength-dependent change in Rayleigh scattered reflectance due to aerosol absorption relative to a pure Rayleigh atmosphere.

AI is defined so that positive values generally correspond to absorbing aerosols and negative values to nonabsorbing aerosols (Hsu et al. 1996 and Herman et al. 1997). The AI measurements are linearly proportional to the aerosol optical thickness (AOT) within the range of AOT observed from ground-based sun photometer instruments in regions covered by burning biomass smoke or wind-blown African dust (Hsu et al. 1999).

In the following sections, the sensitivity of the AI to the detection of various types of absorbing aerosols over blue water is discussed. The effects of phytoplankton on absorbing aerosol detection and how to account for them is also described. Finally, the potential applications of the SeaWiFS AI to general algorithmic issues is outlined.

1.3 SENSITIVITY STUDIES

Sensitivity studies were performed for various types of absorbing and nonabsorbing aerosols using radiative transfer codes (Dave 1972). To use aerosol properties represen-

Table 1. The characteristics of the aerosol properties used in the model simulations for various types of aerosols. The real and imaginary parts of the refractive index are shown in complex notation with i denoting the square root of -1 ($\sqrt{-1}$).

Aerosol Model	$r_0(\mu)$	σ'	*Refractive Index (412 nm)*	*Refractive Index (490 nm)*
Strongly Absorbing Dust	0.25	2.20	$1.57-0.015i$	$1.57-0.010i$
Less Absorbing Dust	0.12	2.20	$1.57-0.015i$	$1.57-0.010i$
Sea Salt	2.00	2.15	$1.38-0.000i$	$1.38-0.000i$
Darker Smoke	0.14	1.45	$1.55-0.040i$	$1.55-0.035i$
Whiter Smoke	0.14	1.45	$1.55-0.023i$	$1.55-0.020i$
Sulfate	0.07	2.03	$1.43-0.000i$	$1.43-0.000i$

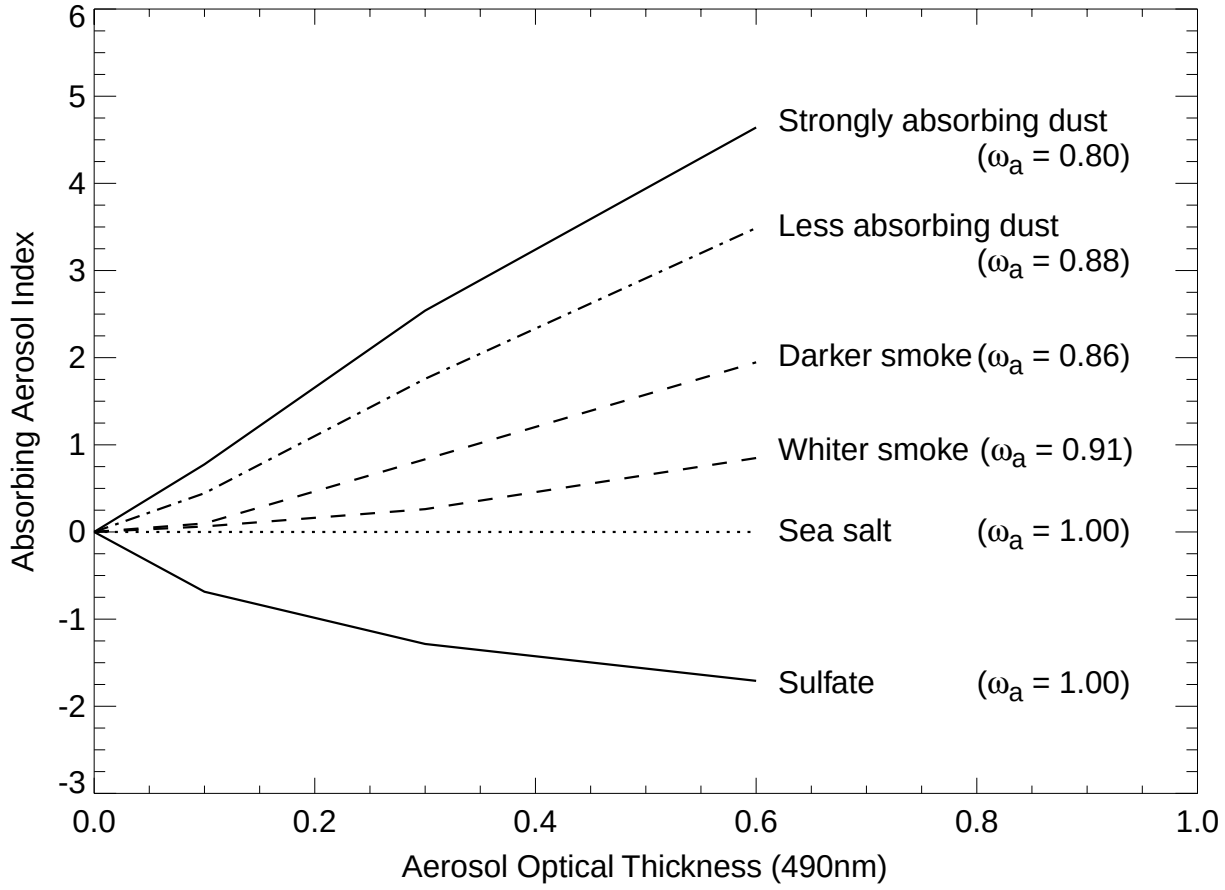

Fig. 1. The relationship between the SeaWiFS AI and AOT at 490 nm for various types of tropospheric aerosols over blue waters. The corresponding single scattering albedo (ω_a) is shown next to the aerosol model. The height of the aerosol layer is assumed to be at 3 km. The viewing geometry is for the condition of the solar zenith angle of 40°, satellite zenith angle of 52°, and relative azimuth angle of 120°.

tative of smoke from biomass burning and dust particles from sandstorms, values based on the results of *in situ* aerosol measurements (Tegen and Lacis 1996, and Remer et al. 1996) were employed in the model simulations. A log-normal particle size distribution was assumed in this study. The mode radius, $r_0(\mu)$, and width, σ', of the particle size distribution and the real and imaginary part of the refractive index at 412 and 490 nm for the aerosol models used in these calculations are listed in Table 1.

Figure 1 illustrates the relationship between the SeaWiFS AI and AOT over blue waters for the aerosol models listed in Table 1. The AOT corresponds to values at 490 nm. The mean aerosol altitude is assumed to be 3.0 km. The results in this figure are calculated for a solar zenith angle of 40°, a satellite zenith angle of 52°, and a relative azimuth angle of 120°. It is apparent that the slope of the AI versus optical depth changes with aerosol type (i.e., single scattering albedo, ω_a). Whiter smoke (e.g., $\omega_a = 0.91$) can only be detected at larger aerosol optical thicknesses. On the other hand, more strongly absorbing dust aerosols (e.g., $\omega_a = 0.80$) can be detected at smaller optical thicknesses using this absorbing aerosol index technique.

1.4 CASE-2 WATER CONSIDERATIONS

The signals over an ocean surface due to highly absorbing phytoplankton can mimic the spectral characteristics of absorbing aerosols in the remotely sensed reflectance. To help distinguish signals due to absorbing aerosols from those due to ocean surfaces with high chlorophyll content, the SeaWiFS 765 nm channel is used. The reflectance measured at this channel is greatly influenced by gas absorption associated with the oxygen A-band. The magnitude of such oxygen absorption depends on the effective altitude of the reflecting surface (e.g., ocean surface, cloud, or aerosol layer surface). It is assumed that the general sources of absorbing aerosols are from land, and the height of a resulting aerosol layer is not close to ocean surfaces. By selecting a threshold on the magnitude of the oxygen A-band signal, low-altitude aerosols (i.e., sea-salt) can be screened out, and conditions where a sufficient amount of absorbing aerosols are present to retrieve their properties can be determined.

When there is a intermediate or high amount of aerosol loading, the detection of absorbing aerosols is less sensitive to surface properties. For a thin aerosol layer over Case-2 water, however, it is very difficult to differentiate between absorbing and nonabsorbing aerosols. There is also a significant uncertainty in modeling the reflectance of various types of constituents over the ocean at 412 and 490 nm. Instead of trying, therefore, to model the effects, a chlorophyll content-based threshold is used as a discriminator. A tighter constraint on this threshold was employed when determining absorbing aerosol contamination for Case-2 water than for the Case-1 water. To determine the threshold level, a simple chlorophyll index was calculated using the SeaWiFS blue and green channels to provide a rough estimate on the degree of deviation of target water from blue water. When a higher level of chlorophyll content is indicated, a larger value of AI is required to pass the confidence level for detecting absorbing aerosols. As a result, the detection limit for absorbing aerosols is higher over Case-2 water than that over Case-1 water.

The combination of procedures mentioned above has provided reasonably good results to distinguish absorbing aerosols from the phytoplankton signature using the remotely sensed reflectance.

1.5 POTENTIAL APPLICATIONS

The SeaWiFS AI provides a fast way to identify the absorbing aerosols on a pixel-by-pixel basis. It can be used in the current operational algorithm as a flag to filter out chlorophyll and water-leaving radiance retrievals contaminated by absorbing aerosols. It will also aid the aerosol model selection process once the absorbing aerosol models are included in the retrieval algorithm.

Chapter 2

Analyses of the SeaWiFS Spectral Band-Pass Effects

Menghua Wang
University of Maryland, Baltimore County
Baltimore, Maryland

Bryan A. Franz and Robert A. Barnes
SAIC General Sciences Corporation
Beltsville, Maryland

Abstract

This chapter describes an effort to study the effects of the SeaWiFS spectral band pass on the retrieved normalized water-leaving radiances and ocean near-surface chlorophyll concentrations. SeaWiFS routinely provides ocean near-surface optical and microphysical property data, however, these retrievals include the effects of the relatively wide SeaWiFS spectral band passes. Because the SeaWiFS bio-optical algorithm was derived using *in situ* measurements, which were acquired at the SeaWiFS nominal band center wavelengths, it was necessary to assess the effects of the SeaWiFS spectral band pass on the retrieved chlorophyll concentrations.

2.1 INTRODUCTION

SeaWiFS, which was successfully launched on 1 August 1997, is one of only a few satellite instruments having complete prelaunch band spectral response measurements covering wavelengths from 380–1,150 nm for the eight SeaWiFS bands. One of the stated goals of the mission is to estimate water-leaving radiances to an accuracy of ±5% (Hooker et al. 1992). Figures 2a–d provide the spectral response function (SRF) for SeaWiFS bands 2, 3, 5, and 6. SeaWiFS not only has in-band response structures, but it also has significant sensor out-of-band contributions.

In ocean color remote sensing, the sensor-measured radiance at the top of the ocean–atmosphere system, measured at a wavelength λ, can be written as,

$$L_t(\lambda) \;=\; L_r(\lambda) \;+ L_a(\lambda) \;+ L_{ra}(\lambda) \;+\; t(\lambda)\, L_W(\lambda), \quad (2)$$

where $L_r(\lambda)$, $L_a(\lambda)$, and $L_{ra}(\lambda)$ are the radiance contributions from the multiple scattering of air molecules, aerosols, and Rayleigh-aerosol interactions, respectively; $L_W(\lambda)$ is the water-leaving radiance, which is the desired quantity for relating the oceanic near-surface physical and bio-optical properties; and $t(\lambda)$ is the atmospheric diffuse transmittance which accounts for the effects of propagating $L_W(\lambda)$ from the sea surface to the TOA (Wang 1999a, and Yang and Gordon 1997).

Because of sensor spectral band responses, the average radiance measured by SeaWiFS is weighted by the sensor spectral response functions. By defining

$$\left\langle L(\lambda_i)\right\rangle \;=\; \frac{\int L(\lambda)\, S_i(\lambda)\, d\lambda}{\int S_i(\lambda)\, d\lambda}, \quad (3)$$

where $S_i(\lambda)$ is the SeaWiFS spectral response function for band i at a nominal center wavelength λ_i, (3) can then be rewritten as

$$\begin{aligned}\left\langle L_t(\lambda_i)\right\rangle \;&= \left\langle L_r(\lambda_i)\right\rangle \;+ \left\langle L_a(\lambda_i) + L_{ra}(\lambda_i)\right\rangle \\ &\quad + \left\langle t(\lambda_i)\, L_W(\lambda_i)\right\rangle.\end{aligned} \quad (4)$$

In (4), i = 1–8 selects the SeaWiFS eight spectral bands and $\left\langle L_t(\lambda_i)\right\rangle$ is the radiance at the TOA measured by the SeaWiFS instrument. The Rayleigh contribution $\left\langle L_r(\lambda_i)\right\rangle$, as well as the aerosol and Rayleigh-aerosol interaction term $\left\langle L_a(\lambda_i) + L_{ra}(\lambda_i)\right\rangle$, can be estimated using methods outlined in Gordon (1995). The Gordon and Wang atmospheric correction algorithm can then be applied (Gordon and Wang 1994a).

Gordon (1995) showed the averaged Rayleigh and ozone optical thicknesses, as weighted by the solar irradiance and the sensor band SRF in computing the atmospheric diffuse transmittance, can be used to rewrite the last term in (4):

$$\left\langle t(\lambda_i)\, L_W(\lambda_i)\right\rangle \;\approx\; t(\lambda_i)\, t_0(\lambda_i)\, \cos\theta_0 \left\langle L_{WN}(\lambda_i)\right\rangle, \quad (5)$$

where $L_{WN}(\lambda_i)$ is the normalized water-leaving radiance for a given band, and $t_0(\lambda_i)$ and $t(\lambda_i)$ are the atmospheric

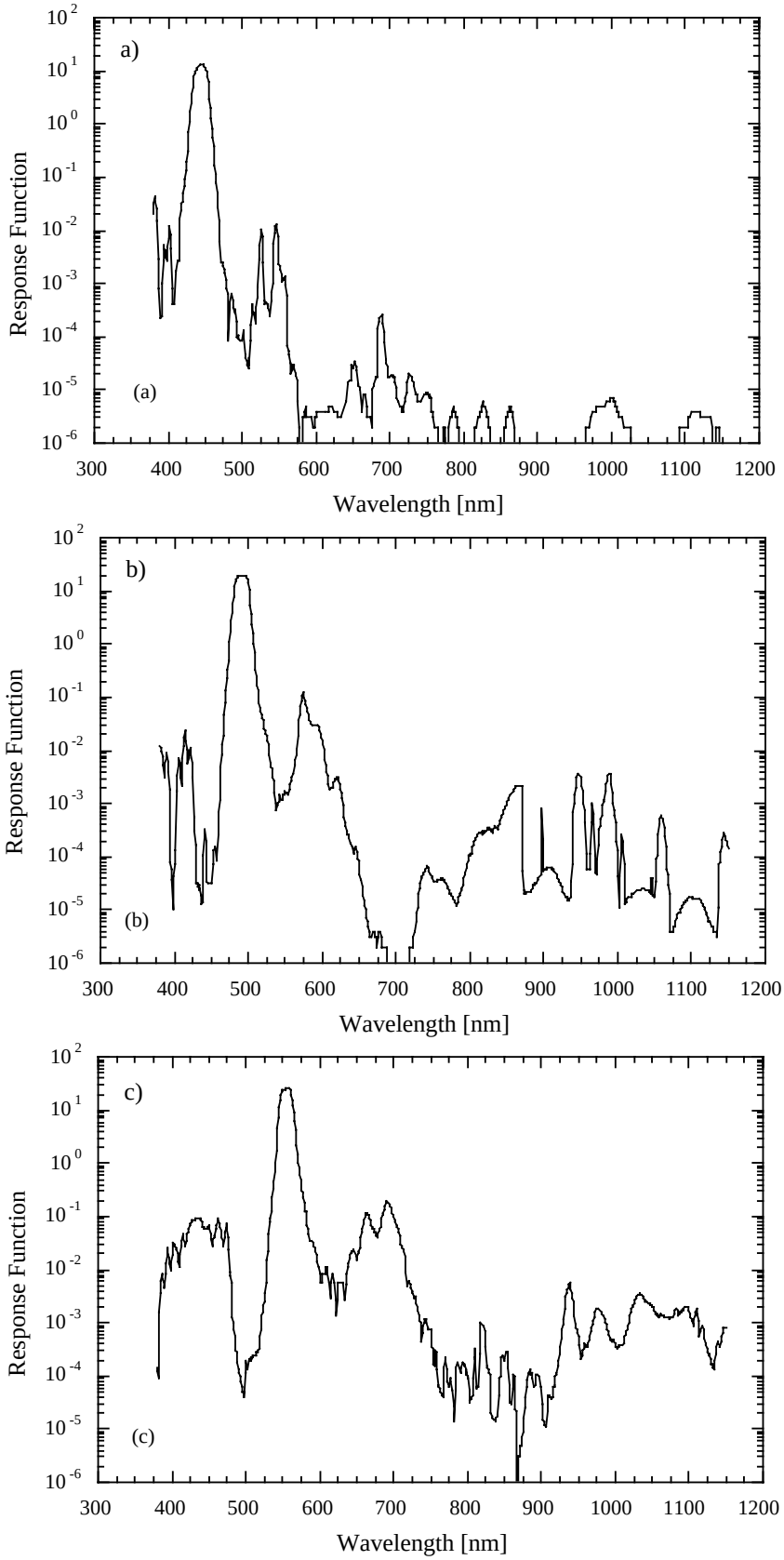

Fig. 2. The SeaWiFS spectral response functions for SeaWiFS: **a)** band 2 (443 nm), **b)** band 3 (490 nm), and **c)** band 5 (555 nm).

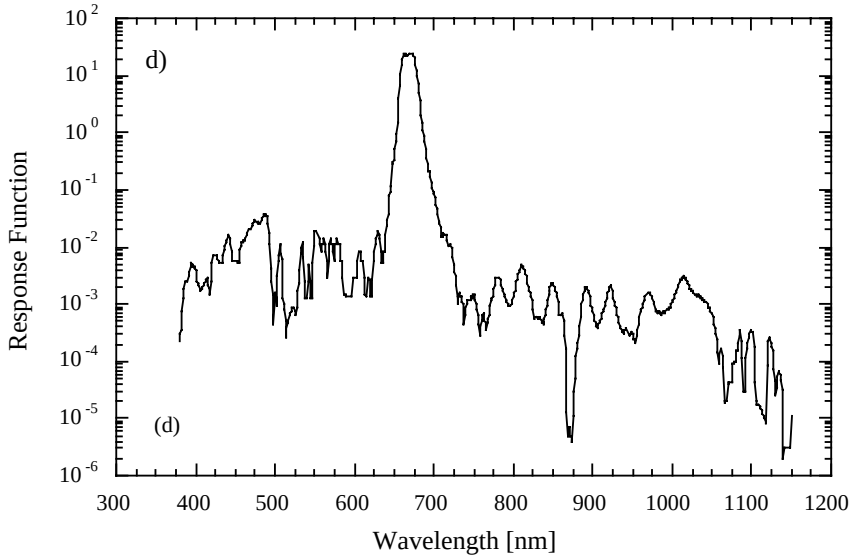

Fig. 2. (cont.) The SeaWiFS spectral response functions for SeaWiFS: **d)** band 6 (670 nm).

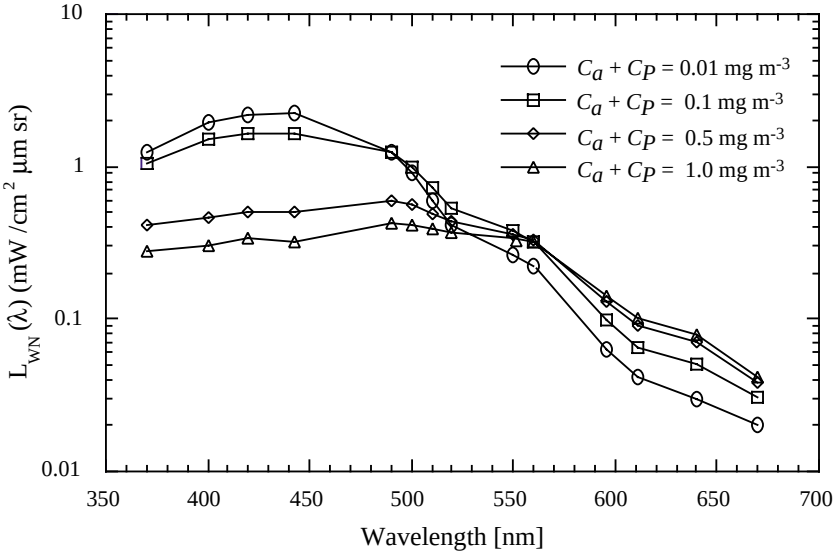

Fig. 3. The spectral distribution of the normalized water-leaving radiance $L_{WN}(\lambda)$ for a typical Case-1 water for various pigment concentrations, derived from Gordon et al. (1988).

diffuse transmittance at the solar and instrument viewing direction, respectively. SeaWiFS, therefore, routinely reports the weighted normalized water-leaving radiances, and it is the ratios of these weighted values that are used to compute the oceaninc near-surface chlorophyll concentrations (O'Reilly et al. 1998).

2.2 SPECTRAL BAND-PASS EFFECTS

To assess the effects of SeaWiFS spectral band responses on the derived normalized water-leaving radiance, it is necessary to derive a consistent set of results for both the nominal center wavelengths, $L_{WN}(\lambda_i)$, and the SRF weighted, $\langle L_{WN}(\lambda_i)\rangle$, cases. The spectral distribution of $L_{WN}(\lambda)$ was, therefore required at various chlorophyll concentrations. Figure 3 provides typical $L_{WN}(\lambda)$ (Case-1 water) spectral distributions obtained from bio-optical model calculations (Gordon et al. 1988) for four pigment concentration values, $C_a + C_P = 0.01$, 0.1, 0.5, and 1.0 mg m^{-3}, where C_a+C_P is the sum of chlorophyll a and phaeophytin a concentrations, respectively.

The Fig. 3 values were used to compute $\langle L_{WN}(\lambda_i)\rangle$ and to estimate the differences between $\langle L_{WN}(\lambda_i)\rangle$ and $L_{WN}(\lambda_i)$. It was found that the values in SeaWiFS bands 4 and 5 (green bands) for clear ocean water (low pigment concentrations) overestimated the $L_{WN}(\lambda_i)$ values by approximately 5% (Fig. 4). Because the SeaWiFS band 5 (555 nm) value was used in deriving the pigment concen-

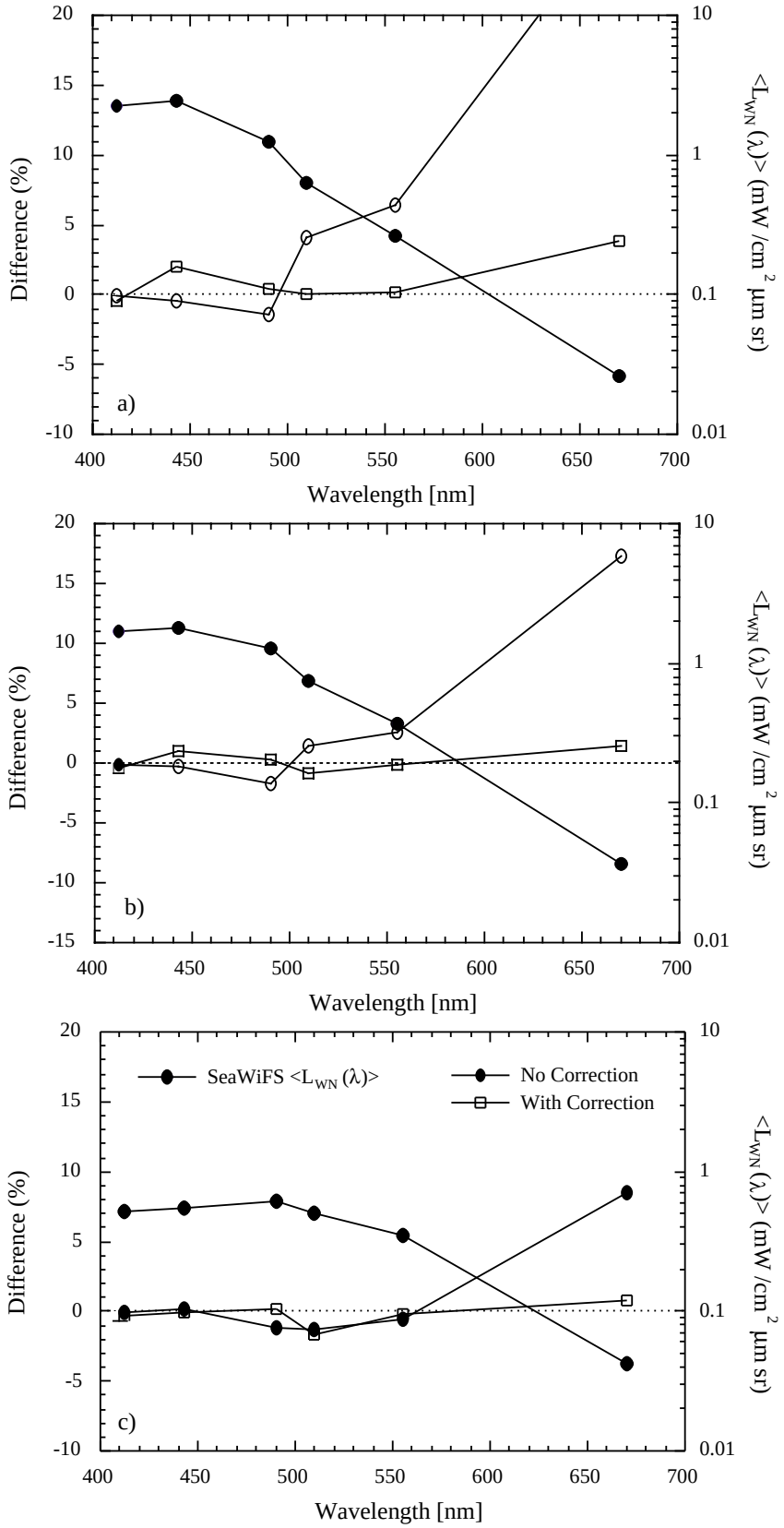

Fig. 4. The difference in percent between values of $\langle L_{WN}(\lambda_i)\rangle$ and $L_{WN}(\lambda_i)$ at the SeaWiFS spectral bands for pigment concentration in milligrams per cubic meter of **a)** 0.01, **b)** 0.1, and **c)** 0.5. Each figure also gives the values of $\langle L_{WN}(\lambda_i)\rangle$ (scale noted in the right side of figure).

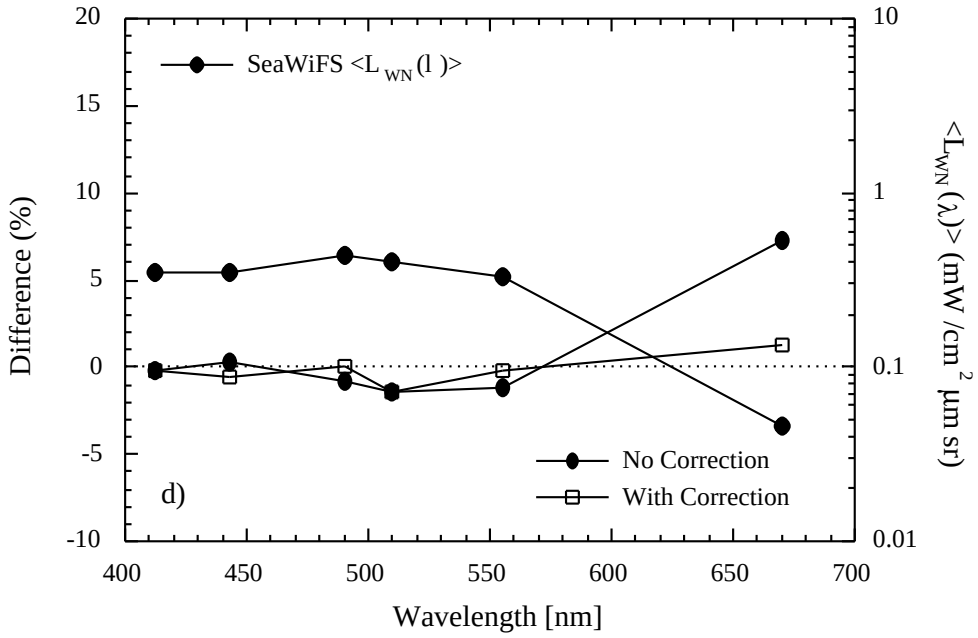

Fig. 4. (cont.) The difference in percent between values of $\langle L_{WN}(\lambda_i)\rangle$ and $L_{WN}(\lambda_i)$ at the SeaWiFS spectral bands for chlorophyll concentration in milligrams per cubic meter of **d)** 1.0. The figure also gives the values of $\langle L_{WN}(\lambda_i)\rangle$ (scale noted in the right side of figure).

trations, it would be useful if the SeaWiFS SRF effects could be removed and converted to the $L_{WN}(\lambda_i)$ value.

2.3 CORRECTIONS

To convert $\langle L_{WN}(\lambda_i)\rangle$ to $L_{WN}(\lambda_i)$ at the SeaWiFS spectral bands, the spectral distribution of $L_{WN}(\lambda_i)$ is needed; this depends on the ocean near-surface optical and microphysical properties. The spectral distribution of $L_{WN}(\lambda_i)$, however, can not be predicted *a priori*. Because SeaWiFS retrieves $\langle L_{WN}(\lambda_i)\rangle$ at the six spectral bands (412, 443, 490, 510, 555, and 670 nm), a first approximation for $L_{WN}(\lambda)$ can be derived by interpolating the $\langle L_{WN}(\lambda_i)\rangle$ values, and then using this measured spectral distribution to derive correction coefficients.

Using this approach, an iterative procedure can be defined to convert the SeaWiFS $\langle L_{WN}(\lambda_i)\rangle$ values to band-centered wavelength values, $L'_{WN}(\lambda_i)$:

1. SeaWiFS retrieved $\langle L_{WN}(\lambda_i)\rangle$ can be approximated as $L_{WN}(\lambda_i)$, i.e., $L_{WN}(\lambda_i) \approx \langle L_{WN}(\lambda_i)\rangle$.
2. Using $L_{WN}(\lambda_i)$ values, the average of the parameter $\langle L(\lambda_i)\rangle$ as weighted by the sensor spectral response function, $\langle\!\langle L_{WN}(\lambda_i)\rangle\!\rangle$, can be derived using (3). The ratio values, $r(\lambda_i)$ (i.e., the ratio value of L_{WN} at the SeaWiFS band-centered wavelength versus the average values weighted by the SeaWiFS spectral response function), can be estimated with

$$r(\lambda_i) \;=\; \frac{L_{WN}(\lambda_i)}{\langle\!\langle L_{WN}(\lambda_i)\rangle\!\rangle}. \qquad (6)$$

3. Finally, the normalized water-leaving radiance SeaWiFS band-centered wavelength, $L'_{WN}(\lambda_i)$, can be obtained with

$$L'_{WN}(\lambda_i) \;=\; r(\lambda_i)\,\langle L_{WN}(\lambda_i)\rangle. \qquad (7)$$

Going from step 2 to step 3 is an iterative process. In testing this approach, it was found that one iteration was usually accurate. It should be noted that to compute the required integrals, a log-linear interpolation was used to convert the six SeaWiFS $\langle L_{WN}(\lambda_i)\rangle$ values to a relatively continuous wavelength distribution covering the SeaWiFS spectral range from 380–1,150 nm.

Figures 4a–d provide results of the correction scheme for pigment concentrations of 0.01, 0.1, 0.5, and 1.0 mg m^{-3}. Although the effects are negligible in the SeaWiFS blue bands, the corrections were performed for all six visible bands to test the efficacy of the approach. In generating Figs. 4a–d, the spectral distribution of $L_{WN}(\lambda)$, as shown in Fig. 3, was used. Note that in Figs. 4a–d, there are three curves in each figure:

a) The SeaWiFS $\langle L_{WN}(\lambda_i)\rangle$ values (the scale is noted on the right side of the figure);

b) The difference between $\langle L_{WN}(\lambda_i)\rangle$ and $L_{WN}(\lambda_i)$ without corrections; and

c) The same as in item b, but with corrections.

The correction scheme works quite well. Differences between true and retrieved values of $L_{WN}(\lambda_i)$ are reduced, in particular, in the SeaWiFS green and red bands. The

correction scheme was also applied to *in situ* data sets acquired from MOBY in Hawaii, and similar results were obtained.

This correction scheme was implemented into the chlorophyll match-up analysis, where the SeaWiFS derived chlorophyll values were compared with co-located *in situ* measurements. The results were plotted as SeaWiFS retrieved values versus the *in situ* measurements, and a linear least-squares fit was then obtained. Table 2 gives the values of intercept (b), slope (m), and the correlation coefficient (R) before and after the SeaWiFS band-pass effects corrections. Note that the perfect match corresponds to values of $b = 0$, $m = 1$, and $R = 1$.

Table 2. Values of coefficients in the linear least-squares fit for the chlorophyll match-up analyses (SeaWiFS versus *in situ* measurements) before and after the SeaWiFS band-pass effects corrections.

Case	b	m	R
Before	0.1093	1.1272	0.8665
After	0.0824	1.0266	0.8504

Chapter 3

Changes Made in the Operational SeaWiFS Processing

Wayne D. Robinson and G. Michael Schmidt
SAIC General Sciences Corporation
Beltsville, Maryland

Charles R. McClain
NASA Goddard Space Flight Center
Greenbelt, Maryland

P. Jeremy Werdell
Science Systems and Applications, Incorporated
Lanham, Maryland

Abstract

This chapter discusses the major changes made in the SeaWiFS processing for the second reprocessing in August 1998 and the third reprocessing in May 2000. Each major change in the processing programs and tables is presented with a description of the effects of the change. For the second reprocessing, a review of the major changes to the data are presented using an eight-day period of data as an example. The effect of the changes for the third reprocessing are also examined and compared to the results of the second reprocessing using two eight-day periods of data. The changes have increased the usefulness of the data in both oceanographic and atmospheric applications.

3.1 INTRODUCTION

This chapter discusses the major changes made in the SeaWiFS level-1, -2, and -3 processing which led to the third reprocessing. Ever since the first SeaWiFS reprocessing of 2 January 1998, SeaWiFS Project personnel have been evaluating the results of the processing and have discovered many problems and improvements. Some problems were fixed in the operational software, but many improvements which required recalibration could not be applied without initiating a complete reprocessing. These changes were accumulated for a period of approximately six months before applying them to all the data in the second reprocessing of the data set. During this period, significant changes in the calibration of SeaWiFS bands 7 and 8 (Eplee and McClain 2000a) made it imperative to include the calibration and other changes into the operational processing, so the quality of the data could be maintained.

The second reprocessing started on 14 August 1998. At that time, the new software was used to reprocess all of the data collected from the start of the mission and to process the real-time data as it was acquired. Since the second reprocessing, a number of minor enhancements and repairs were made to the operational processing software.

Several remaining problems, which were recognized after the second reprocessing, were extensively investigated; many improvements were developed to make the resulting data more useful and to broaden the product suite. All these changes were incorporated in the third reprocessing, which occurred in May 2000.

The next section (Sect. 3.2) discusses the major changes made in the software and tables for the second reprocessing, and the impact of those changes on the products. A brief summary of the combined effect of those changes is discussed in Sect. 3.2.4 and the major changes included in the third reprocessing are presented in Sect. 3.3. Section 3.3.6 presents an analysis of the changes in the derived products from the second to the third reprocessings, which is followed by a summary of the changes and a discussion of future improvements (Sect. 3.4).

3.2 THE SECOND REPROCESSING

In the approximately six months between the first and second SeaWiFS reprocessings, many changes were made in the level-2 and -3 processing software. The most significant changes in that period are shown in Table 3 and are

Table 3. Major changes and their observable effects in the second reprocessing.

Change	*Observable Effect*
Calibration:	
Prelaunch Calibration Change	None
Time dependence of bands 7 and 8	Better temporal stability
Revised vicarious calibration	None
Atmospheric Correction:	
New transmittance tables	Removed L_{WN} as f (scan angle)
Wider range of aerosol models	Reduced number of points outside model range
Other:	
Updated coefficients for the chlorophyll a algorithm	Increased low chlorophyll a concentrations and decreased high chlorophyll a concentrations
Added test for high reflectance ratios	Removed spurious chlorophyll
Tests to decrease chlorophyll speckles	Some reduction on speckles
Improved L_{WN} computation	Less than 1% change in L_{WN}
Noise resistant dark count	No striping in the data
Improved solar radiance computation	None
More accurate anchor point grid	None
Reduced whitecap radiance	Reduced data loss
Binned higher chlorophyll	Retained larger chlorophyll range
Wrote out actual ϵ values	Better diagnostics on ϵ values

discussed briefly here. The details of changes related to the calibration, atmospheric correction, and the new chlorophyll a algorithm are discussed elsewhere in this three-volume set, Volumes 9–11, of the *SeaWiFS Postlaunch Technical Report Series*.

3.2.1 Calibration Related Changes

In the period leading up to the second reprocessing, the calibration of the SeaWiFS instrument became more rigorous, with a more detailed band 7 calibration and better detector characterization. Three changes associated with the calibration are presented here.

3.2.1.1 Prelaunch Calibration Changes

The first reprocessing was conducted using a preliminary set of SeaWiFS calibration values, which were determined in January and April 1997. When an analysis of the calibration data was completed (Johnson et al. 1999), the calibration was modified to include these updates, and was used for the second reprocessing. The changes in the total radiances were less than 0.5%.

3.2.1.2 Time Dependent Calibration

In 1998, the time series of solar and lunar calibration measurements, which began in September 1997, showed that the radiometric responses of bands 7 and 8 were changing as a function of time. The greatest change occurred in band 8, amounting to a 4–5% decrease in the total radiances. The calibration table used during the second reprocessing was adjusted to compensate for these changes and was updated as needed thereafter in the operational processing. A detailed discussion of the calibration is presented in Eplee and Barnes (2000) and Eplee et al. (2000).

3.2.1.3 Revised Vicarious Calibration

Improvements were made in the vicarious calibration of band 7 relative to band 8, and for bands 1–6. Details of the vicarious calibrations are discussed in Robinson and Wang (2000) and Eplee and McClain (2000a), but a short summary is presented here.

The band 7 vicarious calibration was accomplished by adjusting the band 7 gain factor until the ratio of the single-scattering aerosol radiances (the ϵ value) in bands 7 and 8, matched the expected ratio over the open ocean. This process was applied to a limited number of sites in the first reprocessing. The current band 7 calibration extends and improves this procedure by selecting open-ocean sites near Hawaii, evaluating the gain using the time series of SeaWiFS LAC data supporting the MOBY site, and using strict screening procedures for data quality.

The calibration for bands 1–6 was derived by adjusting the gain factors for each band until the water-leaving radiances in those bands matched those measured by MOBY. In the second reprocessing, the calibration was improved with more MOBY observations.

3.2.2 Atmospheric Correction Changes

Wang (2000) presents a more detailed description of the changes made in the atmospheric correction. Two major changes are briefly described here.

3.2.2.1 New Transmittance Tables

The transmittance tables were corrected to include the Fresnel reflectivity of the air–water interface. The introduction of this correction removed a small scan-angle dependence in L_{WN}. The changes reduced L_{WN} in bands 1–5 by 2% at the center of the scan. At the edge of the SeaWiFS global area coverage (GAC) scan, the L_{WN} was reduced by about 5%, and at the edge of a LAC or high resolution picture transmission (HRPT) scan, the reduction was about 10%.

3.2.2.2 Wider Range of Aerosol Models

In the process of performing the atmospheric correction, the level-2 processing determines the atmospheric model most closely matching the ϵ value, or ratio of aerosol radiances in bands 7 and 8. For about 40% of the points processed in the first reprocessing, the ϵ value was below the lowest ϵ value of the available models. In these cases, the atmospheric correction was forced to use the model with the lowest ϵ value to derive the aerosol radiances for the other bands. Although this model was the best available, it was not as correct as a model that would fit the observed ϵ value.

In the second reprocessing, the model suite was expanded to include oceanic aerosol models which contain lower ϵ values. The new atmospheric model suite reduced the occurrence of points below the model range from 40% to about 20%.

3.2.3 Other Changes

Other changes made to the SeaWiFS processing affect both the level-2 and -3 algorithms. The changes correct minor problems, improve algorithms, or reduce noise in the products.

3.2.3.1 Improved Chlorophyll a *Algorithm*

The relationship between L_{WN} and chlorophyll a was updated with additional *in situ* observations (Maritorena and O'Reilly 2000), which resulted in a new set of coefficients for the equation relating the ratio of L_{WN} to chlorophyll in the 490 and 555 nm bands. The new relationship increased chlorophyll values that are less than $0.03\,\mathrm{mg\,m^{-3}}$ and decreased chlorophyll values that are greater than $1.0\,\mathrm{mg\,m^{-3}}$.

It was found that under conditions of very large reflectance ratios, (values greater than 10), the chlorophyll algorithm could return reasonable chlorophyll values. The chlorophyll failure flag was set in these instances, so these values would not be binned. A similar treatment was applied in the third reprocessing.

3.2.3.2 Decreased Chlorophyll a *"Speckling"*

The SeaWiFS level-2 and -3 binned data contained isolated pixels with relatively high chlorophyll a values in fields with otherwise low chlorophyll values. Frequently, these so-called *speckles* were near cloud edges not masked as "cloud" pixels. Methods for removing these points (such as, decreasing the band 8 albedo threshold for cloud masking, or expanding the stray light distance), caused a large number of good data points to be masked (and, thus, removed) in the process of removing a small number of bad points.

An alternative method was used that masked many occurrences of speckles without masking (and removing) good data. A mask was applied to the pixels in which any of the bands 1–8 had zero or negative values after the radiances were corrected to remove the effects of ozone absorption, whitecap radiance, and Rayleigh radiance. The masked data points were assigned the atmospheric correction failure flag (which is usually a mask). The new test reduced the occurrences of speckles, but did not completely eliminate them. This test also revealed cases where the whitecap correction to the radiances was too large (Sect. 3.2.3.7).

3.2.3.3 Improved L_{WN} Computation

The L_W normalization step of the level-2 processing was improved to include a more realistic atmospheric attenuation than the attenuation used in the first reprocessing. In the first reprocessing, the normalization only used the Rayleigh scattering and ozone absorption to correct for the attenuation in the path from the sun to the surface. For the second reprocessing, the effect of aerosol scattering was included, which slightly reduced the L_{WN} values in bands 1–5 by less than 1%.

3.2.3.4 Noise Resistant Dark Count Calculation

Striping was noticed in the radiance data, the cause for which was traced to the *dark count* calculation used in the calibration of the data. The dark count is the digital count value measured by the detectors when looking at a dark surface and, thus, represents a zero radiance value in the calibration equation. The dark count is collected for every scan line of data, has a nominal value of 20 counts, and remains virtually constant throughout an entire data pass. In some of the data, the dark count had a tendency to change by one digital count from one line to the next, which is commonly referred to as *jitter*.

The jitter in the dark counts caused the line-to-line striping in the radiances. To remove the jitter, the dark counts were averaged to estimate a dark count offset for the entire pass. With the onset of data encryption, a number of dark count values that were very different with respect to the standard values from undecrypted lines, were included in the algorithm that computes the average dark count value. The resulting dark count average occasionally produced badly calibrated radiances and caused the entire scene to have radically different normalized water-leaving radiances than expected.

The dark count calculation was improved using the following two steps:

1) Remove from consideration any dark count values that are less than 5 counts or greater than 35 counts, and
2) Take the median value as the dark count for the pass.

The improvements were especially helpful for HRPT data processing, which frequently has trouble with noise at the start and end of a pass. On occasion, it also helped improve the quality of GAC and LAC data.

3.2.3.5 Improved Solar Radiance Computation

A 0.1% error in the value of the correction in the solar irradiance as a function of the time of year, was discovered in the level-2 processing. The correction was improved to reduce this error to 0.001%. A 0.1% error in the solar irradiance roughly translates to approximately a 1.0% error in the L_{WN} values.

3.2.3.6 More Accurate Anchor Point Grid

To speed up the calculation of processing parameters, such as, the ancillary data values and Rayleigh radiances, the level-2 processing program used a set of anchor points at which these quantities were computed exactly. The values of the ancillary data at other points were computed by interpolating the anchor point data to that location. For the first reprocessing, the anchor point separation was eight pixels for LAC and HRPT data, and two pixels for GAC data.

In some cases, the difference between the interpolated Rayleigh values with respect to the exact values was significant, e.g., as great as $0.015\,\mathrm{mW\,cm^{-2}\,\mu m^{-1}\,sr^{-1}}$ in the Rayleigh radiance at 443 nm, which roughly translates to a 1% uncertainty in the L_{WN}. On average, this uncertainty was less than $0.002\,\mathrm{mW\,cm^{-2}\,\mu m^{-1}\,sr^{-1}}$. This uncertainty was reduced to less than $0.004\,\mathrm{mW\,cm^{-2}\,\mu m^{-1}\,sr^{-1}}$ in the second reprocessing by reducing the anchor point separation by a factor of 2 (one pixel in the GAC data and four pixels in the LAC and HRPT data) to improve the accuracy of the Rayleigh and other ancillary data used. (Note that in the third reprocessing, all calculations are done at every point).

3.2.3.7 Reduced Whitecap Radiance Effect

Several instances occurred where a region of ocean was cloud-free, but it was masked out as an atmospheric correction failure, because the ozone, whitecap, and Rayleigh-corrected radiances in some bands were negative (a mask condition intended to reduce speckles in the chlorophyll concentration). It was discovered that in very clear regions with high wind speeds (around $15\,\mathrm{m\,s^{-1}}$), the whitecap correction was so large in bands 7 and 8, the remaining radiance was smaller than the Rayleigh radiance which caused the region to be masked.

A 75% reduction in the whitecap correction was implemented to solve this problem. In discussions with H. Gordon, this reduction factor seemed reasonable. In addition, studies of the whitecap contributions (Gordon and Wang 1994b) showed a large amount of variability in the whitecap radiances under high wind conditions. The main effect of this change in the whitecap correction radiances was to allow previously overcorrected and masked areas to be processed.

3.2.3.8 Binning of Higher Chlorophyll Values

It was noticed that in the process of binning the level-2 data, a large amount of high chlorophyll data was being excluded. The primary reason for this was that many pixels had a valid chlorophyll value (i.e., the L_{WN} in bands 3 and 5 were positive), but the L_{WN} values in bands 1 or 2 were negative. In the first reprocessing, the presence of negative L_{WN} values in a measurement was one of the exclusion conditions for the binning.

To bin more of these excluded chlorophyll values, a number of changes were made in the level-2 and -3 programs. First, the level-2 program was modified to output the actual negative water-leaving radiances that were derived instead of a -1.0 value. This allows an investigator to get a better idea of how large the negative L_{WN} values actually are. The binning routine was modified to bin pixels that have negative L_{WN} values in them, but to bin them as zeros. In addition, the chlorophyll algorithm failure flag (`CHLOR1`) was added as a binning flag, so points which had a chlorophyll algorithm failure (band 3 or 5 where L_{WN} is less than zero or where chlorophyll values are greater than 64) would not get binned. This set of changes restored much of the previously excluded high chlorophyll data.

3.2.3.9 Actual Epsilon Values

In the first reprocessing, the aerosol correction algorithm in the level-2 processing code reported the ϵ value for the nearest aerosol model in cases where the derived ϵ value was actually outside the model range. This caused some uncertainty in the actual value of ϵ, and it also tainted some calculations that used the average value of ϵ.

The aerosol correction algorithm was modified to report and store the actual computed ϵ value. This ϵ value was also used in the aerosol calculations.

3.2.4 Second Reprocessing Analysis

In many cases, changes in L_{WN} values brought about by level-2 processing algorithm changes were compensated for when the vicarious calibration was applied. The only way to understand the effects of all the changes was to consider them after the calibration was implemented. The cumulative effect of all the above changes is discussed in this section. The effect of all the changes to the processing is studied using a sample of typical SeaWiFS data.

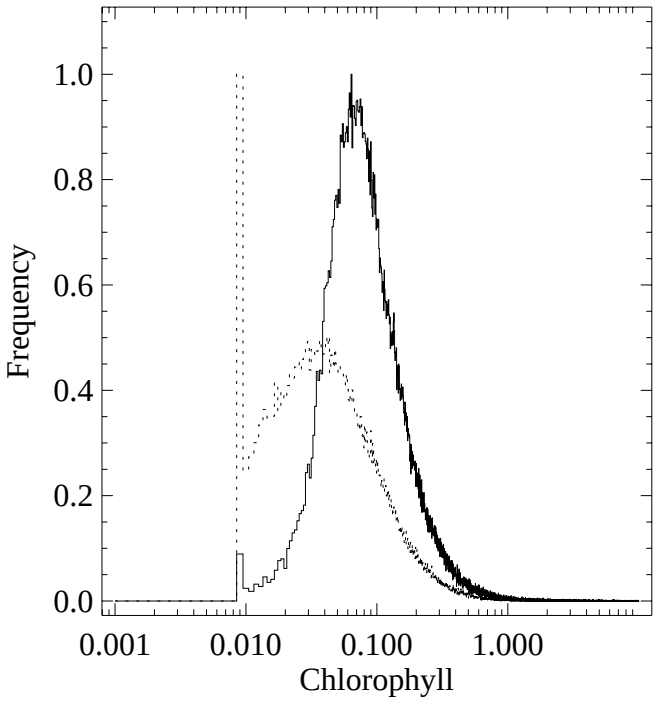

Fig. 5. The SeaWiFS level-3 global chlorophyll *a* frequency distribution for an eight-day period (14–21 March 1998) using the first and second reprocessing algorithms (dotted and solid curves, respectively).

3.2.4.1 Chlorophyll a *Changes*

Figure 5 shows the global frequency distribution of chlorophyll *a* resulting from the first and second reprocessings for an eight-day period. The second reprocessing chlorophyll values are higher in open ocean regions, such as, the South Pacific and Atlantic. Large regions that previously had chlorophyll concentrations at the lowest value of $0.01\,\mathrm{mg\,m^{-3}}$ with the first reprocessing, had their values increase to around $0.03\,\mathrm{mg\,m^{-3}}$ with the second reprocessing. This was mostly the result of the new chlorophyll algorithm, although some contribution resulted from the new transmittance tables and calibration.

The increased chlorophyll values observed in the second reprocessing agreed better with observations of the lowest chlorophyll concentrations, i.e., values of $0.01\,\mathrm{mg\,m^{-3}}$ are rarely observed. The distribution of chlorophyll was raised significantly in the second reprocessing. The peak value of chlorophyll increased from 0.02–$0.05\,\mathrm{mg\,m^{-3}}$ and far fewer points had the lowest chlorophyll value of $0.01\,\mathrm{mg\,m^{-3}}$. A number of observations still appeared below the lower limit of $0.01\,\mathrm{mg\,m^{-3}}$ in the second reprocessing.

Another aspect of the second reprocessing was that the total number of filled bins in the time binned product increased by 5%. Many of the new points were in high chlorophyll areas—a direct result of the new binning strategy which retained a greater number of high chlorophyll values (Sect. 3.2.3.8). Many of the new points were in coastal regions and in the Baltic Sea.

The second reprocessing significantly reduced the magnitude of the highest chlorophyll values (another direct effect of the new chlorophyll *a* algorithm). Chlorophyll concentrations near many coastal regimes, for example, showed decreases up to 30%. The second reprocessing changes also resulted in an increase of the L_{WN} values in bands 3 or 5, so that chlorophyll values could be determined in more coastal areas.

Both the increase in very low chlorophyll *a* values and the decrease in high chlorophyll *a* values were improvements that occurred in the new processing.

3.2.4.2 Water-Leaving Radiance Changes

An analysis of the global distribution of L_{WN} showed a general increase in the L_{WN} values with the second reprocessing. For instance, the mean L_{WN} at 555 nm was increased by 0.06 from 0.26–0.32. The new mode of 0.27 (versus 0.21 in the first reprocessing) had better agreement with the MOBY-derived clear-water L_{WN} value of 0.254 (Eplee and McClain 2000b).

In the blue bands, considerably less change was observed in the L_{WN} distribution. The mean L_{WN} at 412 nm increased only slightly from 1.53–1.56. In some isolated regions along the coast, L_{WN} actually decreased somewhat. The decreases may have been due to the inclusion of zero values of L_{WN} in the binning algorithm (Sect. 3.2.3.8). It was hoped that the second reprocessing changes would reduce the number of negative L_{WN} values in bands 1 and 2. Although L_{WN} increased overall, there were still problems. The next section looks at the distribution of negative L_{WN} values in more detail.

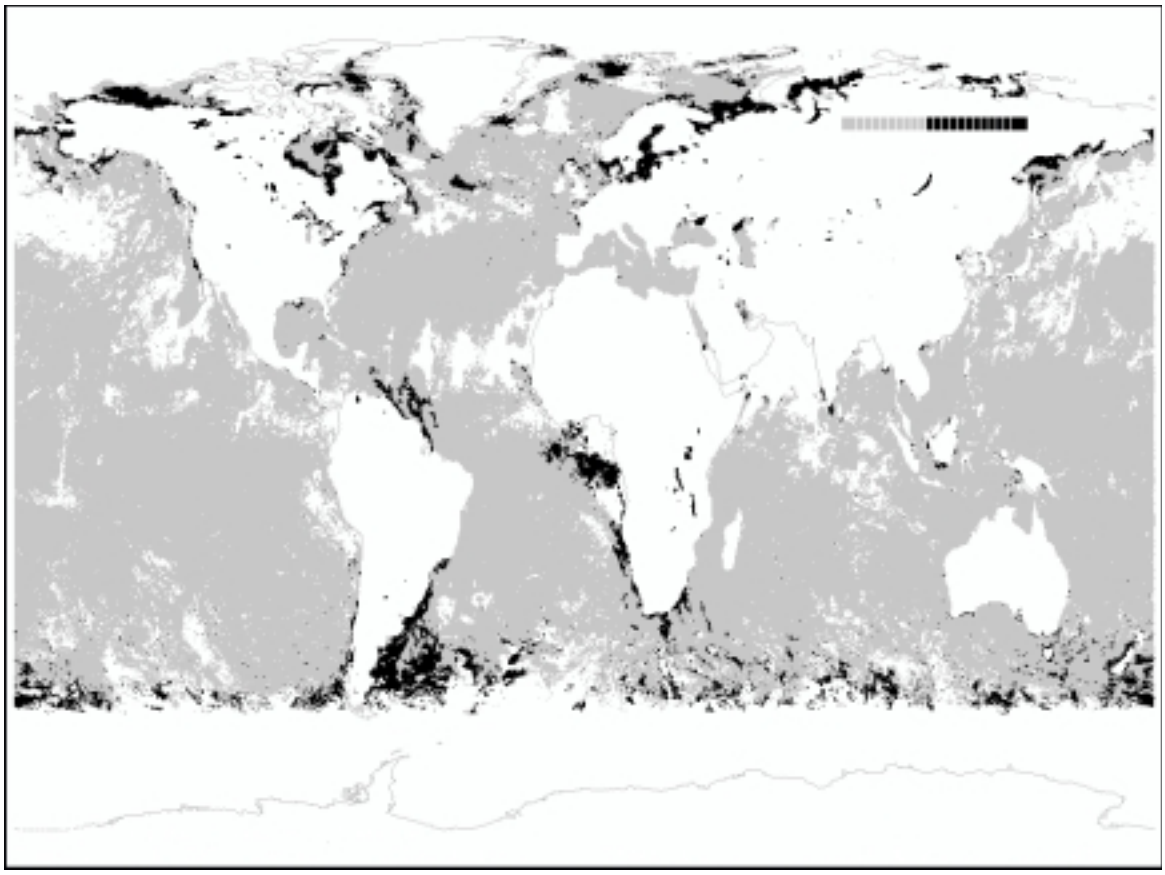

Fig. 6. Percent occurrence of negative L_{WN} values at 412 nm for the eight-day period from 12–19 July 1998. The image was generated using the second reprocessing algorithms and uses data that is excluded by the standard level-2 processing: atmospheric correction algorithm failure, land, sun glint, high total radiance, and clouds. In addition, stray light pixels are excluded. White areas indicate no data—continental land masses make up a large part of this region—while light gray indicates data present with occurrences of negative L_{WN} values of less than 50%. The regions shaded black all have more than 50% occurrence of negative L_{WN} values, indicating areas that are severely affected by negative L_{WN}.

3.2.4.3 Distribution of Negative L_{WN} Values

The occurrence of negative L_{WN} values, particularly in bands 1 and 2, has always been a problem in the SeaWiFS processing scheme. Because the second reprocessing retained the *actual* values of the negative normalized water-leaving radiance instead of setting them to zero, it was possible to look at the distribution of the negative L_{WN} values. The geographic distribution of negative L_{WN} values in the 412 nm band is presented in Fig. 6 for all level-2 data not masked by the level-2 flag conditions in an eight day period from 12–19 July 1998. Regions that had occurrences of negative L_{WN} values greater than 50% are shaded black.

The negative L_{WN} distribution shows the largest problems to be in the coastal margins and in the extreme northern and southern latitude regions. The coastal waters have higher chlorophyll concentrations and are the most likely to have problems with turbid water or dust in the atmosphere affecting the aerosol correction. The non-coastal areas in the Southern Ocean (and to some degree in the extreme North Atlantic) with negative L_{WN} values also have relatively high chlorophyll values, but should not have other coastal problems, such as continental aerosols. The amount of negative L_{WN} in these areas decreases as wavelength increases (not shown) and was fairly negligible at, and above, the 490 nm band.

The distribution of negative L_{WN} values in higher latitude regions suggests the problem may be related to poor treatment of the atmospheric corrections at high solar zenith angles. The 12–19 July data were taken when the sun was at a latitude of 20°N. In that data (Fig. 6), the significant increase in negative L_{WN} values appeared to occur at 40°S and possibly 80°N, which translates into solar zenith angles of around 60°. When the percentage of negative L_{WN} values at 412 nm is plotted as a function of solar zenith angle (Sect. 3.3.6.2), a large increase in the percentage of negative L_{WN} values is seen at a solar zenith angle of 60°. Similar behavior occurred for a period in January

1998 (not shown). This behavior may indicate a breakdown in the plane parallel atmosphere assumption used to derive aerosol model behavior (Ding and Gordon 1994). This possibility was investigated further in preparation for the third reprocessing.

An additional occurrence of negative L_{WN} values was scattered throughout the open ocean areas, but unlike the coastal areas, the frequency of negative L_{WN} values in these areas was relatively small. In the 510 and 555 nm bands (not shown), the distribution of open ocean negative L_{WN} values increased somewhat. This effect was primarily due to the influence of cloud shadows, noise, and stray light on the radiances. When the binning flags, which include masks for low $L_{WN}(555)$ values, were included, this problem was almost entirely removed in band 1 and the other bands.

The binning masks appeared to aid in removing some of the negative L_{WN} values, but large coastal areas remained severely affected by this problem.

3.3 THE THIRD REPROCESSING

The second reprocessing was able to improve on the algorithms used to perform the calibration and processing of the SeaWiFS data to water-leaving radiances and derived geophysical quantities. It also left many important questions to be resolved. The most important concern was to determine what was causing the large number of negative L_{WN} values in coastal areas. The effort to understand and solve this problem and the algorithms chosen for the third reprocessing are presented here.

In the period leading up to the third reprocessing, a number of improvements were also made in the calibration and the atmospheric correction algorithms. Calibration improvements were possible with more measurements, which led to a greater understanding of instrument performance. Another significant change was the migration of the level-2 processing algorithms to a new program, `MSl12`, which greatly improved the ease of use and the incorporation of new algorithms.

The `MSl12` program permitted the selection of many more intermediate and final parameters. With this migration, several basic changes were made in the default operational products and in the available flags. The major operational changes are summarized in Table 4 and brief descriptions of the changes are presented in the following sections along with the results of the third reprocessing (Sect. 3.3.6).

3.3.1 Calibration Related Changes

The changes to the calibration included the routine characterization of the detector degradation, as well as, a better understanding of instrument behavior. Increased use of the SeaWiFS data for cloud and aerosol studies revealed other calibration problems, which were solved for the third reprocessing.

3.3.1.1 Expanded Time-Dependent Calibration

The SeaWiFS CVT has updated the time-dependent calibration as new lunar calibration measurements become available each month. Previously (Sect. 3.2.1.2), a time dependence could only be seen in the two near-infrared bands (765 and 865 nm). A longer time period of observations, and a more accurate treatment of the radiance model of the moon, made it possible to detect and implement a correction for time-dependent changes in the radiometric response in many of the remaining bands (Eplee and Barnes 2000).

The largest changes now seen in bands 7 and 8 are a 2% and 10% decrease, respectively, while bands 1 and 6 (412 and 670 nm) show 1% decreases, and bands 2 and 5 (443 and 555 nm) show 0.5% decreases. Bands 3 and 4 (490 and 510 nm) are assumed to have no change. The SeaWiFS calibration now contains time-dependent corrections for all these bands.

3.3.1.2 Bilinear Gain Adjustments

During work to derive a measure of absorbing aerosols (Hsu et al. 2000 and Fukushima et al. 1999), it was determined that there was a discontinuity in the frequency distribution of total radiances which occurred at the region where the instrument gain changed to a lower sensitivity (the so-called *knee* point). This indicated that the relationship between raw satellite counts and total radiance was incorrect for radiance values above the knee. The radiance value at which this discontinuity occurred was above the range where most ocean color processing is performed and, therefore, has no effect on the oceanic products. It does, however, have an effect on the analysis of dense aerosols, absorbing aerosols, and clouds. It was assumed that the laboratory setting of the knee point was either incorrect or had shifted.

The knee points were redetermined by finding the settings that minimized the discontinuity in the frequency distributions of the total radiances (Eplee and Patt 2000). The implementation of this change reduced the radiances above the knee by 0.8% on average, and increased the radiance below the knee by about 0.1%.

3.3.1.3 Revised Vicarious Calibration

The calibration of bands 1–7 was performed for the third reprocessing in much the same way as it was done for the second reprocessing (Sect. 3.2.1.3, Eplee and McClain 2000a, and Robinson and Wang 2000). This calibration is performed every time the level-2 processing algorithms are modified to ensure that the water-leaving radiances produced by the algorithms match the ground-truth measurements from MOBY.

The vicarious calibration is also performed to include additional SeaWiFS and MOBY measurements taken over time.

Table 4. Major changes and their observable effects in the third reprocessing.

Change	*Observable Effect*
Calibration:	
Expanded time-dependent calibration	Better temporal stability
Bilinear gain adjustments	Smoothed transition to higher radiances
Revised vicarious calibration	None
Temperature correction	None
Atmospheric Correction:	
Modified aerosol model selection	Reduced discontinuity in some fields
Epsilon value extrapolation	Better retrieval of low chlorophyll values
Improved Rayleigh computation	Significant decrease in negative L_{WN} at high solar zenith angles
Pressure dependent transmittance	Small L_{WN} changes
Near-infrared L_{WN} adjustment	Significant decrease in negative L_{WN} and high chlorophyll values in coastal areas
Other:	
Modified C_a:K computation	Eliminated bad data values in binned data
Spectral-dependent whitecap correction	Small reductions in negative L_{WN} values
Sun glint correction	Greatly improved aerosol optical thickness
Ozone data interpolation	None
Improved $K(490)$ algorithm	Better $K(490)$ values in turbid water
Absorbing aerosol flagging	Reduced binning of contaminated data
Trichodesmium flagging	None
Improved chlorophyll algorithm	Slight lowering of low chlorophyll values
Out-of-band correction	Better compatibility to *in situ* measurements
Navigation Improvements	Improved location of data
Improved coastal data inclusion	More coastal retrievals
Structural:	
Product and flag updates	Better flag specificity
Level-2 program code changes	Greater flexibility and faster updates

3.3.1.4 Temperature Correction

A correction was made to the level-0 to -1 conversion software to correctly unpack the focal plane temperatures used in the calibration process. The effect of this correction on the water-leaving radiance values was less than 0.5% in bands 1–4, 1.5% in band 5, and 3.0% in band 6. Recalibration will remove most of these changes.

3.3.2 Atmospheric Correction Changes

A number of improvements were made in the algorithms that remove the radiance contributions of the atmosphere. As with the changes in the calibration (Sect. 3.3.1), some of the changes were made to correct artifacts seen in the data, and others were made to perform a more accurate atmospheric correction.

3.3.2.1 Modified Aerosol Model Selection

It was discovered that the aerosol radiance fields contained noticeable discontinuities in open ocean areas. The discontinuities, which paralleled lines of constant scattering angle, propagated noticeable and unwanted artifacts in the SeaWiFS products. The effect became more noticeable after smoothing of the near-infrared radiance fields—a method under investigation for improving the data quality (e.g., to reduce speckling).

The discontinuity was caused by the transition between the oceanic aerosol model with 90% humidity and other models. This model was removed, leaving the oceanic aerosol model with 99% humidity to handle the very clear, oceanic aerosol conditions. To preserve the 12 model set, the coastal model with 70% humidity was reinstated to the model suite.

3.3.2.2 Epsilon Value Extrapolation

Even with the oceanic aerosol models that extend the coverage to a larger aerosol type range, there were many occasions when this range was exceeded. On these occasions, the ϵ value, which is an indicator of the aerosol type, has a value lower than that of the lowest aerosol model. In the second reprocessing, the ϵ value was used to interpolate between two aerosol models, or in the case of an ϵ value below the lowest model, the value of the lowest model was used (instead of the true value). The result was the removal of more aerosol radiance than if the ϵ value was

extrapolated. The change made for the third reprocessing was to extrapolate the ϵ values for the other bands using an analytical function, so a better aerosol correction could be made.

For test cases in open ocean areas where ϵ value extrapolation would occur, up to 24% of the L_{WN} retrievals benefitted from the extrapolation. No significant changes were observed in the chlorophyll *a* fields, but the 412 nm water-leaving radiances were increased by an average of $0.1\,\mathrm{mW\,cm^{-2}\,\mu m^{-1}\,sr^{-1}}$, an increase of about 6%.

3.3.2.3 Improved Rayleigh Computation

The Rayleigh radiance algorithm, which was used for the second reprocessing, contained no correction for ocean surface roughness. The effect of ocean roughness is negligible at low and moderate solar zenith angles, but becomes significant at solar zenith angles greater than 60°. Without an adjustment for wind roughening, the Rayleigh radiance estimate is too high at large solar zenith angles and greater than zero wind speeds. This results in a reduction of the L_{WN} values and an increase in the occurrence of negative L_{WN} values. Tests of level-2 retrievals with the wind-dependent Rayleigh algorithm showed that negative water-leaving radiances were reduced in the 412 nm band from 80% to 40% at solar zenith angles of 70°, where the problem is most severe. The L_{WN} values at high solar zenith angles also increased significantly. The effects are addressed further in Sect. 3.3.6.2.

3.3.2.4 Pressure Dependent Transmittance

Prior to the third reprocessing, the diffuse transmittance used in the computation of the normalized water-leaving radiance was derived from a look-up table with dependence only on the aerosol model and the viewing geometry. Currently, a pressure correction (through the Rayleigh optical thickness) is also applied to both the sun-to-surface and surface-to-satellite diffuse transmittance (Wang 1999b). The effect on L_{WN} values is small: a large change in the atmospheric pressure of 30 mbar causes about a 1% change in L_{WN} values at 412 nm, while at 865 nm, the change is only 0.05%.

3.3.3 Near-Infrared L_{WN} Value Adjustment

One of the problems noted in the second reprocessing, which was examined closely in preparation for the third reprocessing, was the occurrence of negative water-leaving radiances in the SeaWiFS bands. It was apparent that especially in coastal regions, the water-leaving radiances in the 412 and 443 nm bands were negative for two reasons:

a) High chlorophyll content, which depressed the blue radiances, made water-leaving radiances approximately zero; and

b) Turbid coastal waters confuse the aerosol correction (absorbing aerosols could also be responsible), resulting in the overestimation of aerosol radiance, especially in the blue bands, thereby decreasing the already low radiance value, frequently causing it to become negative.

The negative water-leaving radiances were obviously unrealistic, although radiances approaching zero were common in turbid waters for bands 1 and 2. The negative L_{WN} values made the affected pixels useless for algorithms that rely on the blue bands as input. In the same regions having the negative L_{WN} problem, anomolously high chlorophyll was found, which again indicated that the blue bands were being excessively depressed.

The ocean science community responded to this problem with a number of algorithms to explain the problem and to get better L_{WN} estimates. The solutions fell into two categories:

1. The assumption of zero water-leaving radiance in the near-infrared bands at 765 and 865 nm is wrong in high chlorophyll or turbid waters. The algorithms attempt to use the chlorophyll values to estimate the water-leaving radiances in these bands; the algorithms were contributed by D. Siegel (Siegel et al. 2000), R. Arnone, and R. Stumpf.
2. After the near-infrared contribution is taken into consideration, an assumption can be made about the value of the 412 nm water-leaving radiance so that it and the other L_W values do not become negative (R. Stumpf, pers. comm.).

The most promising combinations of these methods were tested, including the use of band 6 (instead of band 7) with band 8 in the aerosol determination.

The methods were examined in detail for a number of test scenes that were affected by the problem. In addition, the methods were tested in general on two eight-day periods of SeaWiFS GAC data—one in January 1998 and one in July 1998. The results were then compared to the method used in the second reprocessing. Although investigation of the other methods will continue, the Siegel method (Siegel et al. 2000) was chosen for the third reprocessing, because of its simplicity, and because it produced significant decreases in the amount of negative L_{WN} values while lowering coastal chlorophyll values to more reasonable levels.

3.3.4 Other Changes

Several other changes were made in the level-2 and -3 processing in preparation for the third reprocessing. As a result of the level-2 data set format change (Sect. 3.3.5), two new flagging algorithms were added to indicate the presence of absorbing aerosols and *Trichodesmium*. Improvements were made to the chlorophyll, diffuse attenuation, ozone, and whitecap algorithms. A glint correction scheme yielded better atmospheric optical depths and an out-of-band correction permitted better comparison of L_{WN} with *in situ* values.

3.3.4.1 Modified C_a:K Computation

After the second reprocessing was completed, it was discovered that some level-3 binned products had infinite values stored in some bins for the parameter containing the ratio of the chlorophyll *a* concentration values to the diffuse attenuation coefficient at 490 nm, C_a:$K(490)$, hereafter referred to as C_a:K. The problem was introduced because of the new binning policy, which allowed the binning of negative L_{WN} data, combined with some shortcomings in the binning code.

The algorithm for calculating $K(490)$ in the level-2 processing was set to return a zero value for $K(490)$ if the L_{WN} at either 490 or 555 nm was less than zero. When a $K(490)$ value of zero was used in the binner during the calculation of C_a:K, a value of infinity was assigned to that bin. This problem was compounded for products covering longer time periods because once a bin had an infinite value assigned to it, no amount of averaging would lessen or remove it; therefore, eight-day, monthly, and yearly binned products would accumulate more bins with infinite C_a:K values. This problem was fixed in both the $K(490)$ algorithm in the level-2 processing code and in the C_a:K computation in the binner. In the $K(490)$ algorithm, the computation was modified so that zero $K(490)$ values would not be produced.

The following rules were designed to deal with the L_{WN} conditions:

a. If $L_{WN}(490)$ and $L_{WN}(555) > 0$, then compute $K(490)$ normally.

b. If $L_{WN}(490) < 0$, then $K(490) = 6.4\,\mathrm{m}^{-1}$.

c. If $L_{WN}(490) > 0$ and L_{WN} at 555 nm < 0, then $K(490) = 0.016\,\mathrm{m}^{-1}$.

The actions taken for zero L_{WN} values represent the maximum $K(490)$ value that can be stored in the level-2 data set and the lowest possible $K(490)$ value which the algorithm can produce. Tests with SeaWiFS data showed that the default values agreed well with the surrounding $K(490)$ values.

The algorithm for computing C_a:K in the binner was also adjusted to use a $K(490)$ value of $0.016\,\mathrm{m}^{-1}$ in the calculation if a value of zero was encountered. In addition, a modification was made in the masking conditions in the event of an atmospheric failure so that fewer high $K(490)$ values, erroneously derived over open ocean areas, would be binned. If the L_W value for any of the 490, 510, or 555 nm bands are less than zero, the atmospheric warning flag is set in the level-2 file and applied as a mask in the level-3 binning.

3.3.4.2 Changes to Whitecap Correction

For the third reprocessing, three changes were made in the whitecap correction. The first change was to use a correction with a spectral dependence (Frouin et al. 1996). The second change was to increase the strength of the correction by approximately 65% from the values used in the second reprocessing. The third change was to limit the whitecap correction for wind speeds above $8\,\mathrm{m\,s}^{-1}$ to the value found at $8\,\mathrm{m\,s}^{-1}$. This limit was set to avoid overcorrections for whitecaps. This strategy incorporated more recent information on whitecaps (Moore et al. 2000), but avoided overcorrection at high wind speeds.

The effects on the radiances were small, but noticeable. No significant changes were observed for areas with wind speeds less than $10\,\mathrm{m\,s}^{-1}$. For areas with wind speeds from 10–15 $\mathrm{m\,s}^{-1}$, the occurrence of negative water-leaving radiances at 412 nm was reduced by 3%; and for wind speeds above $15\,\mathrm{m\,s}^{-1}$, negative L_{WN} values at 412 nm were reduced by 10%.

3.3.4.3 Sun Glint Correction

The SeaWiFS Project found that the aerosol optical thickness was noticably higher for areas surrounding the subsolar point. The atmospheric correction was accounting for glint outside the glint mask as additional aerosol radiance. This did not noticably affect the L_{WN} and chlorophyll *a* retrievals, but it inflated the aerosol optical thickness, thereby making it less useful.

The level-2 processing program already calculated an estimate of the glint radiance, so the program was changed to remove the glint radiance outside the glint mask as a part of the processing. The glint removal was made more robust by performing a second iteration with a better value of the aerosol optical thickness. Details of the glint correction are presented in Wang and Bailey (2000).

3.3.4.4 Ozone Data Interpolation

In previous reprocessings, TOMS ozone values (the primary SeaWiFS ozone source) were interpolated to the time of the SeaWiFS data pass assuming that the TOMS data were all taken at 12:00 UTC. In fact, the TOMS data were collected over the daylight side of the Earth from east to west with a phasing very close to SeaWiFS (the data were taken almost at the same time). The ancillary data selection and interpolation routines in the level-2 processing were modified to use this information to calculate ozone fields, which would be more representative of the actual conditions at the time of the pass (Ainsworth and Patt 2000). The effect is the smallest around 12:00 UTC, which is near the prime meridian, and the greatest around 0:00 UTC near ±180° longitude.

3.3.4.5 Improved K(490) Algorithm

An improved $K(490)$ algorithm (Mueller 2000) was implemented for the third reprocessing. The previous algorithm used $L_W(443)$ and had errors in regions of highly turbid water and in bloom situations where $L_W(443)$ can be underestimated. The new algorithm estimates $K(490)$ by using the ratio of $L_{WN}(490)$:$L_{WN}(555)$.

3.3.4.6 Absorbing Aerosol Flag

In many oceanic regions, and especially off the west coast of Africa, absorbing aerosols (suspended dust) are not handled by the aerosol determination algorithm. Currently, the suite of aerosol models do not contain absorbing aerosol models. For the third reprocessing, an algorithm was implemented to detect significant amounts of absorbing aerosols (Hsu et al. 2000). A new level-2 flag was made to indicate measurements in regions of excessive absorbing aerosols. This flag is used to exclude data during the level-3 binning phase.

3.3.4.7 Trichodesmium *Flag*

An algorithm was implemented in the third reprocessing that detects the presence of *Trichodesmium* bloom conditions (Subramaniam et al. 2000). The existence of a bloom is indicated by one of the new level-2 flags, which currently is not used for any level-3 exclusion.

3.3.4.8 Improved Chlorophyll a *Algorithm*

The chlorophyll *a* algorithm used for the third reprocessing, the so-called ocean chlorophyll 4 (OC4) algorithm (O'Reilly et al. 1998), was used in place of the ocean chlorophyll 2 (OC2) algorithm (second reprocessing). A larger *in situ* data set was used to refine the OC4 algorithm (O'Reilly et al. 2000), and it also has the property of not reporting negative chlorophyll *a* values as the previous OC2 algorithm did. The range of chlorophyll in the output is expanded at the low end to include values from 0–0.009 mg m^{-3} in steps of 0.001. Previously, the lowest reported chlorophyll value was 0.01 mg m^{-3}. In general, the new algorithm was found to slightly reduce the chlorophyll *a* values in the range from 0.01–0.05 mg m^{-3}.

3.3.4.9 Out-of-Band Correction

The eight SeaWiFS bands have broad response functions compared to most instruments that measure L_W in the field. Although the processing for SeaWiFS water-leaving radiances includes the out-of-band response, the resulting L_W values retain the initial broad response function. For the third reprocessing, an out-of-band correction was applied to the L_W values as the default (Wang et al. 2000). The correction has the greatest effect at 555 nm in low chlorophyll concentrations (high blue radiances), where the corrected L_{WN} values can be 5–10% lower than the uncorrected values. The use of the out-of-band correction slightly decreased the chlorophyll values by about 15% in the range from 0.01–0.05 mg m^{-3}.

3.3.4.10 Navigation Improvements

Improvements were made to the navigation algorithms in the level-0 to -1A software to reduce the seasonal variations in geolocation accuracy and to handle operational changes in the available navigation data from the satellite.

3.3.4.11 Improved Coastal Data Inclusion

Some instances were observed when the radiance at 412 nm—after being corrected for Rayleigh, glint, ozone, and whitecaps—was negative for otherwise clear regions. This condition occurred infrequently along coastal areas, but affected significant regions in any one single data pass. The atmospheric failure masking used in the second reprocessing used this test to exclude observations that had these conditions in any of the eight SeaWiFS bands. In the third reprocessing, this exclusion was removed for the 412 nm band so more coastal areas could be processed. This change was observed to increase the number of retrievels at many coastal regions for approximately one out of every four passes.

3.3.5 Major Product and Flag Changes

Since the SeaWiFS launch, the Project has been creating the same suite of products and flags (McClain et al. 1995 and McClain 2000). With the third reprocessing, the Project took the opportunity to revise the product suite and to expand the flag set to respond to new demands.

3.3.5.1 Product Suite Changes

Table 5 shows the operational product suite used in the third reprocessing and the product names used in SeaDAS. The Coastal Zone Color Scanner (CZCS) pigment product (`CZCS_pigment`) was removed because there was little demand for it, and because a simple equation can be used to derive the pigment from the chlorophyll *a* product. In addition, the two products of the aerosol radiance at 670 nm and at 865 nm (`La_670` and `La_865`, respectively) were removed in favor of the normalized water-leaving radiance at 670 nm (`nLw_670`). The Ångström coefficient at 510 nm (`angstrom_510`), was included because many researchers use the Ångström coefficient to characterize the aerosol type.

Table 5. Operational products for the third reprocessing.

Product Name	*Description*
`nLw_412`	L_{WN} values at 412 nm
`nLw_443`	L_{WN} values at 443 nm
`nLw_490`	L_{WN} values at 490 nm
`nLw_510`	L_{WN} values at 510 nm
`nLw_555`	L_{WN} values at 555 nm
`nLw_670`	L_{WN} values at 670 nm
`angstrom_510`	Ångström coefficient at 510 and 865 nm
`chlor_a`	Chlorophyll *a* concentration
`K_490`	Diffuse attenuation coefficient at 490 nm
`eps_78`	Epsilon at 765 and 865 nm
`tau_865`	Aerosol optical thickness at in 865 nm

Table 6. Flags for the third reprocessing. The "Flag Name" column denotes the flag names as of the third reprocessing, whereas the "Old Name" column is the flag name used in the second reprocessing. The "Mask In" columns indicate that no geophysical data is created in the level-2 (L2) or level-3 (L3) data set if the flag conditions marked "Y" exist for that observation.

Flag Number	*Flag Name*	*Mask In L2*	*Mask In L3*	*Old Name*	*Description*
1	ATMFAIL	Y	Y	EPSILON1	Atmospheric algorithm failure
2	LAND	Y	Y	LAND1	Land
3	BADANC			ANCIL1	Missing ancillary data
4	HIGLINT	Y	Y	SUNGLINT1	Sun glint contamination
5	HILT	Y	Y	HIGHLT1	Total radiance above the knee in any band
6	HISATZEN		Y	SATZEN1	Satellite zenith angle above the limit
7	COASTZ			COASTZ1	Shallow water
8	NEGLW			NEGLW1	Negative water-leaving radiance in any band
9	STRAYLIGHT		Y	STRAYLIGHT1	Stray light contamination
10	CLDICE	Y	Y	CLDICE1	Clouds or ice
11	COCCOLITH		Y	COCCOLITH1	Coccolithophore bloom
12	TURBIDW		Y	TURBIDW1	Turbid (Case-2) water
13	HISOLZEN		Y	SOLZEN1	Solar zenith angle above the limit
14	HITAU			HIGHTAU1	High aerosol concentration
15	LOWLW		Y	LOWLW1	Low water-leaving radiance at 555 nm
16	CHLFAIL	†	Y	CHLOR1	Chlorophyll not calculable
17	NAVWARN		Y		Questionable navigation (tilt change)
18	ABSAER		Y		Absorbing aerosol index above the threshold
19	TRICHO				*Trichodesmium* bloom condition
20	MAXAERITER		Y		Maximum number of iterations in the NIR algorithm
21	MODGLINT				Glint corrected measurement
22	CHLWARN				Chlorophyll is out of range
23	ATMWARN		Y		Epsilon value is outside the reasonable range or L_W in 510, at 490, or 555 nm is less than zero
24	DARKPIXEL				Rayleigh corrected radiance is less than zero for any band

† The chlorophyll value is not computed, but *first guess* L_{WN} values are computed.

Similar changes were made in the level-3 binned products. In place of the La_670 and CZCS_pigment products are the nLw_670 and angstrom_510 products.

3.3.5.2 Flag Changes

For previous reprocessings, the suite of flags was limited to 16 by the format of the level-2 data set. In the third reprocessing, the available room for flags was expanded to 32, of which only 24 flags are currently defined. Table 6 lists these flags and their status as masks in excluding data in the level-2 and -3 operational products.

The original 16 flags have much the same meaning as before with some exceptions. In the second reprocessing, the atmospheric algorithm failure flag (EPSILON1) included many conditions that prevented the calculation of the aerosol radiances and, thus, the L_{WN} values. It also indicated times when the ϵ value was outside reasonable limits defined by the standard aerosol models; hence, the name EPSILON1. Now, the atmospheric algorithm failure flag (renamed to ATMFAIL), only indicates conditions where L_{WN} values could not be calculated. The new ATMWARN flag indicates when the ϵ value is outside the reasonable range, but L_{WN} values could be calculated. It also indicates observations where L_W values in the 490, 510, and 555 nm bands are negative. A serious problem condition, when the Rayleigh corrected radiances are negative, is indicated in the new DARKPIXEL flag so that this condition can be monitored more easily.

In the second reprocessing, the chlorophyll algorithm failure flag (CHLOR1) indicated two problems: a) chlorophyll could not be computed, and b) chlorophyll exceeded the high threshold. Now, the CHLFAIL flag only indicates when chlorophyll can not be calculated, because the input L_{WN} values are less than zero, or when the calculated chlorophyll is outside physical limits (greater than 640 mg m^{-3}). The new CHLWARN flag signals chlorophyll values which exceed the high value that can be stored in the product (greater than 64 mg m^{-3}), or very small values (less than 0.01 mg m^{-3}).

The remaining six new flags address new conditions or are used to more consistently handle current conditions.

Table 7. Average chlorophyll in the Chesapeake Bay derived from *in situ* measurements (SeaWiFS second and third data reprocessings). The mean chlorophyll *a* values ($\bar{C}_a$) are in milligrams per cubic meter ($\mathrm{mg\,m^{-3}}$). The standard deviation (σ) and number of observations are also given.

Date	*In Situ*			*Second Reprocessing*			*Third Reprocessing*		
	$\bar{C}_a$	σ	*Obs.*	$\bar{C}_a$	σ	*Obs.*	$\bar{C}_a$	σ	*Obs.*
11–19 April 1998	11.93	11.31	91	42.64	18.42	1755	16.01	7.96	1960
4–12 August 1998	10.83	10.61	89	25.93	13.93	1804	11.06	3.71	1810
19–23 October 1998	7.43	4.08	67	16.85	9.76	1815	7.96	2.97	2133

The `NAVWARN` flag is used primarily to indicate where less reliable navigation is expected, such as when the instrument tilt is changing. The level-3 binning can use the `NAVWARN` flag to decide on binning instead of having to use the tilt indicator in the level-2 data. `The ABSAER` and `TRICHO` flags indicate the existence of absorbing aerosols and *Trichodesmium* blooms detected by new algorithms, respectively. The `MAXAERITER` flag indicates when the near-infrared (NIR) correction algorithm (Sect. 3.3.3) has been unable to converge on a NIR L_{WN} estimate. Finally, the `MODGLINT` flag indicates pixels where the glint correction was applied.

3.3.6 Third Reprocessing Analysis

The software for the third reprocessing was updated with all the changes mentioned in Sects. 3.3.1–3.3.5. The vicarious calibration for bands 1–7 was performed with the new algorithms. The new algorithms and the new calibration were used to process two eight-day periods: 17–24 January 1998 and 12–19 July 1998. The results of these runs, in comparison to the second reprocessing runs, is discussed next.

3.3.6.1 Chlorophyll a

Figure 7 is a plot of the global distribution of chlorophyll *a* concentration for the January and July periods. The inclusion of binned chlorophyll in the 0–0.009 $\mathrm{mg\,m^{-3}}$ range for the third reprocessing can be seen, as can the artificial accumulation of values, at 0.01 $\mathrm{mg\,m^{-3}}$, for the second reprocessing. The third reprocessing produced a greater number of chlorophyll values in the 0–0.04 $\mathrm{mg\,m^{-3}}$ range than the second reprocessing, which indicates that the chlorophyll values in this range are reduced. For a test area in the Pacific located in one of the lowest chlorophyll areas in the data, around (135°E,12°N), the average chlorophyll value dropped from 0.057–0.0381 $\mathrm{mg\,m^{-3}}$, a 34% decrease. In the chlorophyll range above 0.07 $\mathrm{mg\,m^{-3}}$, the third reprocessing increased the chlorophyll values. The magnitude of the changes in July period are less, but still follow the same trend.

Figure 8 shows the change that occurred in chlorophyll *a* concentration more clearly for the intermediate and high values of chlorophyll, and it summarizes a scatterplot comparing binned chlorophyll from the third reprocessing versus the second reprocessing. For a number of chlorophyll ranges in the second reprocessing, the statistics are plotted with the matching third reprocessing chlorophyll values. In the 0.2–1.0 $\mathrm{mg\,m^{-3}}$ range, the third reprocessing shows a slight increase in the chlorophyll value of about 10%, as was seen in the histograms (Fig. 7). For chlorophyll values greater than 2 $\mathrm{mg\,m^{-3}}$, the third reprocessing significantly lowered the chlorophyll value. In the 5–10 $\mathrm{mg\,m^{-3}}$ range, the third reprocessing lowered the chlorophyll values by about 40%, and lowers it even more for higher values. This lowering of high chlorophyll is primarily due to the Siegel NIR algorithm (Siegel et al. 2000) and greatly reduces chlorophyll values in all the coastal and upwelling regions.

To illustrate how the third reprocessing improves chlorophyll *a* retrievals in coastal waters, SeaWiFS chlorophyll values were compared with *in situ* pigment data from the Chesapeake Bay. Three time periods in 1998 were selected for this analysis: 11–19 April, 4–12 August, and 19–23 October. For each time period, HRPT data were processed to level-2 chlorophyll using both the second and third reprocessings and methodologies, and were then space- and time-binned. *In situ* data (originally provided by L. Harding, University of Maryland), were obtained from SeaBASS (see Sect. 7.1.1 for an overview of SeaBASS). Only the lower Chesapeake Bay, south of 38.5°N latitude, was considered in the analysis.

For all three time periods, the mean SeaWiFS-retrieved chlorophyll value exceeds that of the mean *in situ* value. The third reprocessing values, however, are 62.5, 57.3, and 52.8% lower than the second reprocessing values, for April, August, and October, respectively (Table 7). Additionally, the ratio of mean SeaWiFS-to-mean *in situ* chlorophyll values is reduced from 3.57–1.34 for April, 2.39–1.02 for August, and 2.27–1.07 for October. Results from these comparisons (especially the latter) indicate that the methodology for the third reprocessing significantly improves SeaWiFS chlorophyll *a* retrievals in coastal regions. The number of successful chlorophyll retrievals also increased by more than 10% for two of the three time periods.

3.3.6.2 Negative L_{WN} Values

The use of the Siegel NIR algorithm (Siegel et al. 2000) and the wind speed correction to the Rayleigh radiance algorithm (Sect. 3.3.2.3) significantly helped reduce the number of negative L_{WN} values globally. In the January time

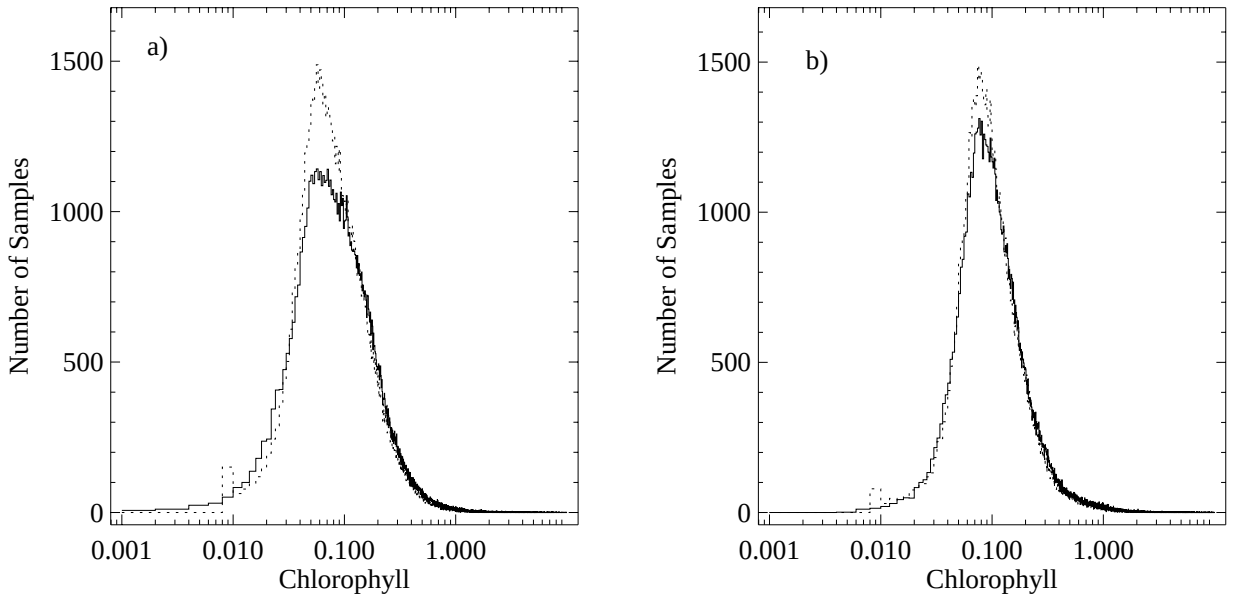

Fig. 7. The SeaWiFS level-3 global chlorophyll *a* frequency distribution for the eight day period of: **a)** 17–24 January 1998, and **b)** 12–19 July 1998, made with the second reprocessing (dotted curve) and the third reprocessing (solid curve).

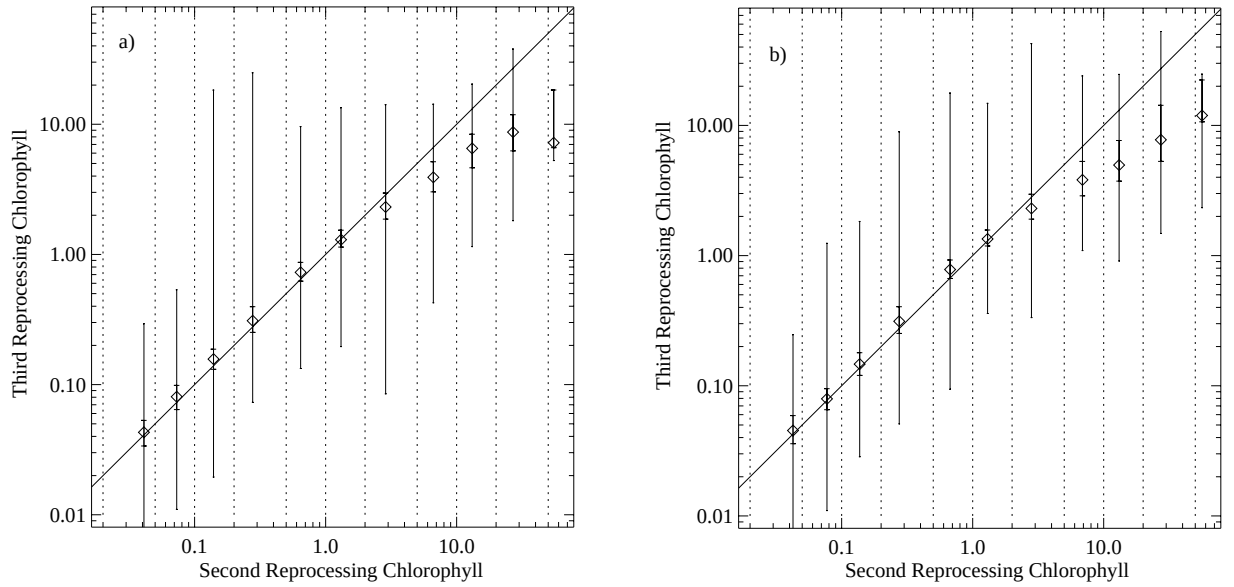

Fig. 8. Comparison of the chlorophyll retrieved in the third reprocessing (y-axis) to that retrieved in the second reprocessing (x-axis) for: **a)** 17–24 January 1998, and **b)** 12–19 July 1998. For level-3 binned chlorophyll *a* concentration from the second reprocessing in 11 ranges from 0.02–64.0 $\mathrm{mg\,m^{-3}}$, the median third reprocessing chlorophyll value is plotted as diamonds. The nearest set of bars is the range of data in the second-to-third quartiles, while the outer bars show the extreme range of the third reprocessing chlorophyll values. Chlorophyll values greater than 2 $\mathrm{mg\,m^{-3}}$ were significantly reduced in the third reprocessing.

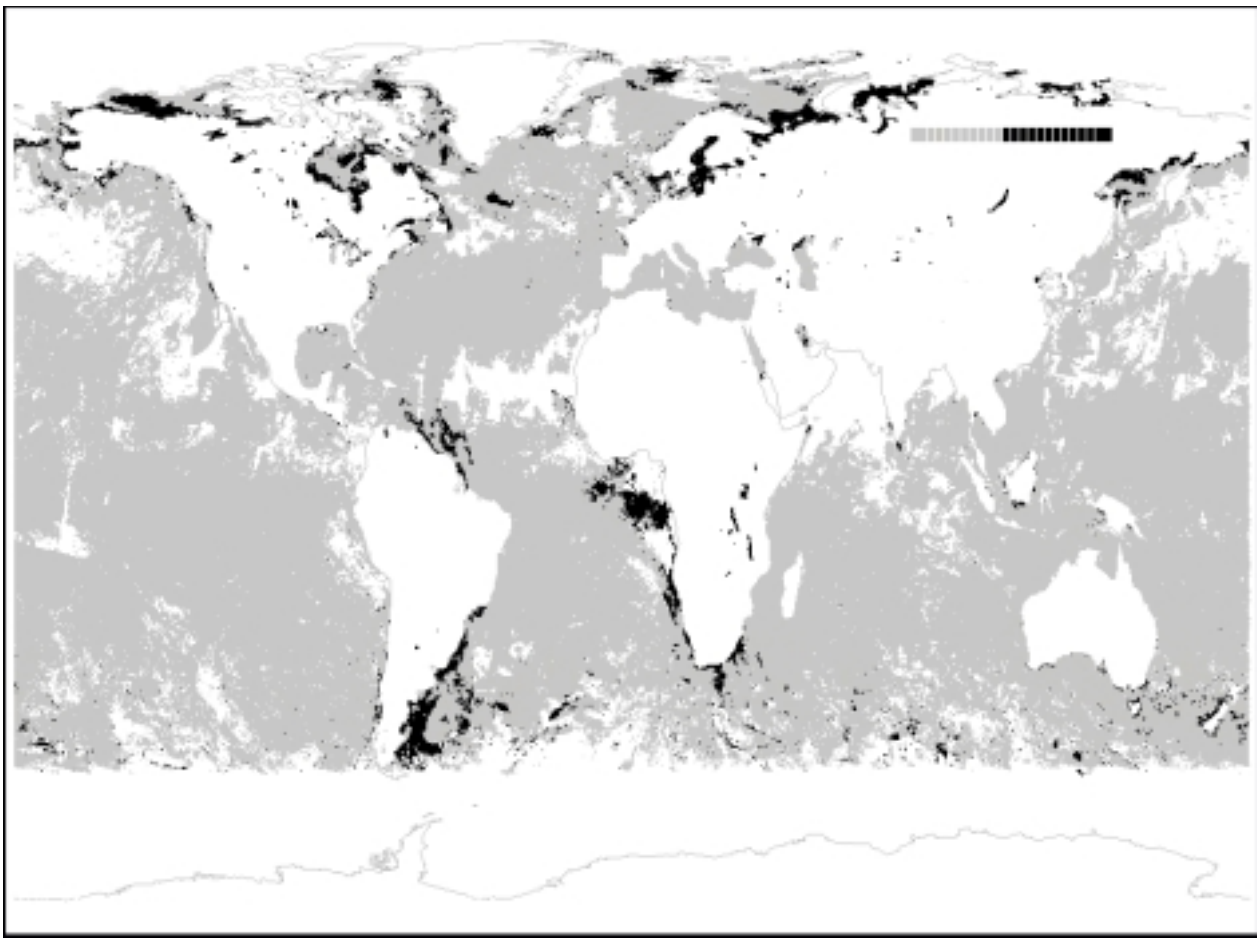

Fig. 9. The percent occurrence of negative L_{WN} values at 412 nm for the eight-day period from 12–19 July 1998. This image was generated using the third reprocessing algorithms and used data excluded by the standard level-2 processing: atmospheric correction algorithm failure, land, sun glint, high total radiance, and clouds. In addition, stray light pixels were excluded. White areas indicate no data—continental land masses make up a great part of this region—while light gray indicates data present with occurrences of negative L_{WN} values of less than 50%. The black regions all have more than 50% occurrence of negative L_{WN} values, indicating areas that were severely affected by negative L_{WN} values. In regions where the solar zenith angle is high, such as the Southern Ocean and along the coast, the amount of negative L_{WN} values were reduced relative to the second reprocessing (Fig. 6).

period, the number of negative L_{WN} values in the binned data for the 412 nm band was reduced from 2.5–2.1% of the total, while in the July time period, the reduction was from 5.2–4.7%. Figure 9 shows the geographical regions, in the July time period, wherein the percentage of negative L_{WN} values are higher than 50% for the third reprocessing. Compared with the same display for the second reprocessing (Fig. 6), the reduction in negative L_{WN} values at high solar zenith angles, and especially in the Southern Ocean, is dramatic. The improved performance of the atmospheric correction with the wind-dependent Rayleigh radiances is the main reason why the solar zenith limit for useful data was increased from 70–75°. Slight reductions can also be seen in the occurrence of negative L_{WN} values along coastal areas.

When the wind speed correction to the Rayleigh radiances is made, the amount of negative L_{WN} values is reduced. This effect is illustrated in Fig. 10, which shows the percentage of negative L_{WN} as a function of solar zenith angle for the 412, 490, and 555 nm SeaWiFS bands in the July time period (the other bands and the January time period show similar behavior). In the 412 nm band, at solar zenith angles from 65–70°, the percentage of measurements with negative L_{WN} values dropped from 60% to 20%, with similar decreases in the other bands.

Figure 11 shows the mean of the L_{WN} values as a function of solar zenith angle for the same SeaWiFS bands in the July time period. The decrease in the mean L_{WN} values, which begins at solar zenith angles of about 60°, could lower the L_{WN} values in the 412 nm band to less than

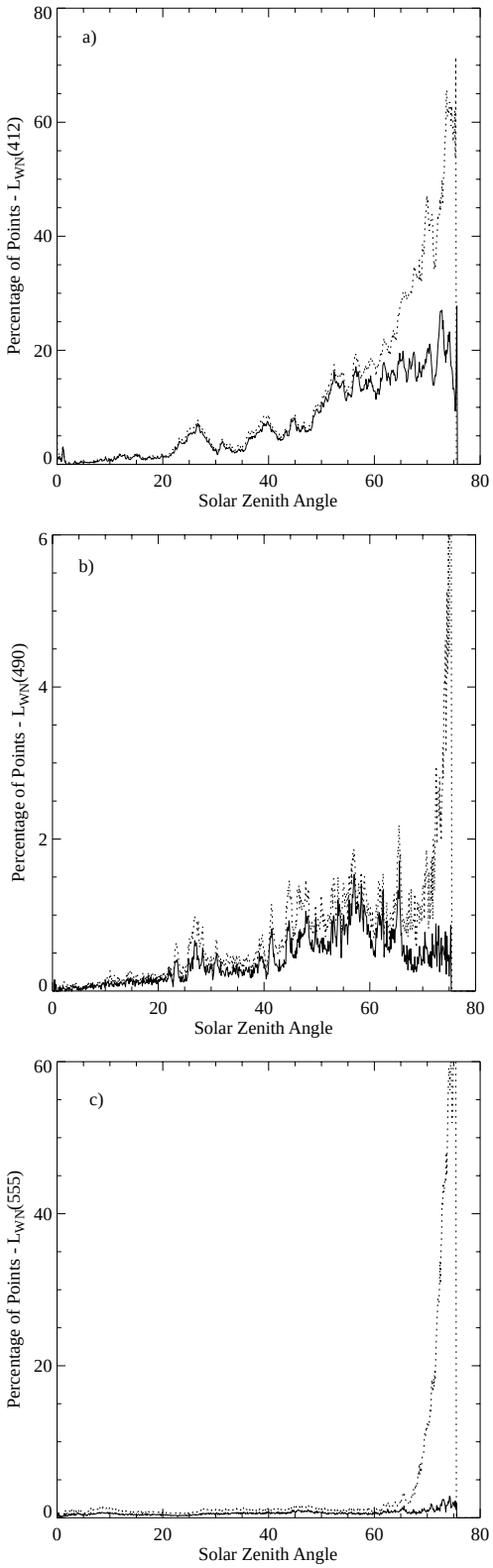

Fig. 10. The percentage of negative L_{WN} values as a function of the solar zenith angle for the eight-day period of 12–19 July 1998 for the second (dotted curves) and third (solid curves) reprocessings. The SeaWiFS bands at **a)** 412, **b)** 490, and **c)** 555 nm are shown.

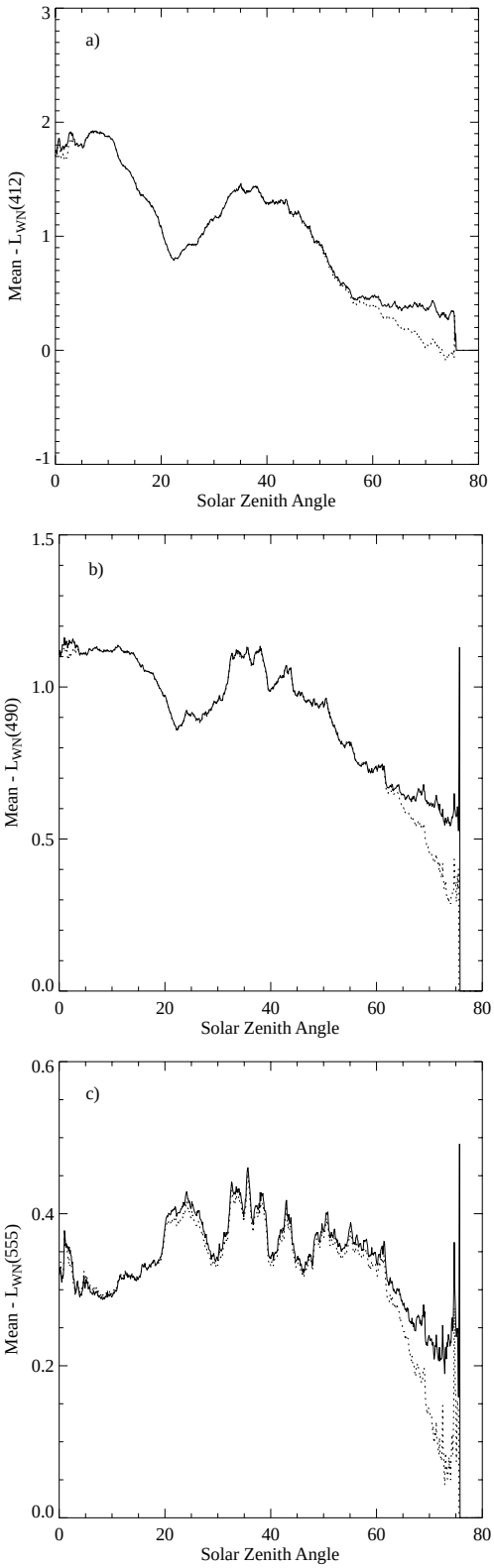

Fig. 11. Mean L_{WN} values as a function of solar zenith angle for the eight-day period of 12–19 July 1998 for the second (dotted curves) and third (solid curves) reprocessings. The SeaWiFS bands at **a)** 412, **b)** 490, and **c)** 555 nm are shown.

zero in the second reprocessing (Fig. 11a). In addition, the 555 nm band average (Fig. 11c) dropped below 0.15, which is a masking threshold for removing data contaminated by cloud shadows. The third reprocessing significantly increased these means at high solar zenith angles and greatly reduced the aforementioned problems in both the 412 and 555 nm bands, as well as yielding increased L_{WN} values in the other bands and restoring a more constant value of L_{WN} in the green bands (i.e., 510 and 555 nm).

In general, the number of level-3 bins filled in the eight-day time bins of the third reprocessing increased over those in the second reprocessing by 1.2% and 2.4% for the January and July test periods, respectively. This corresponds to an increase of 1.8×10^6 and 3.8×10^6 km^2 in ocean coverage for the same respective time periods. Much of this increase is due to the improved, wind-dependent Rayleigh radiance algorithm, and the opening of the solar zenith angle cutoff for binning from 70–75°.

More results of the quality of the SeaWiFS L_{WN} values and derived chlorophyll *a* concentrations can be found in Bailey et al. (2000). These comparisons show marked improvement in the L_{WN} and chlorophyll values compared to *in situ* measurements.

3.4 CONCLUSIONS

The second reprocessing repaired many large problems and brought about favorable changes in both the chlorophyll and L_{WN} distributions. The changes increased very low chlorophyll values in open-ocean regions, and decreased the values of high chlorophyll values greater than 1.0 mg m^{-3} and in many cases, allowed more chlorophyll retrievals to be made and binned in the level-3 data. L_{WN} values generally increased, although the prevalence of negative L_{WN} was recognized as a major problem remaining. Negative L_{WN} values were found to be most prevalent in bands 1 and 2, at higher solar zenith angles, and around coastal areas where turbid, high chlorophyll concentrations exist.

The third reprocessing increased the usefulness of SeaWiFS data in both oceanic and atmospheric applications. The negative L_{WN} problem, which was recognized and characterized in the second reprocessing, was addressed and significantly reduced in the third reprocessing through the use of a) a correction of the NIR L_{WN} values, and b) a wind-dependent correction to the Rayleigh radiance calculation. Abnormally high coastal chlorophyll *a* concentrations were decreased, and data at higher solar zenith angles were retrieved, as a result of these improvements. A chlorophyll algorithm that benefits from an increased observation set improved the retrieval of chlorophyll from the L_{WN} data. These and many other changes combined to improve the agreement between SeaWiFS L_{WN}, chlorophyll, and aerosol optical thickness with corresponding *in situ* observations.

In summary, the changes made for the second and third reprocessings have been wide ranging and have had a positive influence on all of the SeaWiFS products. Even so, there are many more possible improvements in future reprocessings that will be explored. The occurrence of negative L_{WN} values, although reduced, is still a problem in the coastal regions. More work is planned to improve the NIR methods and possibly will include absorbing aerosols in the aerosol model suite. Work is under way to improve the cloud detection and masking algorithm. Other algorithms will be examined and improved, such as the algorithm for the turbid water flag.

Chapter 4

SeaWiFS Global Clear-Water Analysis

Robert E. Eplee, Jr.
SAIC General Sciences Corporation
Beltsville, Maryland

Charles R. McClain
NASA Goddard Space Flight Center
Greenbelt, Maryland

Abstract

The SeaWiFS CVT made a comparison of global clear-water radiances retrieved by SeaWiFS with normalized water-leaving radiances measured by MOBY as a check on the accuracy and stability of the vicarious calibration of SeaWiFS. The procedures and results of this comparison are described in this chapter.

4.1 INTRODUCTION

The SeaWiFS CVT performed a vicarious calibration of SeaWiFS (Eplee and McClain 2000a) using data from MOBY (Clark et al. 1997), deployed off of Lanai, Hawaii. As a check on the accuracy and stability of the vicarious calibration, the CVT made a comparison of global clear-water radiances, retrieved by SeaWiFS, with normalized water-leaving radiances (L_{WN}) measured by MOBY. For the purposes of this analysis, deep-water radiances are defined to be normalized water-leaving radiances (Gordon and Clark 1981) collected from ocean areas having a minimum depth of 1 km, while clear-water radiances are deep-water radiances collected from ocean areas with a maximum chlorophyll a concentration of $0.15\,\mathrm{mg\,m^{-3}}$. Radiances measured by MOBY met the clear-water criteria.

4.2 CLEAR-WATER ANALYSIS

The CVT computed global mean clear-water radiances for bands 1–6 from the time series of eight-day composite SeaWiFS images produced by the Project using the calibration table and vicarious gains implemented for the third reprocessing. In this analysis, 124 eight-day composites were used in the analysis, spanning a time range of 15 September 1997 through 24 May 2000.

As is discussed in Eplee and McClain (2000a), problems with the surface irradiance (E_s) measurements for MOBY require the computation of L_{WN} for MOBY from measurements of water-leaving radiance (L_W), using the solar zenith angle and the atmospheric diffuse transmittance. Because the clear-water analysis requires the determination of L_{WN} at MOBY for clear-sky conditions, the CVT used the mean L_{WN} determined for MOBY during the vicarious calibration as the comparison for the SeaWiFS clear-water radiances.

The comparison of the two sets of radiances is shown in Table 8. The SeaWiFS clear-water radiances are slightly higher than the MOBY radiances because MOBY is located in water containing a marginally higher chlorophyll a concentration than that found for the global clear-water means. The SeaWiFS global clear-water radiances agree with the MOBY measurements of L_{WN}, verifying the validity of the vicarious calibration of SeaWiFS. The apparent difference between SeaWiFS and MOBY in band 6 (670 nm) occurs because radiance values near zero make the characterization of the vicarious gain difficult for this band (Eplee and McClain 2000a). For comparison, the nominal clear-water L_{WN} for the CZCS 520 and 550 nm bands are 0.495 and $0.280\,\mathrm{mW\,cm^{-2}\,\mu m^{-1}\,sr^{-1}}$, respectively (Gordon and Clark 1981).

Table 8. Clear-water radiance comparison between the MOBY vicarious radiances (in units of mW $\mathrm{cm^{-2}\,sr^{-1}\,\mu m^{-1}}$) and the SeaWiFS clear-water radiances. The values shown are the arithmetic means.

λ [nm]	*MOBY Vicarious Radiance*	*SeaWiFS Clear-Water Radiance*
412	1.83536	1.95934
443	1.61899	1.75631
490	1.11291	1.17869
510	0.651690	0.697108
555	0.271239	0.296487
670	0.0147519	0.0348858

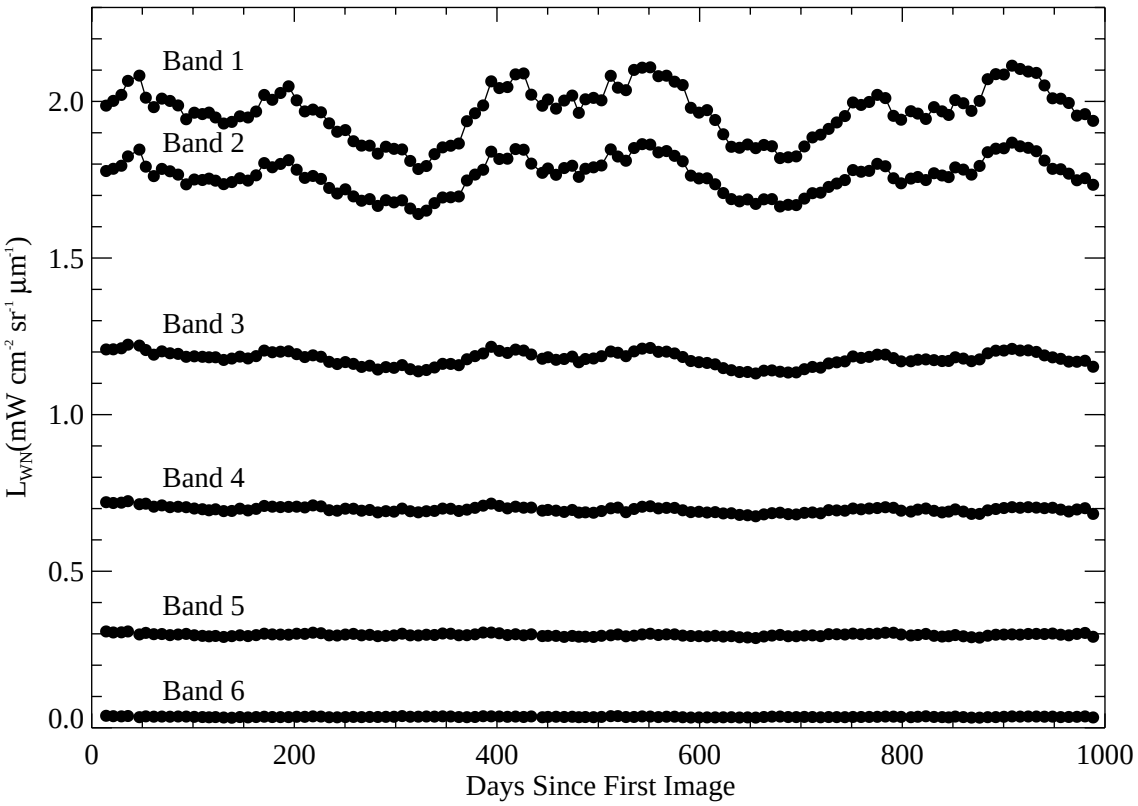

Fig. 12. The mean clear-water radiances retrieved by SeaWiFS.

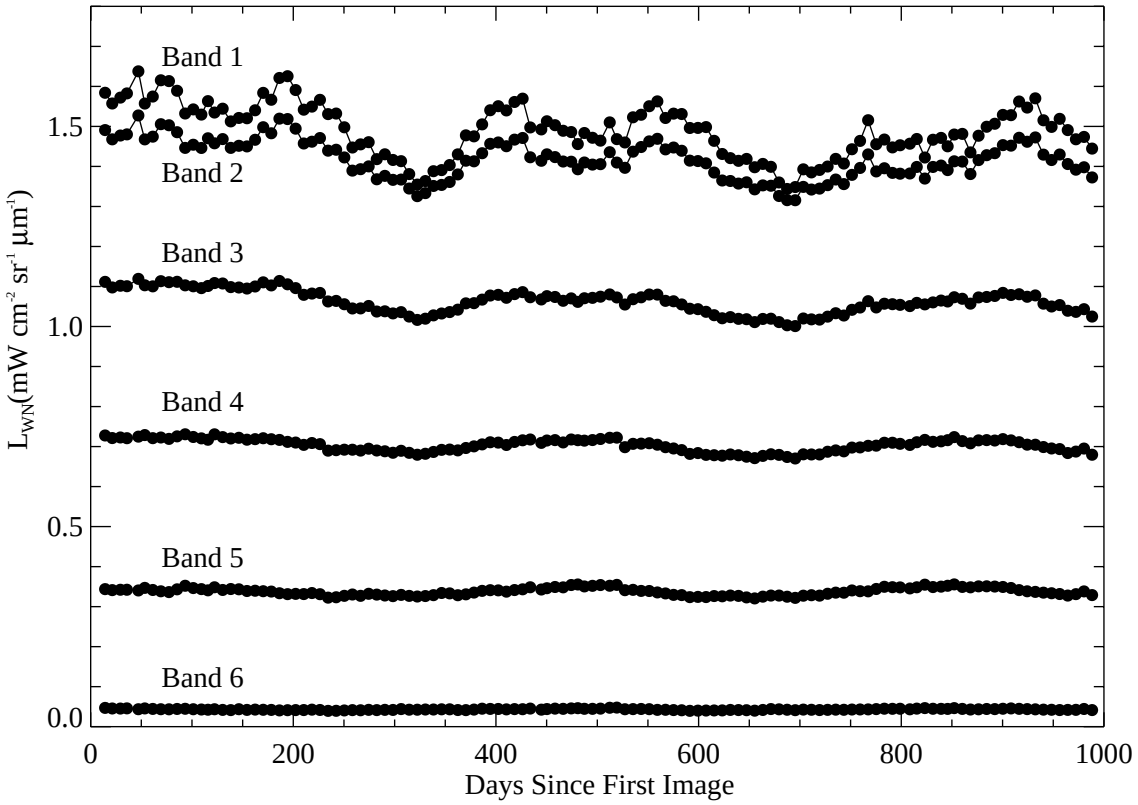

Fig. 13. The mean chlorophyll *a* concentrations retrieved by SeaWiFS.

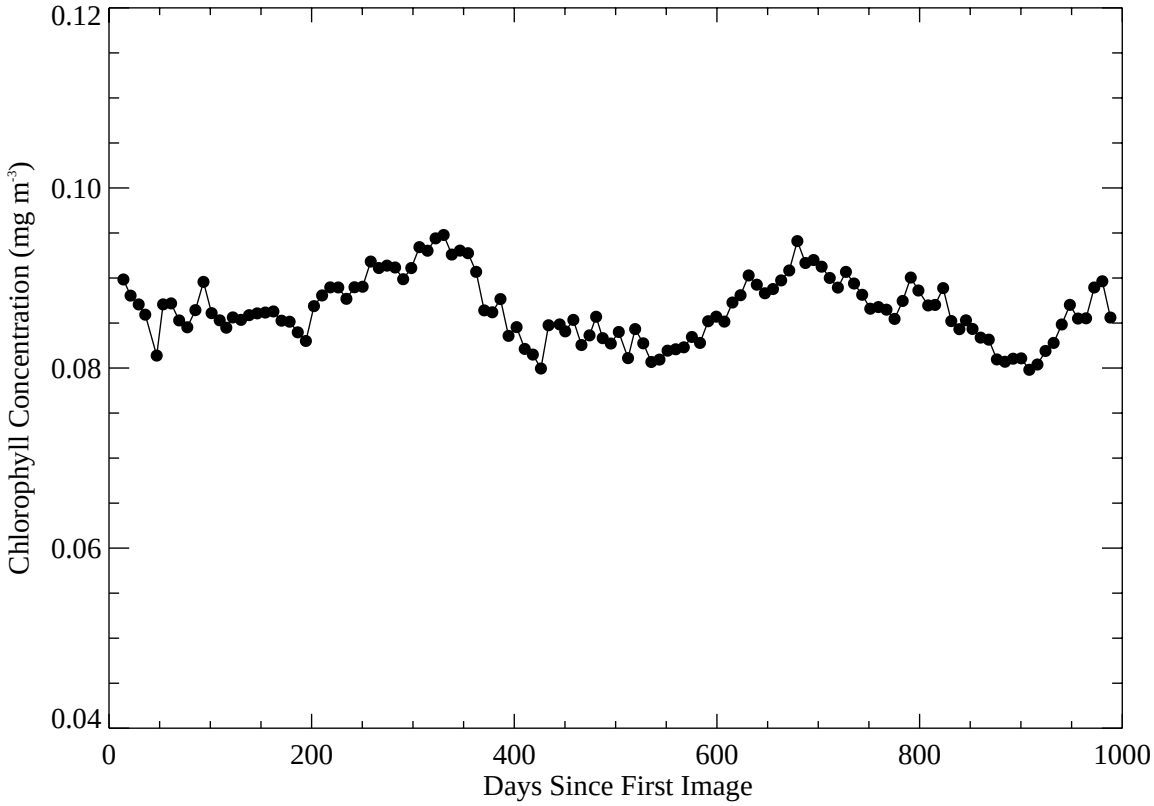

Fig. 14. The mean clear-water chlorophyll concentrations retrieved by SeaWiFS.

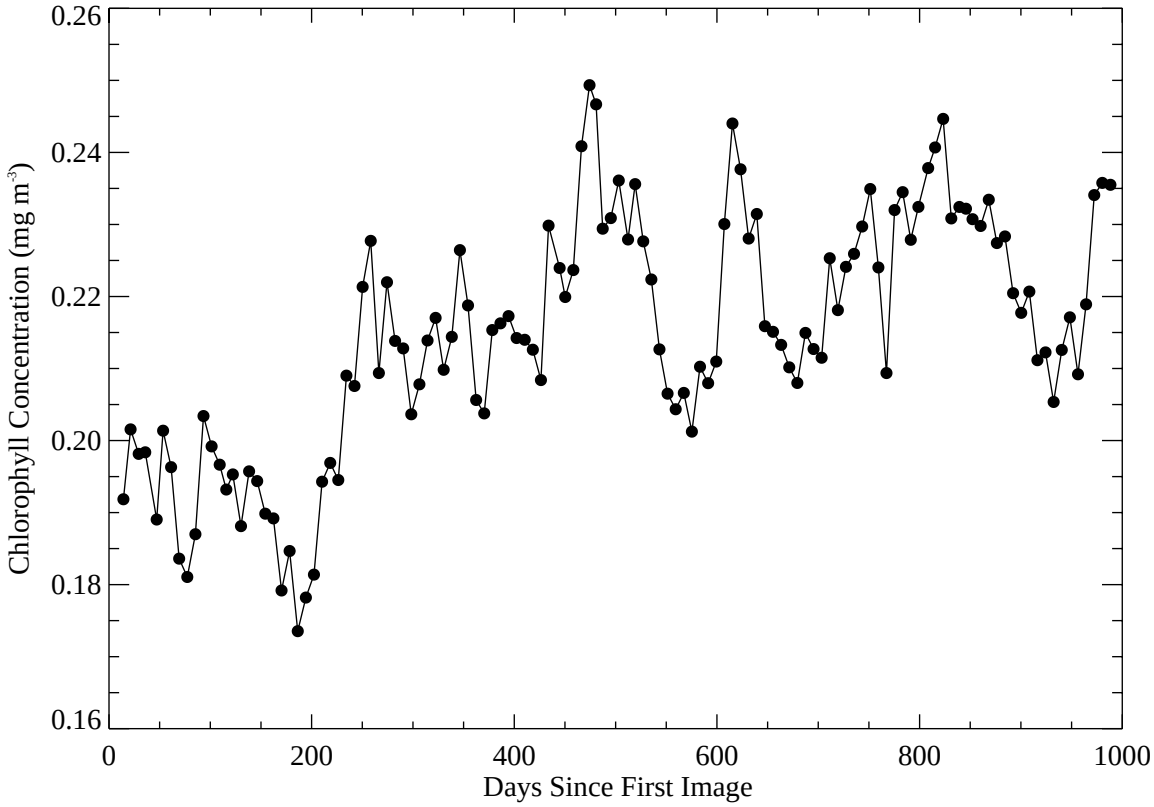

Fig. 15. The mean deep-water chlorophyll *a* concentrations retreived by SeaWiFS.

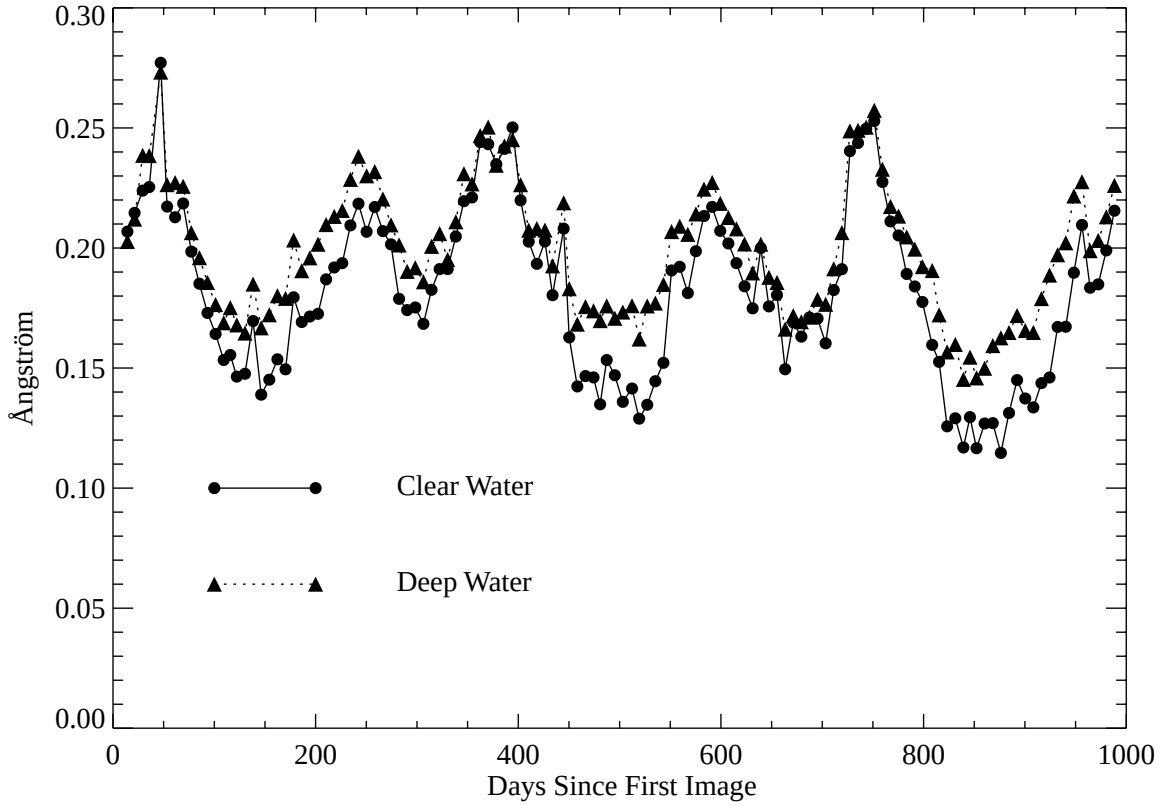

Fig. 16. Epsilon values at 765 and 865 nm [$\epsilon(765, 865)$, the atmospheric correction parameter] retrieved by SeaWiFS.

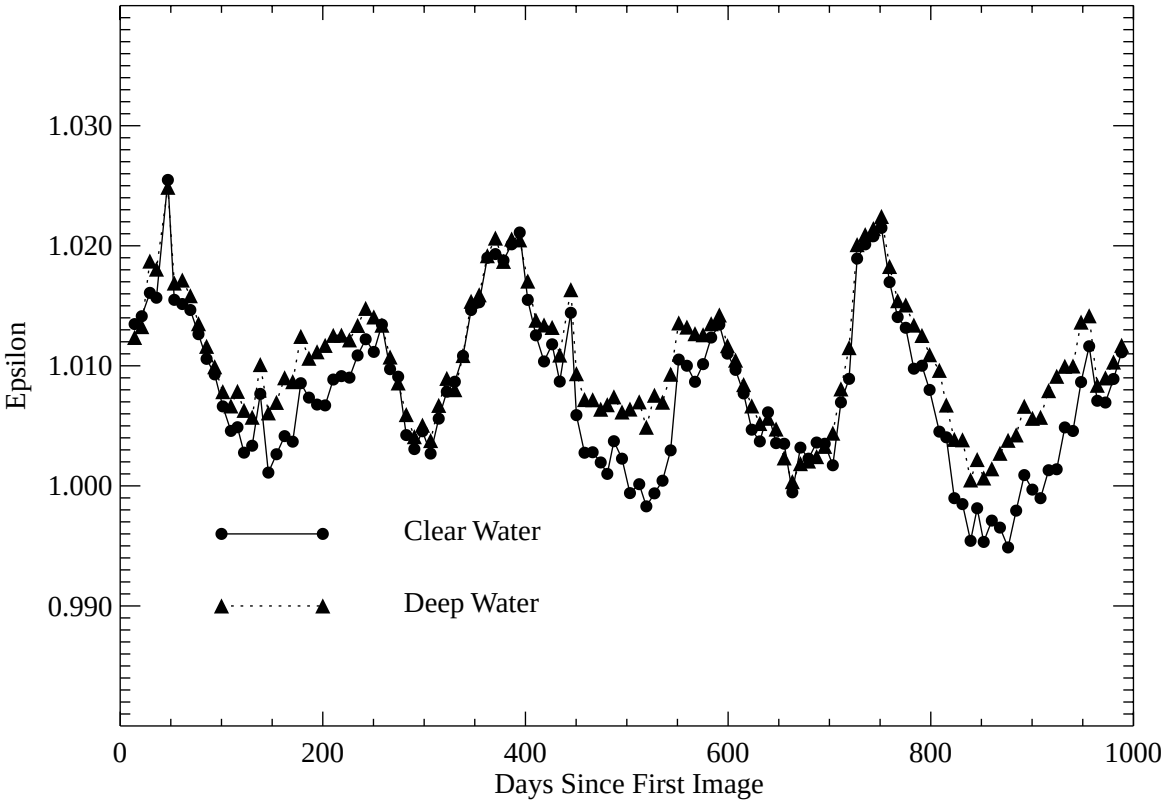

Fig. 17. The mean Ångström exponent at 510 nm retrieved by SeaWiFS.

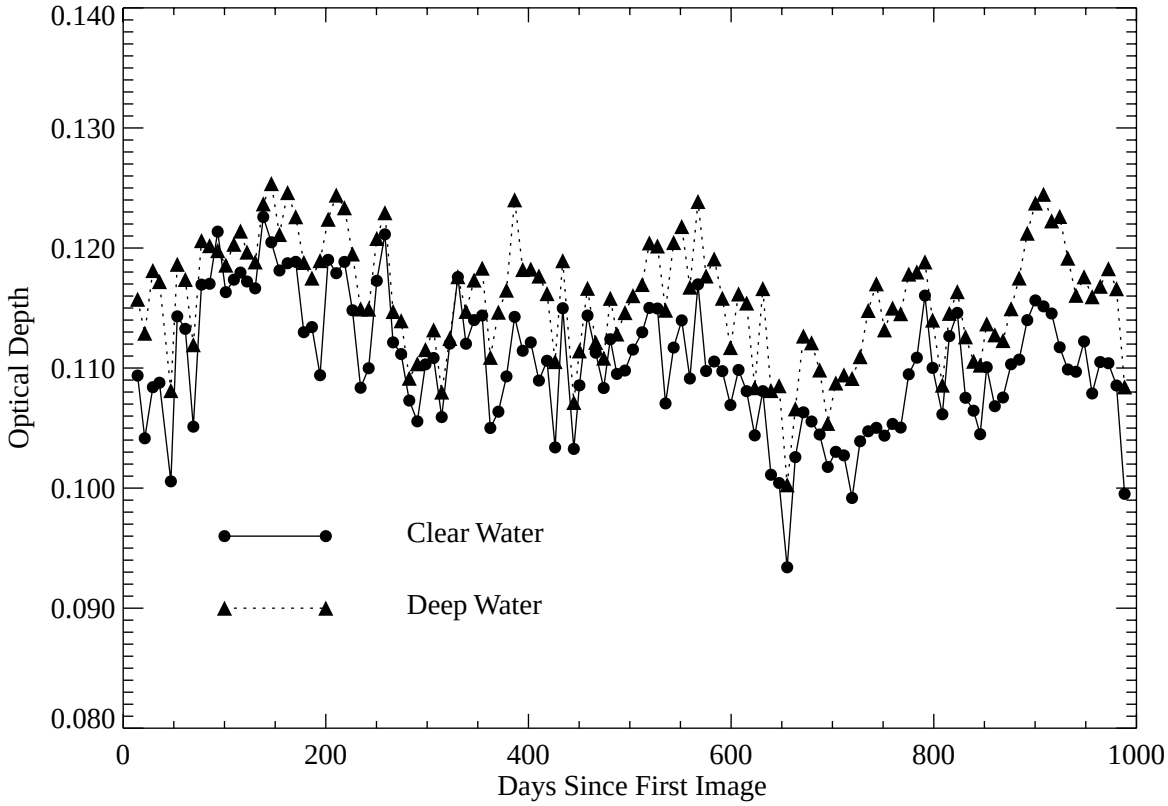

Fig. 18. The mean aerosol optical depth at 865 nm retrieved by SeaWiFS.

4.3 TIME-SERIES ANALYSIS

The time series of the mean SeaWiFS clear-water and deep-water radiances are plotted in Figs. 12 and 13, respectively. The figures establish that the vicarious calibration and the time corrections for each of the SeaWiFS bands are stable over the course of the mission. The radiances for bands 1–3 in the two figures show the differences expected for clear-water and deep-water comparisons. Bands 1 and 2 show slight periodicities, which may be a result of the interannual variability of global chlorophyll *a* concentrations (e.g., El Niño–La Niña) and due to the fact that the sampling of the ocean on a global basis shifts north and south seasonally.

The stability of the vicarious calibration and time corrections is also demonstrated by the plot of the mean clear-water chlorophyll time series in Fig. 14. The periodic trends observed in the radiances for bands 1 and 2 are also apparent in the chlorophyll concentration. The mean deep-water chlorophyll time series plotted in Fig. 15 shows the effects of the El Niño–La Niña transition on the global chlorophyll abundance.

The stability of the atmospheric correction over the course of the mission is shown by plots of the time series of the mean atmospheric correction parameter $\epsilon(765, 865)$, the mean Ångström exponent at 510 nm, and the mean aerosol optical depth at 865 nm, shown for both the clear-water and deep-water analyses in Figs. 16–18, respectively.

Chapter 5

Along-Scan Effects in SeaWiFS Data

Robert E. Eplee, Jr.
SAIC General Sciences Corporation
Beltsville, Maryland

Charles R. McClain
NASA Goddard Space Flight Center
Greenbelt, Maryland

Abstract

The SeaWiFS CVT has looked for along-scan effects in SeaWiFS data by examining mean radiances of LAC scenes over MOBY and by analyzing the ratio of SeaWiFS-to-MOBY (S:M) match-up data. Analyses of the SeaWiFS along-scan data and S:M ratios show decreases in the water-leaving radiances retrieved by SeaWiFS as the scan angles or optical paths of the observations increase. These two analyses, which are independent of each other, both point to an overcorrection of the SeaWiFS data by the SeaWiFS atmospheric correction algorithm.

5.1 INTRODUCTION

SeaWiFS data can show variations in response as a function of pixel number within the scan. These along-scan effects have three primary sources:

1) Variations in the instrument response as a function of pixel number within the scan (scan modulation effects),
2) Variations in the atmospheric correction as a function of optical path length, and
3) Variations in ocean reflectance.

The variations in instrument response were measured in the laboratory calibration of SeaWiFS (Barnes et al. 1994) and are accounted for by the scan modulation corrections applied during the calibration of the data. The analysis discussed in this chapter investigates possible variations in the atmospheric correction.

5.2 ATMOSPHERIC EFFECTS

The CVT analyzed variations in response as a function of pixel number within the scan by averaging the scan lines in LAC scenes over MOBY on a pixel-by-pixel basis for all of the clear pixels in each of the scenes. The MOBY LAC data were selected to minimize areal variations in ocean reflectance while including coverage of a high quality *in situ* time series. For this analysis, 149 scenes, spanning the mission from 19 September 1997 until 4 February 2000, were processed to level-2 and the resulting normalized water-leaving radiances were averaged for bands 1–6. The average chlorophyll a concentration for these data is approximately $0.1\,\mathrm{mg\,m^{-3}}$. The results of the analysis are mean radiances as functions of pixel number for the time period of the analysis.

The mean L_{WN} values are plotted in Fig. 19. These plots show a possible trend with pixel number, especially for bands 1 and 2. The trend for band 1 is particularly evident in Fig. 20, where the L_{WN} values are plotted as a function of the secant of the scan angle at each pixel. The two sides of the scan (before and after nadir) are plotted separately. The GAC cutoff in the LAC data occurs at a scan angle of 45%; the first and last 146 pixels of LAC data are excluded from the GAC data sampling. Figure 20 implies that the atmospheric correction of the data is not symmetric about nadir and that there is a rolloff in the measured radiances of approximately 10% at the GAC data cutoff. Examination of Figs. 19 and 20 suggests that the atmospheric correction algorithm overcorrects the radiances as the scan angle increases.

To look for seasonal effects, the data were broken down into three periods of the year, based on the sequential day of the year. Period 1 covers days 1–99, and includes data from 1998, 1999, and 2000, and has 57 scenes. Period 2 covers days 100–299, and includes data from 1997, 1998, and 1999, and has 54 scenes. Period 3 covers days 300–365, and includes data from 1997, 1998, and 1999, and has 38 scenes. (Period 2 encompasses 200 days because sun glint during summer leads to a loss of data during this time.) The L_{WN} values in band 1 for these periods are plotted in Fig. 21. The different amplitudes of the radiances for

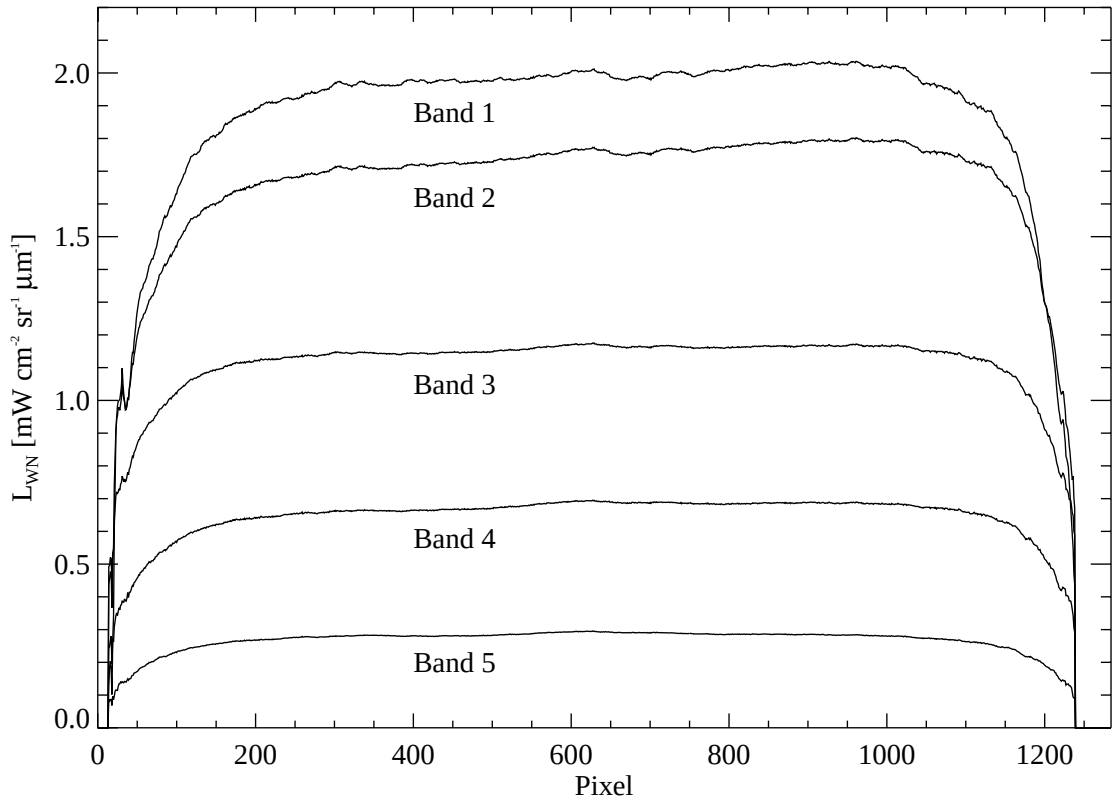

Fig. 19. The mean L_{WN} values as a function of pixel number along the scan line.

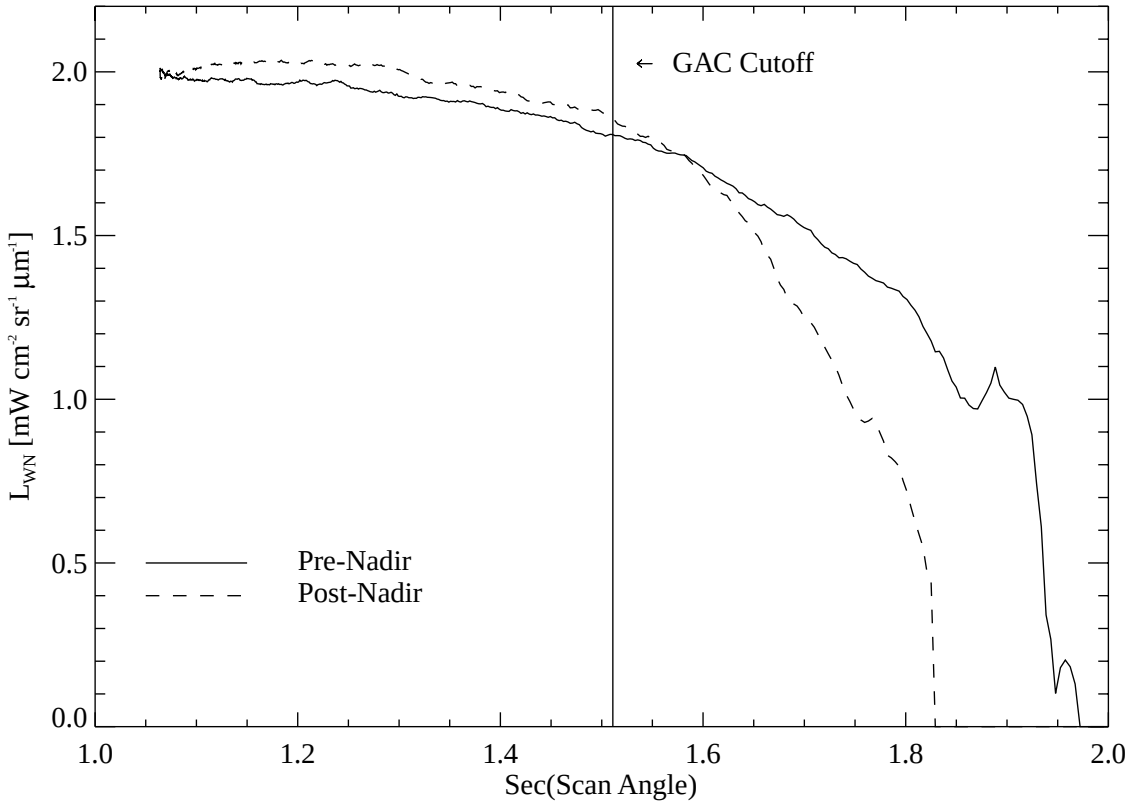

Fig. 20. The mean L_{WN} values as a function of the secant of the scan angle for each pixel.

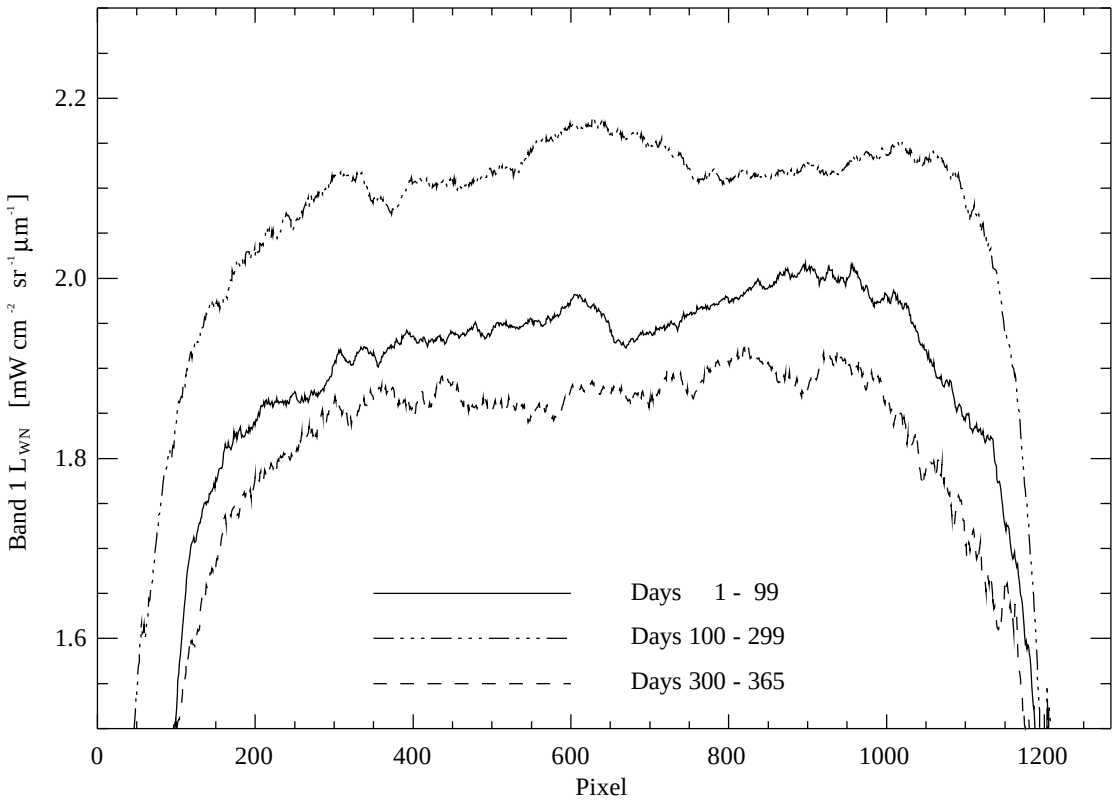

Fig. 21. The seasonal means of L_{WN} values as a function of pixel number along the scan line.

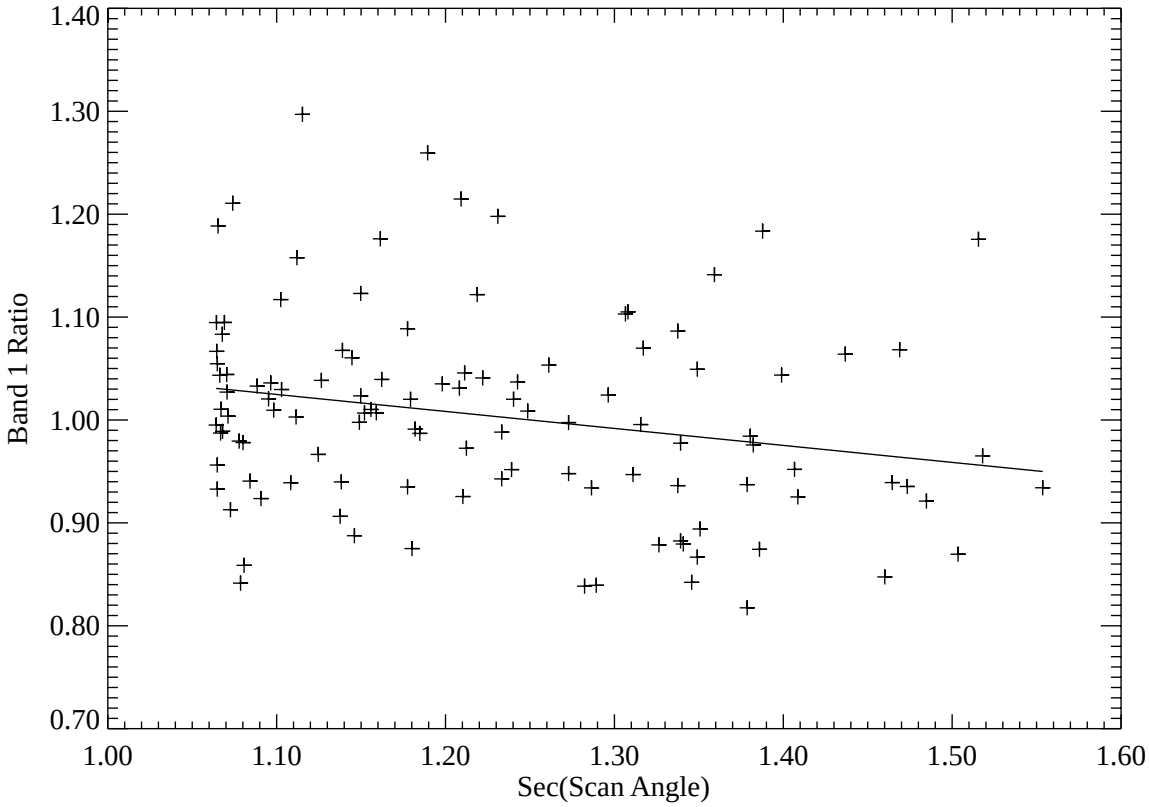

Fig. 22. The S:M MOBY matchups for band 1 as a function of the secant of the scan angle.

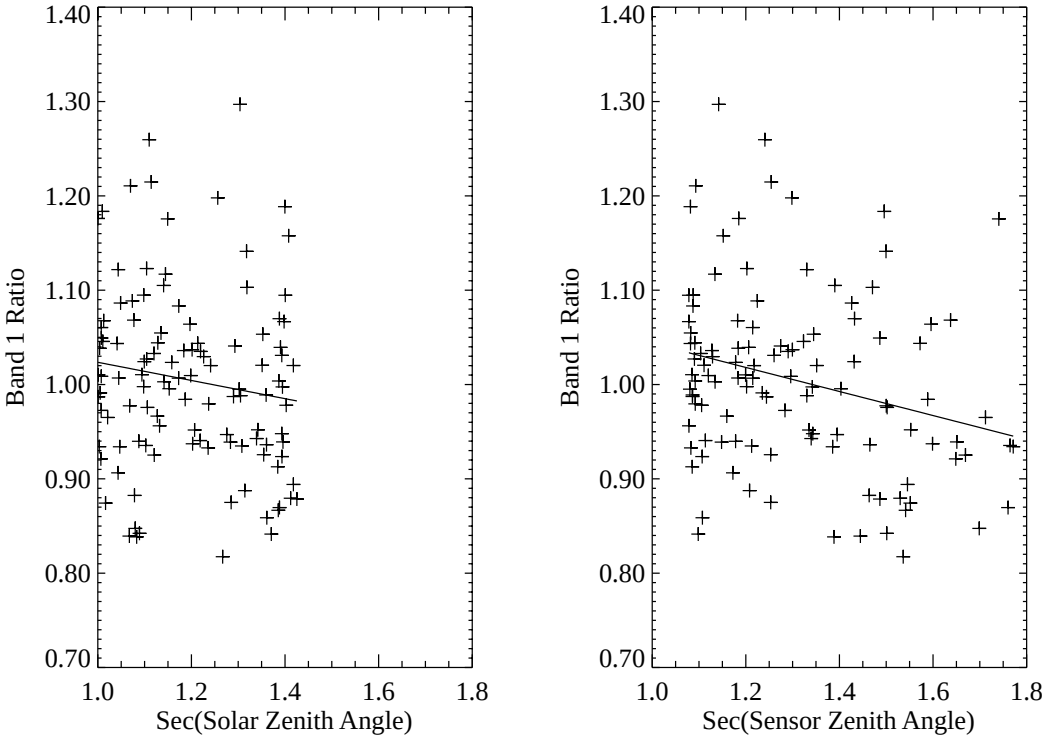

Fig. 23. The S:M matchups for band 1 as functions of the secants of the solar and sensor zenith angles.

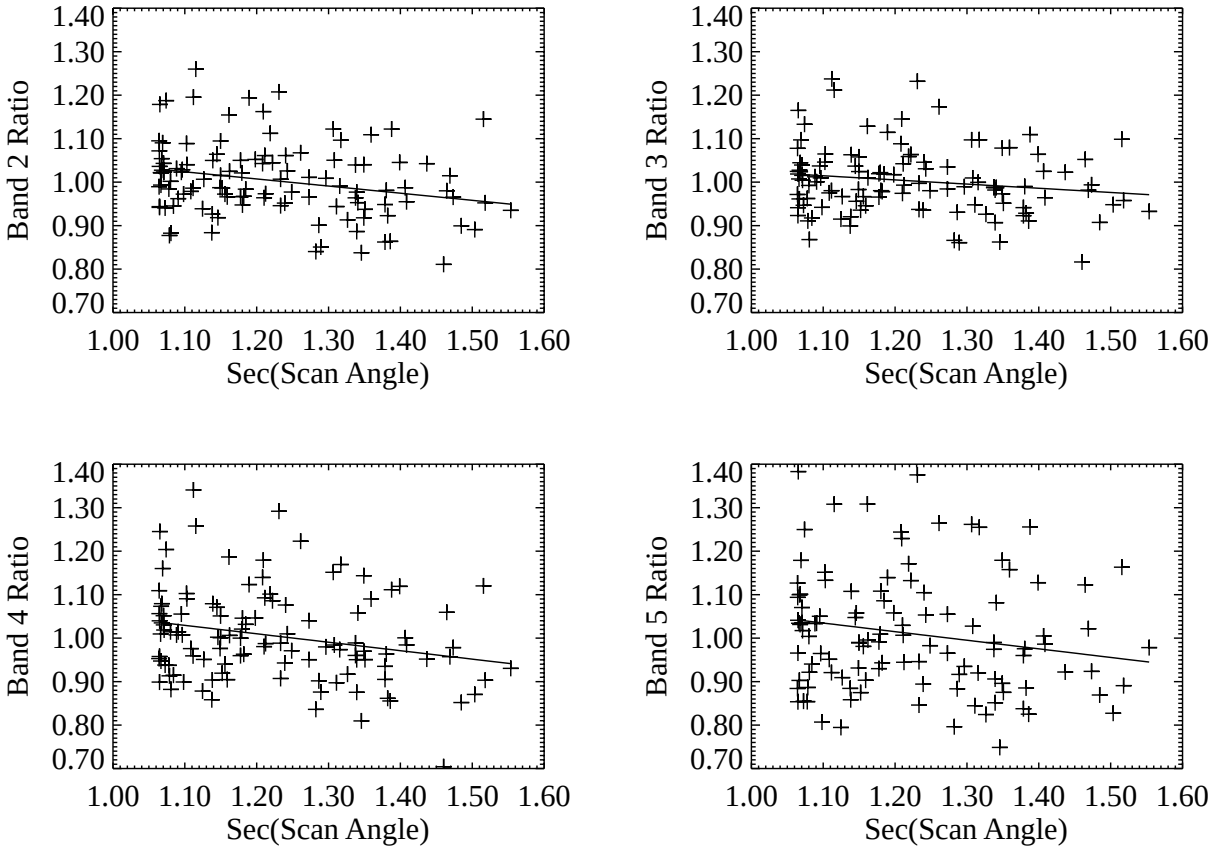

Fig. 24. The S:M matchups for bands 2–5 as functions of the secant of the scan angle.

each period are presumably due to seasonal variations in the chlorophyll concentration. The mean radiance for each period still shows a trend with pixel number.

5.3 SCAN ANGLE OF MATCHUPS

Because the along-scan analysis indicates an overcorrection by the atmospheric correction algorithm as the scan angle increases, the CVT examined the SeaWiFS-to-MOBY (S:M) matchups discussed in Eplee and McClain (2000a) as functions of scan angle, solar zenith angle, and sensor zenith angle. The match-up ratios for band 1 are plotted as a function of the secant of the scan angle in Fig. 22. The band 1 ratios are plotted as functions of the secant of the solar and sensor zenith angles in Fig. 23. Similar effects are observed for bands 2–5. The match-up ratios for these bands are plotted as functions of the secant of the scan angle in Fig. 24. Each of these figures also show linear fits to the data.

Examination of Figs. 22–24 shows a decrease in the SeaWiFS radiances as the various angles increase, or as the optical path through the atmosphere increases. The decrease is approximately 10% at scan angles and sensor zenith angles of 45%, which are correlated parameters. The magnitude of the decrease as a function of scan angle is comparable to the effect observed in the along-scan analysis. The decrease is approximately 7% for the solar zenith angle. The decrease in the match-up ratios as a function of the secant of the scan angle is comparable to the decrease in the water-leaving radiances observed in the along-scan analysis as a function of the secant of the scan angle. Because the water-leaving radiances measured by MOBY are independent of the sensor geometry, the decrease in the match-up ratios with scan angle are due to decreases in the water-leaving radiances retrieved by SeaWiFS, as a function of scan angle.

5.4 DISCUSSION

Analyses of the SeaWiFS along-scan data and the S:M match-up ratios show decreases in the water-leaving radiances retrieved by SeaWiFS as the scan angles or optical paths of the observations increase. These two analyses, which are independent of each other, both point to an overcorrection of the SeaWiFS data by the SeaWiFS atmospheric correction algorithm. An alternative explanation, however, may be the bidirectional reflectance of the ocean surface, or f/Q effect (Morel and Gentili 1996), but preliminary evaluations were inconclusive.

Chapter 6

SeaWiFS Aerosol Optical Thickness Match-up Analyses

Menghua Wang
University of Maryland, Baltimore County
Baltimore, Maryland

Sean W. Bailey
Futuretech Corporation
Greenbelt, Maryland

Christophe M. Pietras
SAIC General Sciences Corporation
Beltsville, Maryland

Charles R. McClain
NASA Goddard Space Flight Center
Greenbelt, Maryland

Abstract

In this chapter, a match-up procedure is described which compares the retrieved SeaWiFS aerosol optical thicknesses with data from *in situ* measurements. The aerosol optical thickness at 865 nm is a by-product of the SeaWiFS atmospheric correction and is routinely retrieved from SeaWiFS measurements. This work is part of the SeaWiFS calibration and validation efforts in studying the aerosol optical properties over the ocean, thereby, validating aerosol models used in the atmospheric correction of ocean color sensors. The aerosol model is an integral part of the SeaWiFS atmospheric correction. The SeaWiFS aerosol retrieval algorithm, the data acquisitions from both SeaWiFS and the *in situ* measurements, and the match-up procedure are described. Finally, some preliminary comparison results are presented and discussed.

6.1 INTRODUCTION

Aerosols play an important role in climate forcing and biogeochemical cycling. They not only directly influence radiative transfer in the atmosphere and, hence, change the radiance reflected to space, but they also indirectly affect the radiation budget by providing cloud condensation nucleii that lead to cloud formation (Charlson et al. 1987 and 1992). There have been continuous efforts in recent years with both ground *in situ* measurements and remote retrieval of aerosol optical properties using aircraft and satellite sensors. The primary goals of the SeaWiFS mission are routine global ocean color measurements and ocean bio-optical property data (Hooker et al. 1992 and McClain et al. 1998). In retrieving the ocean near-surface signals from sensor-measured radiances at the satellite, however, the atmospheric effects must be removed. This is known as *atmospheric correction*, which removes more than 90% of the observed radiance in the visible spectrum (Gordon and Wang 1994a).

The SeaWiFS atmospheric correction algorithm uses two NIR bands (765 and 865 nm) to estimate the aerosol optical properties and extrapolate these into the visible spectrum. Aerosol optical properties, in particular, aerosol optical thickness, is a by-product of the SeaWiFS atmospheric correction. Aerosol optical thickness at 865 nm, $\tau_a(865)$, is routinely retrieved from SeaWiFS measurements. The aerosol optical thickness is proportional to aerosol particle concentration, and is one of the most important aerosol optical parameters.

In this chapter, the effort to compare and validate the SeaWiFS aerosol optical products with *in situ* measurements, principally from Aerosol Robotic Network (AERONET) data (Holben et al. 1998), are outlined. Some other *in situ* measurements from calibration and validation campaigns within the SIMBIOS Project are also analyzed. There are two primary objectives behind these comparisons. First, because $\tau_a(865)$ is part of the SeaWiFS standard product suite, it warrants validation. With global

ground-based measurements of the τ_a data readily available through AERONET, comparisons between the SeaWiFS derived values and ground-based *in situ* measurements are very useful in evaluating the algorithm performance. The second objective of this work is to determine the validity of the suite of aerosol models currently used by the SeaWiFS Project for atmospheric correction.

6.2 PROCEDURES

In this section, the SeaWiFS aerosol optical thickness retrieval algorithm and its implementation in the SeaWiFS image processing system are described. Then, the algorithm is extended to retrieve the aerosol optical thicknesses in all of the SeaWiFS bands. Next, the data acquisition procedure and match-up criteria for both SeaWiFS and *in situ* observations are outlined. Finally, a data analysis strategy for both SeaWiFS and the *in situ* ground measurements is discussed.

6.2.1 Theoretical Bases

By defining the reflectance $\rho = \pi L/(F_0 \cos\theta_0)$, where L is the radiance in the given viewing direction, F_0 is the extraterrestrial solar irradiance constant, and θ_0 is the solar zenith angle. The total upward reflectance at the top of the ocean–atmosphere system, $\rho_t(\lambda)$, measured at the two SeaWiFS NIR bands (765 and 865 nm) can be written as:

$$\rho_t(\lambda) \;=\; \rho_r(\lambda) \;+\; \rho_a(\lambda) \;+\; \rho_{ra}(\lambda), \tag{8}$$

where $\rho_r(\lambda)$, $\rho_a(\lambda)$, and $\rho_{ra}(\lambda)$ are the contributions from multiple scattering of air molecules (Rayleigh scattering), aerosols, and Rayleigh-aerosol interactions, respectively. Note that the surface sun glint and whitecap terms in the above equation have been ignored. This equation can be rewritten as

$$\rho_t(\lambda) \;-\; \rho_r(\lambda) \;=\; \rho_a(\lambda) \;+\; \rho_{ra}(\lambda). \tag{9}$$

The value of the left hand side of (9) can be estimated from the sensor-measured radiance, $\rho_t(\lambda)$, and the computed Rayleigh scattering reflectance, $\rho_r(\lambda)$, if the surface atmospheric pressure is known. This gives the aerosol and Rayleigh-aerosol interaction contributions of $\rho_a(\lambda)+\rho_{ra}(\lambda)$ at the two SeaWiFS NIR wavelengths. By using a set of candidate aerosol models, the effects of the spectral variation of the $\rho_a(\lambda)+\rho_{ra}(\lambda)$ values at the two NIR bands are then extrapolated into the SeaWiFS visible bands (Gordon and Wang 1994a). The extrapolation was achieved through a process of aerosol model selection from evaluating the atmospheric correction parameter, $\epsilon(\lambda_i, \lambda_j)$, defined as

$$\epsilon(\lambda_i, \lambda_j) \;=\; \frac{\rho_{as}(\lambda_i)}{\rho_{as}(\lambda_j)}, \tag{10}$$

(Gordon and Wang 1994a, and Wang and Gordon 1994), where $\rho_{as}(\lambda_j)$ is the single scattering aerosol reflectance at SeaWiFS band λ_j, which is given by

$$\rho_{as}(\lambda_j) \;=\; \frac{\tau_a(\lambda_j)\,\omega_a(\lambda_j)\,p_a(\theta, \theta_0, \lambda_j)}{4\,\cos\theta\,\cos\theta_0}. \tag{11}$$

The parameters $\tau_a(\lambda_j)$, $\omega_a(\lambda_j)$, and $p_a(\theta, \theta_0, \lambda_j)$ are the aerosol optical thickness, the aerosol single scattering albedo, and the effective value of aerosol scattering phase function related to the single scattering case, respectively. The θ term is the sensor zenith angles.

In computing $\epsilon(\lambda_i, \lambda_j)$, λ_j is usually taken at the longer NIR band, i.e., 865 nm for SeaWiFS. The value of $\epsilon(\lambda_i, \lambda_j)$ characterizes the spectral variation of aerosol optical properties. For a given solar and viewing geometry, $\epsilon(\lambda_i, \lambda_j)$ depends only on the aerosol model; therefore, it forms the link between $\epsilon(\lambda_i, \lambda_j)$ and the aerosol model.

Using lookup tables, which were generated with a set of candidate aerosol models developed by Shettle and Fenn (1979), the $\rho_a(\lambda) + \rho_{ra}(\lambda)$ values at the two SeaWiFS NIR bands can be converted to the single scattering reflectance $\rho_{as}(\lambda)$, thereby providing $\epsilon(765, 865)$ values for given aerosol models. Hereafter, all $\epsilon(765, 865)$ values will be denoted as ϵ with sub- and superscripts, as applicable. The SeaWiFS retrieved atmospheric correction parameter, $\overline{\epsilon}$, was obtained by a weighted averaging over individual ϵ values derived from a set of aerosol models. Two aerosol models with ϵ^- and ϵ^+ such that

$$\begin{aligned} \epsilon^- \;&\leq\; \overline{\epsilon} \\ &<\; \epsilon^+ \end{aligned} \tag{12}$$

can be obtained, where ϵ^- is for the aerosol model with the largest ϵ value less than or equal to $\overline{\epsilon}$, and ϵ^+ is for the aerosol model with the smallest ϵ value greater than $\overline{\epsilon}$.

With the two retrieved aerosol models, the corresponding aerosol optical thicknesses (τ_a) for a given wavelength λ, $\tau_a^-(\lambda)$ and $\tau_a^+(\lambda)$, can then be estimated using (11). Finally, the SeaWiFS aerosol optical thickness was obtained by interpolating between the two models as

$$\tau_a(\lambda) \;=\; (1 - r_a)\,\tau_a^-(\lambda) \;+\; r_a \tau_a^+(\lambda), \tag{13}$$

where

$$r_a \;=\; \frac{\overline{\epsilon} \;-\; \epsilon^-}{\epsilon^+ \;-\; \epsilon^-} \tag{14}$$

is the interpolation ratio (r_a) between the two models.

SeaWiFS routinely retrieves the aerosol optical thickness at 865 nm as a standard product. It is straightforward, however, to extend the current aerosol optical thickness retrievals to the remaining SeaWiFS wavelengths using (13). After making a necessary interpolation for wavelengths that are slightly shifted from the SeaWiFS bands, comparisons between SeaWiFS results and *in situ* measurements are possible. Both the Cimel sun–sky scanning radiometer and the MicroTops II sun photometer have spectral

Table 9. AERONET sites used for the aerosol match-up analyses.

AERONET Station	*Latitude*	*Longitude*	*AERONET PI*
Bahrain	26.32	50.50	C. McClain
Bermuda	32.37	−64.70	B. Holben
Dry Tortugas	24.60	−82.80	K. Voss and H. Gordon
Kaashidhoo	4.97	73.47	B. Holben
Lanai	20.83	−156.99	C. McClain
San Nicolas Island	33.26	−119.49	R. Frouin

wavelengths at 440, 500, 670, and 870 nm corresponding to SeaWiFS bands 2 (443 nm), 4 (510 nm), 6 (670 nm), and 8 (865 nm), respectively. The aerosol optical thicknesses, therefore, can be compared at these four wavelengths.

It should be noted that the satellite and *in situ* data usually differ in both temporal and spatial characteristics. The *in situ* data are temporally averaged, while the satellite data are spatially averaged.

6.2.2 SeaWiFS Data Acquisition

The SeaWiFS aerosol optical thickness data were obtained by spatially co-locating a 25×25 pixel grid box around the pixel containing the ground-based measurement station, thereby providing a maximum of 625 SeaWiFS retrievals in each matchup. A spatial homogeneity (uniformity) test in the retrieved $\tau_a(865)$ value was then conducted to screen thin cirrus and high altitude aerosol contamination, because the *in situ* and satellite measurements are often looking through different atmospheric paths. Only those satellite data sets which passed the spatial homogeneity test were used for the match-up analyses. The SeaWiFS operational code has been modified to output, at a pixel-by-pixel level, the aerosol optical thickness at a wavelength of 865 nm, values of retrieved two aerosol models, and the model partition ratio r_a value. Aerosol optical thicknesses at all of the SeaWiFS wavelengths can be calculated using (13).

6.2.3 *In Situ* Data Acquisition

The ground-based measurements, used for the aerosol optical thickness match-up analyses, come from two primary sources: the automated Cimel sun–sky scanning radiometer managed as part of the AERONET network, and handheld MicroTops II sun photometers. In the following two sections, the data acquisition procedures from these two instruments are discussed.

6.2.3.1 In Situ *Data from Cimel*

A select group of ground stations from AERONET was chosen. These instruments were located at either coastal or island stations and were operational for a reasonable length of time after SeaWiFS went into operation. Table 9 provides the AERONET station name, location (latitude and longitude), and the corresponding responsible AERONET principal investigator (PI). Currently, efforts are underway to include additional AERONET stations. The retrieval of data from AERONET was automated to facilitate the match-up analyses. Once per month, a script is automatically run to access the AERONET database and retrieve τ_a data for the predetermined sites.

For the match-up purpose, the ground-based measurements from AERONET were first reduced to include only those records within ±3 h of the SeaWiFS overpass time for a given station. These records include the aerosol optical thicknesses measured at the four spectral wavelengths (440, 500, 670, and 870 nm). As an initial quality control step, the data were averaged and some variation parameters were computed to screen possible cloud contamination. Only those data sets that have low temporal variations (stable atmosphere) were then further reduced to ±1 h of the SeaWiFS overpass time and used for the match-up analyses. Usually, the Cimel instruments routinely take one measurement every 15 min near local noon; therefore, for a given SeaWiFS file, there may be as many as eight AERONET measurements that qualify as a match for the 2 h time window. Figure 25 shows the flow chart of the match-up procedure for the aerosol optical thickness obtained from SeaWiFS and Cimel measurements. The strategy in the validation study is not to compromise good data with bad data for the purpose of more matchups, i.e., it is preferred to screen out some good data to keep the high quality of data sets.

6.2.3.2 In Situ *Data from MicroTops*

The hand-held MicroTops sun photometer data, were collected by various investigators in field campaigns associated with the SIMBIOS project. The cruises from which the MicroTops data were collected, along with the locations and investigators, are listed in Table 10. Data from the MicroTops instruments are reprocessed from raw voltages using code adapted from the AERONET standard Cimel processing routines. This ensures that the τ_a data derived from the MicroTops measurements will be comparable to the data provided by AERONET. The number

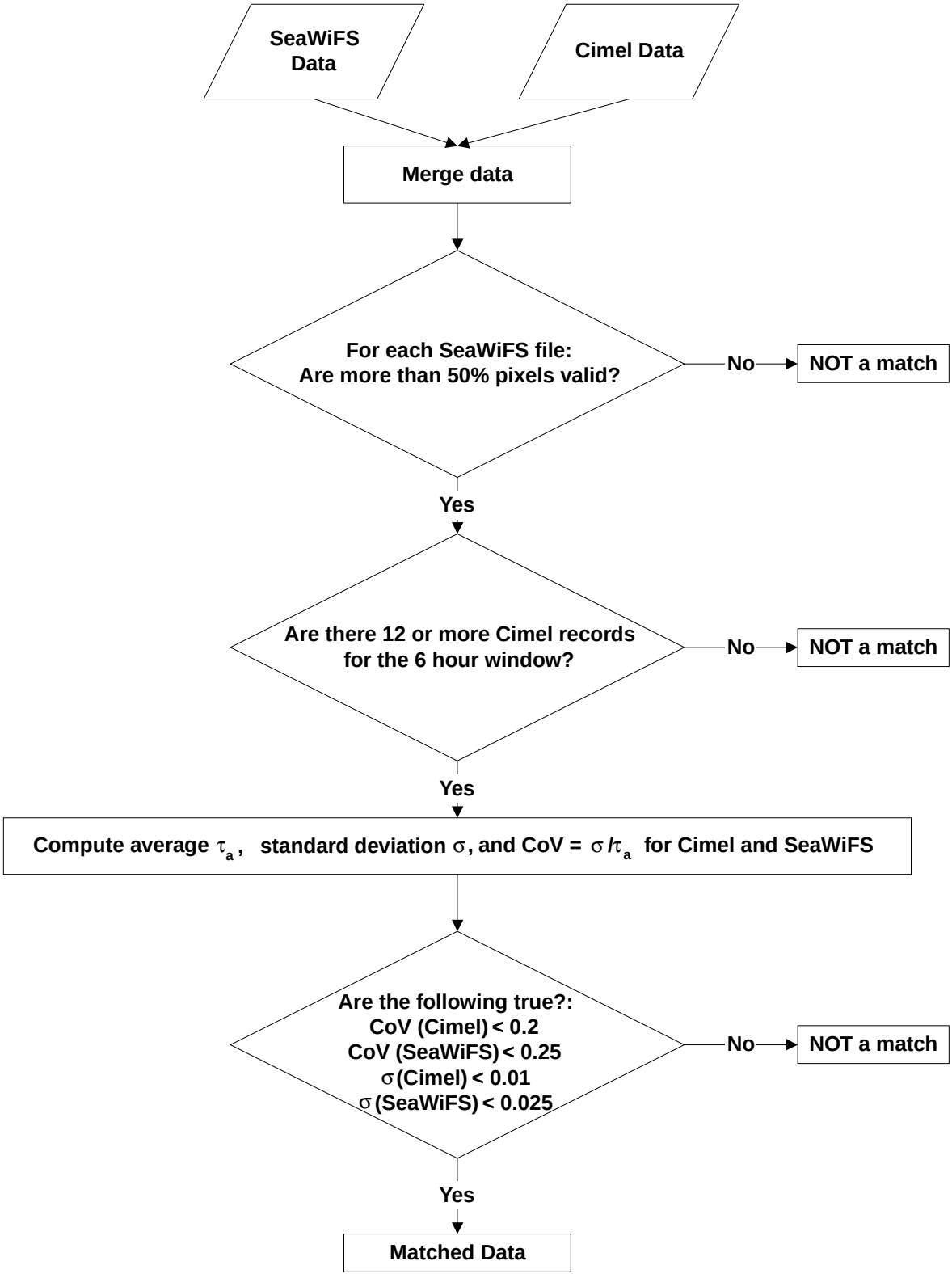

Fig. 25. A flow chart of the match-up procedure for the aerosol optical thickness obtained from SeaWiFS and Cimel measurements.

Table 10. MicroTops data used for the aerosol match-up analyses.

Cruise	*Location*	*Investigator*
MOBY Refit[1]	MOBY Station, Hawaii	D. Clark
Jason Project[2]	Sea of Cortez	G. Feldman
GoCal97-98[3]	Gulf of California	J. Mueller
JUL98NAN[4]	Massachusetts Bay	B. Schieber and A. Subramaniam
HOTS[5]	HOTS Station, Hawaii	J. Porter and C. Motell
HMS *Rose*[6]	East Coast of US	G. Feldman
USF–BNL[7]	TOTO, Bahamas	M. Miller

1) MOBY refit: Measurements obtained at the Marine Optical Buoy site at Hawaii.
2) Jason Project: An expedition to the Sea of Cortez with Robert Ballard and the Jason Project.
3) GoCal: A cruise to the Gulf of California (Sea of Cortez).
4) JUL98NAN: A National Oceanic and Atmospheric Administration (NOAA)-sponsored cruise off Nantucket Island, Massachusetts in July 1998.
5) HOTS: Hawaiian Ocean Time Series cruise.
6) HMS *Rose*: A cruise aboard Her Majesty's Ship (HMS) *Rose*, a wooden tall sailing ship, which went from Miami, Florida to New York, New York.
7) USF–BNL: A cruise to the Tongue of the Ocean (TOTO) by a group from the University of South Florida (USF) and Brookhaven National Laboratory (BNL).

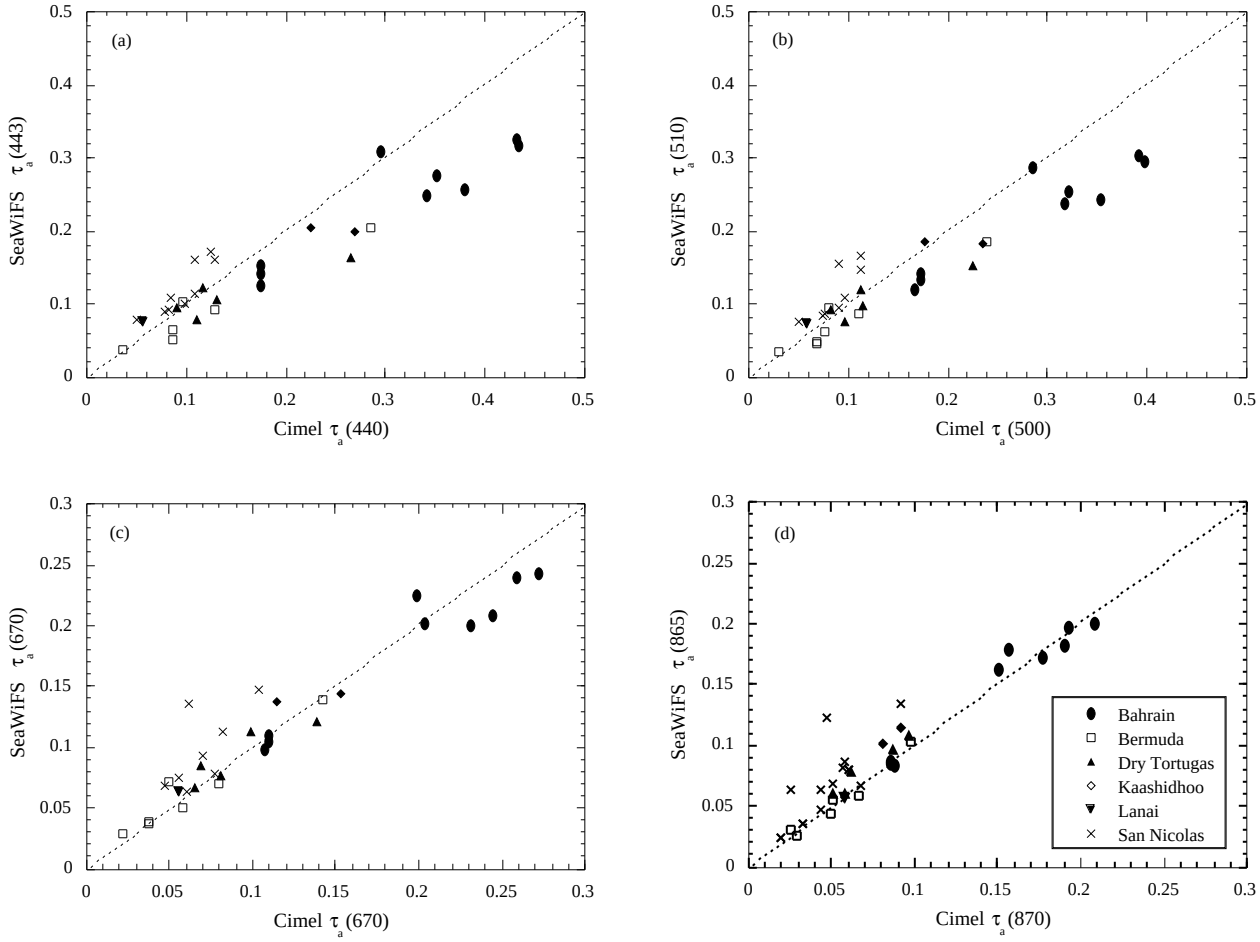

Fig. 26. The retrieved SeaWiFS aerosol optical thicknesses $\tau_a(\lambda)$ compared with the ground *in situ* measurements from the various AERONET stations for four wavelengths: **a)** 440 nm; **b)** 500 nm; **c)** 670 nm; and **d)** 870 nm.

Table 11. Five aerosol optical thickness, $\tau_a(865)$, samples of MicroTops data compared with SeaWiFS $\tau_a(865)$ data. $\tau_a^{\min}$, $\tau_a^{\max}$, and τ_a^{avg} are the miniumum, manximum, and average from each set of measurements, respectively.

Cruise	*MicroTops Data* $\tau_a^{\min}$	$\tau_a^{\max}$	τ_a^{avg}	*SeaWiFS* τ_a^{avg}
GoCal97	0.0196	0.0821	0.0342	0.0632
GoCal98	0.0191	0.0548	0.0258	0.0341
Jason Project	0.0285	0.0727	0.0433	0.0297
HMS *Rose*	0.0638	0.5829	0.1500	0.0692
JUL98NAN	0.0573	0.1764	0.0877	0.0889

of hand-held MicroTops measurements that match a given SeaWiFS file varies greatly because the measurement protocol for these instruments is not well defined. In general, there should be a minimum of three MicroTops measurements per matched SeaWiFS file. The MicroTops data, however, tends to be much more variable than the Cimel data. The *in situ* data screening procedure, as outlined for the Cimel data set, was therefore not applied.

6.3 PRELIMINARY RESULTS

The SeaWiFS derived aerosol optical thicknesses with those from the ground *in situ* measurements were compared. As this is an ongoing research project, all results shown here are preliminary. Figures 26a–d provide an overall comparison results of $\tau_a(\lambda)$ between SeaWiFS and Cimel measurements at the four wavelengths 440, 500, 670, and 865 nm. The Cimel measurements were from the AERONET stations listed in Table 9. The number of data contributed to each plot in Fig. 6 from individual stations, from the top of the list to the bottom in Table 9, are 9, 8, 5, 2, 1, and 8. The station at Lanai, therefore, only contributed one point, whereas the Bahrain station provided nine points shown in Figs. 26a–d. The dotted lines in Fig. 26 are the 1:1 line. Although the comparison results vary both in time and location, Fig. 26 shows that the comparisons agree reasonably well at the longer wavelengths (670 and 865 nm) for most of the AERONET stations.

There is no obvious bias in the retrieved aerosol optical thicknesses. This implicitly indicates that the calibration at the SeaWiFS 865 nm wavelength is reasonably accurate. At the short wavelengths, however, it appears that SeaWiFS has the tendency of overestimating $\tau_a(\lambda)$ with respect to the *in situ* measurements, in particular, for the relatively large aerosol optical thicknesses ($\tau_a > 0.15$). This is most evident with the SeaWiFS $\tau_a(443)$ comparison results. Some possible sources that contributed to the comparison differences are from both satellite measurements (calibration, aerosol models, and cloud and thin cirrus contamination) and *in situ* data (mainly from instrument calibration and cloud contamination). More studies are needed to understand all of these.

Similarly, the *in situ* MicroTops II data, which were from the various SIMBIOS calibration and validation campaigns, were compared with the SeaWiFS measurements. Table 11 shows five sample comparison results from five field experiments. For the MicroTops data in Table 11, the minimum $\tau_a^{\min}$, the maximum $\tau_a^{\max}$, and average τ_a^{avg} from each set of measurements are listed. There are high variations in the MicroTops measurements. Applying a data screen procedure for MicroTops data was not possible, as was for the Cimel data, because none of MicroTops data were able to pass this data screening process.

Acknowledgments

The authors are grateful to J.T. Riley for the instrument calibrations, and the AERONET PIs for collecting and providing Cimel data, in particular the PIs listed in Table 9. Thanks go to B. Holben's group at GSFC for maintaining a global AERONET database and providing useful comments. Thanks also go to the investigators who provided the MicroTops II data, as listed in Table 10, in particular, measurements that were used in the analyses from G. Feldman, J. Mueller, and B. Schieber and A. Subramanian.

Chapter 7

Normalized Water-Leaving Radiance and Chlorophyll *a* Match-up Analyses

Sean W. Bailey
Futuretech Corporation
Greenbelt, Maryland

Charles R. McClain
NASA Goddard Space Flight Center
Greenbelt, Maryland

P. Jeremy Werdell
Science Systems and Applications, Incorporated
Lanham, Maryland

Brian D. Schieber
SAIC General Sciences Corporation
Beltsville, Maryland

Abstract

Validation of SeaWiFS requires the use of *in situ* (field collected) data sets. The SeaWiFS and SIMBIOS Projects have sponsored numerous PIs to collect *in situ* optics and chlorophyll data for the purpose of comparing values to those derived from the SeaWiFS instrument. The match-up design described here uses field data stored in SeaBASS, match-up analysis software, and a plotting and statistics package to validate the primary SeaWiFS derived ocean products, i.e., normalized water-leaving radiance, chlorophyll *a* concentration, and the diffuse attenuation coefficient.

7.1 INTRODUCTION

A key method for validating SeaWiFS data is to compare the remote sensing values with coincident *in situ* measurements collected from ships or other oceanic platforms. NASA has sponsored field research activities to build a database of optical, pigment, and related *in situ* data for use in validating the derived products (McClain et al. 1992 and 1998). These data, which are stored in SeaBASS, have been made available to those assisting in the SeaWiFS algorithm development and validation effort, e.g., the SIMBIOS Science Team and the Moderate Resolution Imaging Spectroradiometer (MODIS) Oceans Team.

Data from SeaBASS were employed in developing the first version of OC2 (OC2v1) during the first SeaWiFS Bio-optical Algorithm Mini-workshop (SeaBAM, O'Reilly et al. 1998) and the second version (OC2v2, O'Reilly et al. 2000). The prelaunch strategy for the match-up comparison process is described in McClain et al. (1996) and has been updated since launch (Hooker and McClain 2000). In this chapter, a brief overview of SeaBASS is followed by a discussion of the match-up procedures for the validation process. Finally, results of the current match-up analysis (October 2000) are presented.

7.1.1 SeaBASS Data Archive

The SeaWiFS Project built SeaBASS (Hooker et al. 1994) as a local repository for *in situ* optical and pigment data to be used in satellite calibration and validation activities (e.g., *in situ* and satellite match-up analyses). The system is composed of two separate databases: a bio-optical archive with data from over 350 field campaigns, and a historical pigment archive which holds in excess of 300,000 fluorometric and high-performance liquid chromotography (HPLC) pigment data records. Bio-optical data include worldwide measurements of apparent and inherent optical properties from research vessels, moorings, drifters, and other platforms. Other oceanographic and atmospheric data, such as, estimates of primary productivity and aerosol optical thickness, are also archived in SeaBASS.

Participants in the SIMBIOS Project are contractually obligated to submit data to SeaBASS, so the size of the archive has grown rapidly (McClain and Fargion 1999). SeaBASS also includes data contributions from the SeaWiFS Field Program (Stanford Hooker, PI) and other US and foreign researchers. Access to SeaBASS is provided via the world wide web at `http://seabass.gsfc.nasa.gov`, and users may both browse the archive directories and query the bio-optical and pigment databases. To protect the publication rights of its contributors, access to SeaBASS is limited (via a password) to members of the SeaWiFS and SIMBIOS Science Teams and to other regularly contributing investigators who have been granted access on an individual basis.

SeaBASS supports standard (two-dimensional) American Standard Code for Information Interchange (ASCII) data files, which are easily managed from any computer platform and by most programming languages. This approach also avoids the use of proprietary software on the part of a contributing investigator and allows easy integration of the files into the world wide web. The architecture of a SeaBASS data file is simple: data are presented in columns (delimited by a space, tab, or comma) and preceded by a series of predefined metadata headers. The headers provide descriptive information on the data file, such as date, time, location, column name and units, investigators, and additional ancillary information.

To assist with the standardization of SeaBASS data files, the Project developed feedback software and protocols to evaluate the format of submitted data files. A complete description of SeaBASS data formats, format verification protocols, and quality control is provided at the SeaBASS web site at `http://seabass.gsfc.nasa.gov`.

7.2 METHODS

The procedure for comparing SeaWiFS image data to *in situ* data is described here, with particular attention given to the description of the exclusion criteria used. The procedure described, and the exclusion critera used, are designed to minimize the effect of bad data on the comparison while not biasing the results.

7.2.1 *In Situ* Match-up Data Files

In situ data are compared to SeaWiFS image files by matching the two data sources in time and space. Each *in situ* data set is first summarized in a single ASCII file, known as a *match-up* file. The match-up file adheres to the aforementioned SeaBASS data format. The data included in the match-up file are $L_W(\lambda)$; $E_s(\lambda)$, either measured directly or extrapolated from profiled downwelling irradiance, $E_d(0^+)(\lambda)$; C_a; and $K_d(490)$. Location and measurement times are also necessary for each record in the match-up file.

For all incoming data, proper descriptive documentation and possibly, interactions with the data provider, are required to assure the usefulness of the *in situ* data for matchups. Many types of instrumentation and operational procedures produce data for SeaWiFS matchups. The majority of the optical data come from well-known profiling radiometers, but a growing number of other approaches are being tested that collect data at a few discrete depths or from above the surface.

7.2.2 The Match-up Procedure

The SeaWiFS match-up procedure includes using both UNIX C-shell scripts (CSH) and Interactive Data Language (IDL) procedures. These are used to compare individual SeaWiFS Hierarchical Data Format (HDF) files to *in situ* data records of individual measurements, i.e., stations. To generate the initial list of SeaWiFS files for consideration, the SeaWiFS Project HDF file database is queried for files that spatially and temporally match records in the *in situ* data source. The pixel and line number of the SeaWiFS file that matches the *in situ* location is determined. A region encompassing 101×101 pixels centered on the matched pixel is extracted from each of the resulting initial level-1a (L1A) files (GAC, LAC, and HRPT). These extracted data files are saved to a new file for local disk storage.

For all valid L1A matches, a level-2 (L2) product is generated from the extracted file for further analysis. A comprehensive suite of SeaWiFS L2 products are generated, including all $L_W(\lambda)$, $L_{WN}(\lambda)$, $E_s(\lambda)$, C_a, $K_d(490)$, and ancillary data (ozone, windspeed, and atmospheric pressure). In the generation of the L2 products, the Siegel NIR correction (Siegel et al. 2000) is applied, as well as the sun glint and out-of-band corrections. As with the extracted L1A files, the L2 files are saved to local disk storage. For each successful L2 file generated, a record including the path to the L2 file, the matched pixel and line number, and associated latitude and longitude are written to a file. This list file and the *in situ* match-up file are used as input to the IDL program where the match-up exclusion criteria are applied and the match-up plots and statistics are generated.

7.2.3 Match-up Exclusion Criteria

Only a small percentage of the candidate SeaWiFS files become final valid matches. A number of exclusion criteria have been formulated to provide an objective set of points for SeaWiFS validation which removes invalid or redundant data from consideration. The approach presented here is a result of numerous iterations. Nevertheless, future modifications to the existing set of exclusion logic is likely as a better understanding of both the SeaWiFS and *in situ* data are attained.

The first exclusion criterion applied is a time difference between the *in situ* record and the satellite overpass. A time window of ±180 min from the satellite overpass is used

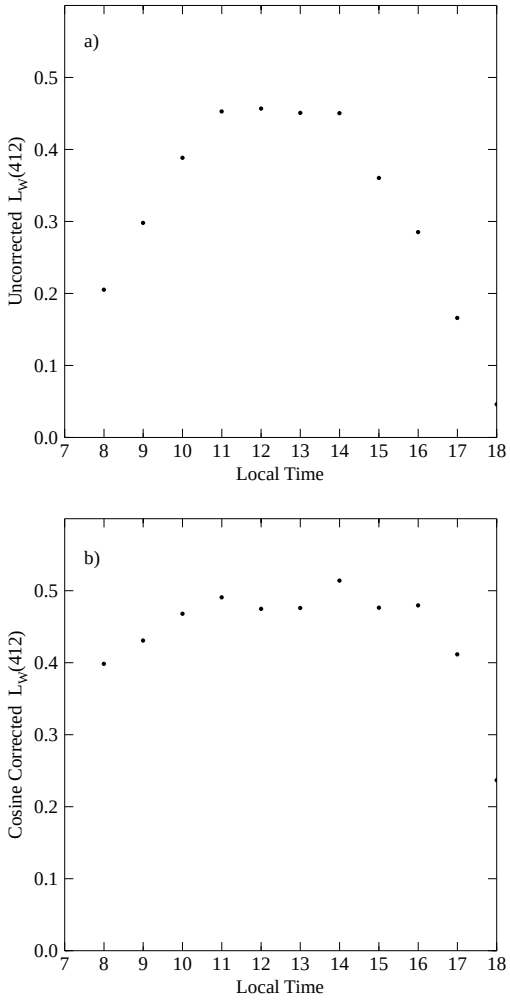

Fig. 27. Plots of hourly $L_W(412)$ measurements from the BTBM over the course of a clear day: **a)** uncorrected $L_W(412)$ measurements; and **b)** $L_W(412)$ measurements corrected for the cosine of the solar zenith angle.

because this window is the time period of reasonable illumination in most situations and, presumably, constant atmospheric conditions. An analysis of $L_W(412)$ normalized to the cosine of the solar zenith angle from the Bermuda Test-Bed Mooring (BTBM) throughout a clear day shows that a ± 180 min window is reasonable (Fig. 27).

In the current match-up set, the majority of candidate SeaWiFS files (i.e., those that coincide with *in situ* stations), are eliminated from consideration as a result of the SeaWiFS image pixels being flagged (excluded), usually because of clouds and stray light, although other factors are often present. Pixels are excluded if any of the following flags are applied: atmospheric correction failure, land, sun glint, total radiance above the knee value, high satellite zenith angle, stray light, clouds or ice, coccolithophores, and low $L_{WN}(555)$. Currently, pixels are not excluded with the turbid water flag applied. The authors have found that the current turbid water flag is not robust. It may erroneously flag pixels near cloud edges and fail to set in extremely turbid water if the SeaWiFS derived chlorophyll concentration is high (greater than approximately $10\,\mathrm{mg\,m^{-3}}$).

If a matchup passes the temporal exclusion criterion, the valid SeaWiFS pixels are averaged for a region encompassing the matched pixel, and simple statistics are recorded. The match-up approach uses a 3×3 pixel *box* for this spatial comparison. It should be noted that SeaWiFS GAC files have a lower sampling resolution than the LAC or HRPT products (approximately 4 km samples versus approximately 1 km samples, respectively). This sampling aspect results in a poorer representation of *in situ* conditions.

Once the match-up code has reported all unflagged matches, the routine reviews the records for further refinement. Calculations currently used for the exclusion of points and the match-up values include:

1. Minimum number of valid pixels: At least five out of nine pixels in the 3×3 box considered from the Sea-

WiFS image must be valid (unflagged) to avoid contaminated data.

2. SeaWiFS file reduction: If there are GAC, onboard LAC, and HRPT matches corresponding to the same *in situ* point, the order of preference is onboard LAC, HRPT, and GAC. When multiple files of the same preferred type match a single *in situ* record, the closest temporal match is selected. This selection is necessary when multiple HRPT stations or multiple GAC swaths cover the *in situ* point. Permanent real-time HRPT stations are given precedence over other HRPT sources.
3. Duplicate *in situ* data reduction: Cases where multiple *in situ* casts are performed at the same station are reduced to one representative record before the matchup by selecting the cast with the highest $L_W(490)$ value normalized to the theoretical E_s value.
4. Multiple *in situ* measurements for each SeaWiFS file: Along-track measurements are included in the *in situ* match-up files where adjoining measurements are greaer than 12 km apart.
5. Surface irradiance calculation: Theoretical E_s values are calculated using time and location for each *in situ* data record. This value can be used for later L_{WN} analysis.
6. Solar elevation correction: A $\cos(\theta_0)$ correction is applied to L_W match-up points (*in situ* and satellite). This adjustment helps remove time dependencies due to changes in the solar elevation and allows for a larger time window to be used.
7. Out-of-range $K_d(490)$values: Cases where the $K_d(490)$ values are below the $K_d(490)$ value of pure water (0.016 m^{-1}) or above a value of 6.4 m^{-1} are removed.
8. Large coefficient of variation elimination: Satellite matchups with extreme variation between pixels in the SeaWiFS 3×3 pixel *box* (coefficient of variation, or the standard deviation divided by the mean value, greater than 0.2) are excluded. These typically represent frontal regions or other anomalies (e.g., cloud edges) in the SeaWiFS imagery, which make the match-up validity questionable. The coefficient of variation value was selected because the satellite data appeared to form separate clusters of both fairly uniform data and highly variable data with a gap between them at about 0.2. Presently, this test is applied to each geophysical field (L_{WN}, C_a, etc.) independently.

Currently, three comparisons can be performed for each candidate matchup:

a) SeaWiFS L_W to *in situ* L_W;

b) SeaWiFS L_{WN} to *in situ* L_{WN} using observed L_W and E_s ($L_{WN} = F_0 L_W / E_s$; and

c) SeaWiFS L_{WN} to *in situ* L_{WN} using observed L_W, and theoretical E_s.

Values of E_s are usually measured directly (above the surface), but are often estimated by extrapolating subsurface measurements of E_d through the air–sea interface, denoted as $E_d(0^+$, although, there may be errors introduced in doing so (D. Clark, pers. comm.). The second calculation of L_{WN} (item c in the list above) is determined using the L_W values and a theoretical estimate of E_s (M. Wang, pers. comm.):

$$E_s(\lambda) \;=\; F_0(\theta_0)\,\cos(\theta_0)\exp\!\left[-\frac{\gamma}{\cos(\theta_0)}\right], \qquad (15)$$

where

$$\gamma \;=\; \frac{\tau_r(\lambda)}{2} \;+\; \Omega_{\mathrm{tc}}\,a_{\mathrm{oz}}(\lambda) \;+\; 0.0054, \qquad (16)$$

λ is the wavelength, θ_0 is the solar zenith angle, τ_r is the Rayleigh optical thickness, a_{oz} is the ozone absorption coefficient, and Ω_{tc} is the total columnar ozone in Dobson units (DU). The wavelength-independent constant value of 0.0054 accounts for the effects of aerosols and was estimated using an aerosol optical thickness of 0.1 and the M90 aerosol model. The ozone value used is an average of the ozone values for the 3×3 pixel box surrounding the matched pixel. This same ozone value is the one used in the operational processing.

An extensive comparison of both *in situ* and theoretical clear-sky E_s values for the valid matchups was conducted. The comparison showed reasonably good agreement between the measured and theoretical $E_s(\lambda)$ values. There were, however, several values above the maximum theoretical value. These may be the result of cloud reflection effects, poor calibrations, etc. The theoretical E_s value was shown to give similar match-up comparisons than those using the *in situ* E_s values. The theoretical E_s values, therefore, are used to compute the L_{WN} values for the *in situ* data.

Previous versions of the exclusion criteria eliminated match-up points in cases where the measured (*in situ*) E_s values differed substantially from the theoretical value in (15). This step was originally included to remove matches that may have been contaminated by clouds, but were not flagged as such in the level-2 processing. This step was later removed as it was noted the approach does not generally exclude any additional points from the final matchups. Other steps in the exclusion processing removed faulty records. Another test was to compare the difference in solar zenith angles between the satellite and *in situ* measurement times for L_W measurements. This condition, however, was ameliorated by applying the $\cos(\theta_0)$ correction for L_W comparisons as mentioned above, so this exclusion criteria was also dropped.

Once all the exclusion criteria are applied, statistics are generated for each $L_W(\lambda)$, $L_{WN}(\lambda)$, C_a, and $K_d(490)$ comparison. These are written to an ASCII file. The final matched data set is saved as an IDL *saveset* (Table 12) for future reference and analysis.

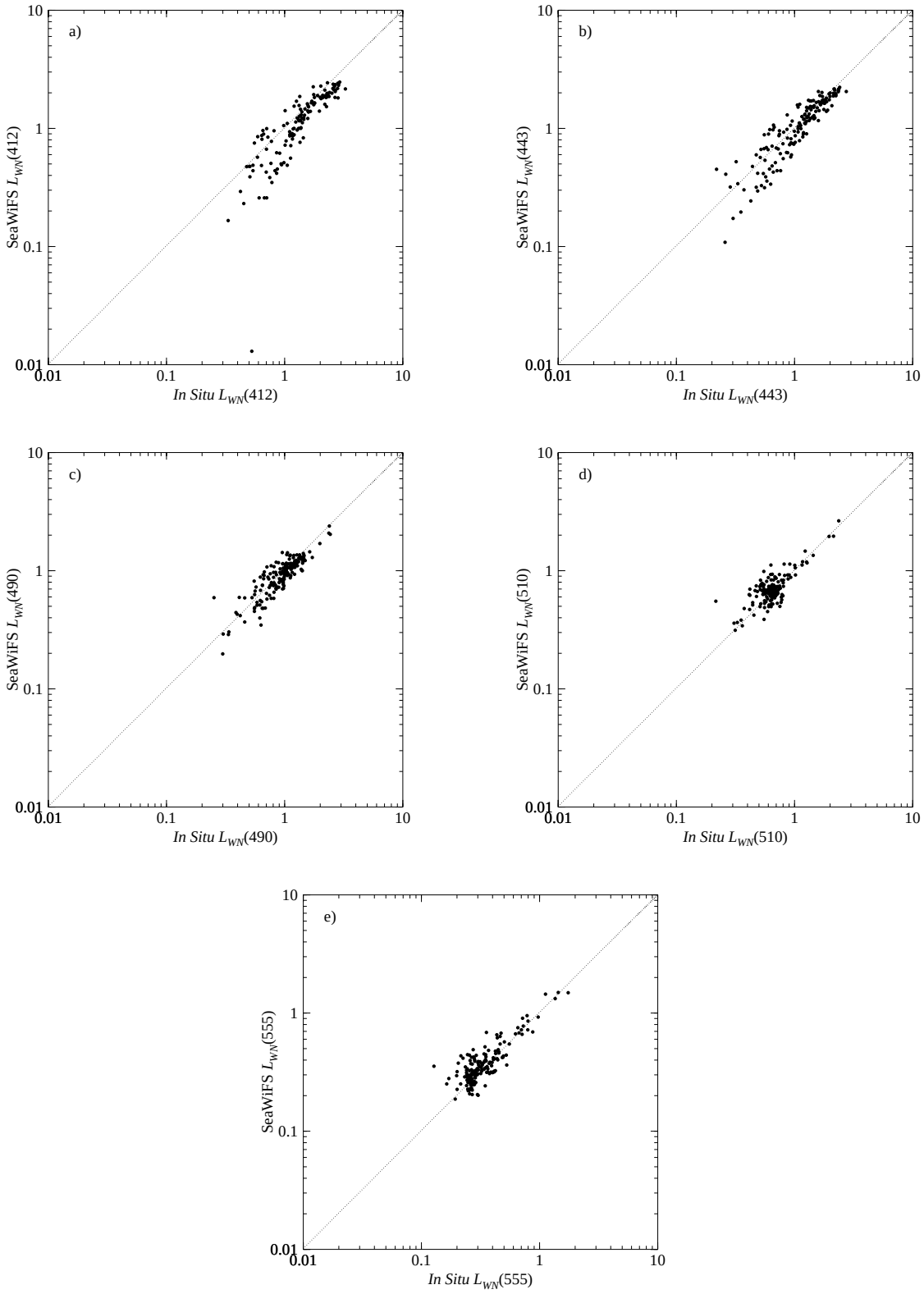

Fig. 28. Comparisons of SeaWiFS and *in situ* measurements of L_{WN} at five wavelengths: **a)** 412 nm, **b)** 443 nm, **c)** 490 nm, **d)** 510 nm, and **e)** 555 nm. Negative L_{WN} values have been excluded.

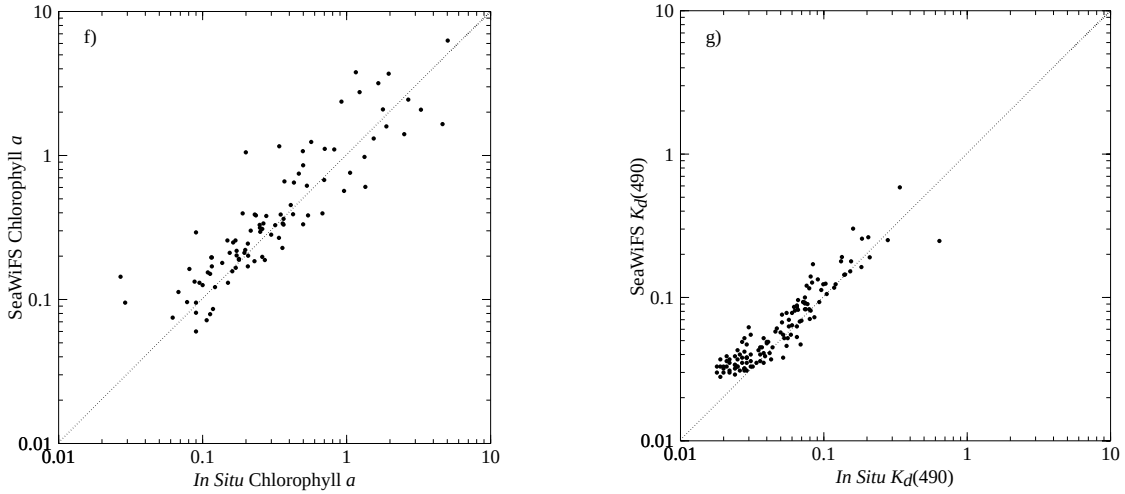

Fig. 28. (cont.) Comparisons of SeaWiFS and *in situ* measurements of L_{WN} and **f)** chlorophyll a, and **g)** $K(490)$. Negative L_{WN} values have been excluded.

Table 12. Fields stored in a match-up results summary file.

Name	*Description*
CRUISEID	Cruise identifier
ENV_YEAR	Year of *in situ* measurement
ENV_MONTH	Month of *in situ* measurement
ENV_DAY	Day of *in situ* measurement
ENV_HOUR	Hour of *in situ* measurement
ENV_MINUTE	Minute of *in situ* measurement
ENV_SECOND	Second of *in situ* measurement
ENV_LAT	Latitude of *in situ* measurement
ENV_LON	Longitude of *in situ* measurement
ENV_LW(λ)	*In situ* L_W at wavelength λ
ENV_ES(λ)	*In situ* E_s at wavelength λ
ENV_KD490	*In situ* $K_d(490)$
ENV_CHL	*In situ* chlorophyll concentration
TDIFF	Time difference between *in situ* measurement and satellite overpass
SAT_FILE	Satellite extract file name
SAT_COUNTS	Number of valid pixels in 3×3 box surrounding *in situ* lat/lon
SAT_SOLZ	Solar zenith angle at satellite overpass
SAT_SOLA	Solar azimuth angle at satellite overpass
SAT_SENZ	Satellite zenith angle at satellite overpass
SAT_SENA	Satellite azimuth angle at satellite overpass
SAT_LW_(λ)	Satellite L_W at wavelength λ
SAT_ES_(λ)	Satellite E_s at wavelength λ
SAT_NLW_(λ)	Satellite L_{WN} at wavelength λ
SAT_TAUA_(λ)	Satellite aerosol optical thickness at wavelength λ
SAT_ANGSTROM_555	Satellite Ångström exponent between 865–555 nm
SAT_EPSILON	Satellite ϵ value
SAT_OZONE	Ancillary ozone value
SAT_WINDSPEED	Ancillary wind speed
SAT_PRESSURE	Ancillary atmospheric pressure
SAT_CHL_OC2	Satellite-derived chlorophyll using OC2v2 (operational algoithm at the time of this writing)

Table 12. (cont.) Fields stored in a match-up results summary file.

Name	*Description*
SAT_K_490	Satellite-derived $K_d(490)$
SAT_(λ)_STATS	Simple statistics on satellite measurements (minimum, maximum, and standard deviation)
ENV_ES(λ)_CALC	Calculated *in situ* E_s using the Gordon clear sky model (Gordon et al. 1988)

Table 3. Decrease in the number of matches as different criteria are applied, in order, to the match-up set.

Processing Step	*Number of Matches Remaining*
Initial set (at least one valid SeaWiFS pixel)	886
Five out of nine pixels valid	659
Duplicate satellite coverage	361
Duplicate *in situ* measurements	198
Coefficient of determination tests (negative L_W values excluded):	
$L_W(412)$	119
$L_W(443)$	141
$L_W(490)$	153
$L_W(510)$	136
$L_W(555)$	149
C_a	76
$K_d(490)$	125

Table 14. L_W statistics are presented for the first five wavelengths and C_a values. The mean ratios are the SeaWiFS-to-*in situ* values, σ is the standard deviation, and CV is the coefficient of variance. The number of points for each parameter is not the same because of differences in the specific wavelengths measured *in situ* by different investigators. C_a values were sometimes measured without coincident optics, or, in other cases, the reverse was true. Some matchups were dropped because of negative L_W values.

Parameter	*Mean Ratio*	σ	*CV*	*Number of Observations*	*Range of In Situ Values*
$L_W(412)$	0.856	0.222	0.259	119	0.330–3.238
$L_W(443)$	0.957	0.246	0.256	141	0.219–2.709
$L_W(490)$	0.973	0.206	0.211	153	0.252–1.695
$L_W(510)$	1.075	0.236	0.219	136	0.215–0.857
$L_W(555)$	1.106	0.279	0.252	149	0.127–0.538
C_a	1.061	0.498	0.434	76	0.062–4.650
$K_d(490)$	1.255	0.287	0.222	125	0.018–0.340

7.2.4 Match-up Results

The current (October 2000) *in situ* data records in SeaBASS were processed for each exclusion criterion outlined above (Table 13). Of the 2,389 *in situ* records considered (39 data sets and 4,248 SeaWiFS files), 198, or 8.3% passed all exclusions to become final matches.

Comparisons of L_{WN} between *in situ* sites and SeaWiFS show generally good agreement in the radiance values (Figs. 28a–e and Table 14), especially at the higher radiance values. Note the lower number of match-up points in the $L_{WN}(412)$ and, to a lesser extent, $L_{WN}(443)$ band. This reduction at lower wavelengths occurs in coastal areas where the spectral water-leaving radiance in the NIR wavelengths is greater than zero, a condition that causes the overestimation of aerosol radiances and low, often negative, L_W values in these bands.

Negative L_W values can also result when absorbing aerosols are present with the most severe effects being at the shortest wavelengths. In nearly all cases, this anomaly

occurred in Case-2 waters or in a phytoplankton plume with relatively high C_a concentrations. Many of these values exhibited high coefficients of determination (greater than 0.5) in the 3×3 pixel set. Note that the lower number of points in the $L_W(510)$ panel is not due to overestimation of the aerosol radiance, but stems from the absence of this channel in some field radiometers.

The comparison of $L_{WN}(412)$ (Fig. 28a) shows that SeaWiFS retrievals have a slight negative bias, which increases at lower values. The conditions reported above that resulted in negative L_{WN} retrievals are influencing the retrievals at low values as well. The $L_{WN}(443)$ comparison (Fig. 28b) does not show the same bias seen in the $L_{WN}(412)$ comparison, although it is possible that the effect is present at this band, except at a much smaller extent. SeaWiFS compares quite well with the *in situ* measurements for $L_{WN}(490)$, $L_{WN}(510)$, and $L_{WN}(555)$ (Figs. 28c–e, respectively), although $L_{WN}(555)$ may be slightly positively biased.

The comparison of SeaWiFS and *in situ* chlorophyll values (Fig. 28f) demonstrates the reasonably high quality of the chlorophyll *a* data product for *in situ* values from about 0.02–7 $\mathrm{mg\,m^{-3}}$. For this comparison, SeaWiFS derived chlorophyll *a* values were determined using a different ocean chlorophyll algorithm (OC4v4). A comparison of the two algorithms showed that the OC4 algorithm performed better than the OC2 algorithm. OC4 became the operational algorithm with the third reprocessing of SeaWiFS data. These results are affected not only by variations in SeaWiFS imagery, but from inaccuracies in field chlorophyll measurement techniques. Ongoing work continues to improve the SeaWiFS and *in situ* comparisons from both the SeaWiFS imagery and field measurement aspects of the effort.

7.3 CONCLUSIONS

The SeaWiFS validation effort has demonstrated the capability of matching SeaWiFS and *in situ* measurements. The comparison of SeaWiFS and *in situ* chlorophyll concentration demonstrates that the SeaWiFS C_a values are reasonably good. A weakness in the validation effort has been the quality of the *in situ* data used as *truth* against the SeaWiFS products. Problems of instrument deployment, calibration, pigment estimation, data processing, and documentation have resulted in errors leading to invalid matchups despite the calibration and data analysis round-robins, protocol development, quality control, and other activities initiated by the SeaWiFS Project to improve data quality. Improvements, however, are being realized as stricter data ingest methods (i.e., `FCHECK`) and other activities proceed.

The SeaWiFS and *in situ* match-up effort has provided a quantitative evaluation of the data products, although, it is limited to regions where data have been reported. At present, the global representation of Case-1 (open ocean) waters is not complete, especially in areas where chlorophyll *a* concentrations are less than 0.05 $\mathrm{mg\,m^{-3}}$ and in polar regions. Figure 29 provides the locations of the current match-up data set, which corresponds to the points in Fig. 28. The SeaWiFS and SIMBIOS Projects are actively supporting continued field research in these undersampled areas.

Efforts to report individual match-up results from the ongoing validation effort on-line have been undertaken to allow individual investigators the opportunity to assess their data further and perhaps explore methods for future *in situ* data improvements. It is hoped this exchange of ideas will continue to improve the accuracy and usefulness of the validation data set. In addition, other approaches to validating pigment concentrations are being explored, e.g., comparing regional and seasonal statistics where sufficient *in situ* data are available. As the ongoing calibration and validation efforts expand under SIMBIOS and other missions, and as improvements in the atmospheric correction and bio-optical algorithms are developed, the accuracy of the products will continue to improve.

Future enhancements planned for the match-up analysis include the addition of an exclusion criterion based on the optical depth of the water column. If the optical depth is greater than the depth of the water column, bottom reflection will influence the L_{WN} values retrieved by SeaWiFS. Currently, there is no way of excluding these points from the match-up data set. Plans are also underway to improve the SeaWiFS turbid water flag. Should a sufficiently robust flag be developed, the match-up data set will be partitioned into Case-1 and Case-2 water types.

Glossary

AERONET	Aerosol Robotic Network
AI	Absorbing Aerosol Index
AOT	Aerosol Optical Thickness
ASCII	American Standard Code for Information Interchange
BNL	Brookhaven National Laboratory
BTBM	Bermuda Test Bed Mooring
CSH	UNIX "C-shell" script programming utility
CVT	Calibration and Validation Team
CZCS	Coastal Zone Color Scanner
DU	Dobson Unit of total ozone
GAC	Global Area Coverage
GoCal	Gulf of California
HDF	Hierarchical Data Format
HMS	Her Majesty's Ship
HPLC	High-Performance Liquid Chromotography
HRPT	High Resolution Picture Transmission
IDL	Interactive Data Language
JUL98NAN	A NOAA-sponsored cruise off Nantucket Island, Massachusetts in July 1998.
L1	Level-1 SeaWiFS data product
L1A	Level-1a SeaWiFS data product with navigation information
L2	Level-2 SeaWiFS data product
L3	Level-3 SeaWiFS data product
LAC	Local Area Coverage
MOBY	Marine Optical Buoy
MODIS	Moderate Resolution Imaging Spectroradiometer
NASA	National Aeronautics and Space Administration
NIR	Near-Infrared
NOAA	National Oceanographic and Atmospheric Administration
OC2	Ocean Chlorophyll 2 algorithm
OC2v1	OC2 version 1
OC2v2	OC2 version 2
OC4	Ocean Chlorophyll 4 algorithm
OC4v3	OC4 version 3
PI	Principal Investigator
SeaBAM	SeaWiFS Bio-optical Algorithm Mini-workshop
SeaBASS	SeaWiFS Bio-optical Archive and Storage System
SeaWiFS	Sea-viewing Wide Field-of-view Sensor
SIMBIOS	Sensor Intercomparison and Merger for Biological and Interdisciplinary Oceanic Studies
SRF	Spectral Response Function
TOA	Top of the Atmosphere
TOMS	Total Ozone Mapping Spectrometer
TOTO	Tongue of the Ocean study (Bahamas)
USF	University of South Florida

Symbols

a_{oz}	Ozone absorption coefficient.
b	Intercept.
C_a	Chlorophyll *a*.
$\bar{C}_a$	Mean chlorophyll *a* values.
C_P	Phaeophytin *a*.
CV	Coefficient of variance.
$E_d(\lambda)$	Downwelling irradiance.
$E_d(0^+)$	Extrapolated subsurface measures of $E_d(\lambda)$ through the air–sea interface.
$E_s(\lambda)$	Surface irradiance incident at the ocean surface, $E_d(0^+)$.
f	Scan angle.
$F_0(\lambda)$	Solar irradiance constant adjusted for the Earth–sun distance variations.
f/Q	Ocean surface bidirectional reflectance parameter.
i	Square root of -1.
I	Aerosol index.
$K(490)$	Diffuse attenuation coefficient of seawater measured at 490 nm.
$K_d(490)$	Diffuse attenuation coefficient of downwelling irradiance at 490 nm.
$L(\lambda)$	Radiance.
$L_a(\lambda)$	Radiance measured at the TOA from aerosol scattering alone.
$\langle L_a(\lambda_i)\rangle$	Aerosol interaction term.
$L_r(\lambda)$	Radiance measured at the TOA from Rayleigh scattering alone.
$\langle L_r(\lambda_i)\rangle$	The Rayleigh contribution.
$L_{ra}(\lambda)$	Radiance at the TOA from Rayleigh-aerosol interactive scattering.
$\langle L_{ra}(\lambda_i)\rangle$	Rayleigh-aerosol interaction term.
$L_t(\lambda)$	Radiance measured at the TOA.
$\langle L_t(\lambda_i)\rangle$	The radiance at the TOA measured by the SeaWiFS instrument.
$L_W(\lambda)$	Water-leaving radiance.
$L_{WN}(\lambda)$	Normalized water-leaving radiance.
$L_{WN}(\lambda_i)$	Normalized water-leaving radiance for a given band.
$L'_{WN}(\lambda_i)$	Normalized water-leaving radiance at the band-centered wavelength.
$\langle L(\lambda_i)\rangle$	Average radiance for band i as weighted by the sensor spectral response function.
$\langle\langle L_{WN}(\lambda_i)\rangle\rangle$	Average of the parameter $\langle L(\lambda_i)\rangle$ as weighted by the sensor spectral response function.
m	Slope.
$p_a(\lambda)$	The effective value of aerosol scattering phase function related to the single scattering case.
R	Correlation coefficient.
$\tilde{R}^{412}_{490}$	The TOA reflectance ratio measured by SeaWiFS.
$\hat{R}^{412}_{490}$	The reflectance ratio calculated assuming an atmosphere containing only large nonabsorbing particles and Rayleigh scattering molecules.
$r(\lambda_i)$	Ratio value of L_{WN} at the SeaWiFS band-centered wavelength versus the average values weighted by the SeaWiFS spectral response function.
$r_0(\mu)$	Mode radius of the particle size distribution in microns.

r_a Interpolation ratio between two models in the derived epsilon values.

$r_i(\lambda_i)$ Ratio value of L_{WN} at the SeaWiFS band-centered wavelength versus the average values weighted by the SeaWiFS spectral response function.

$R_{\rm rs}(\lambda)$ Remote sensing reflectance.

$\tilde{R}_{\rm rs}(\lambda)$ Measured remote sensing reflectance.

$\hat{R}_{\rm rs}(\lambda)$ Calculated remote sensing reflectance.

$R^{\lambda_i}_{\lambda_j}$ A compact notation to represent $R_{\rm rs}(\lambda_i)/R_{\rm rs}(\lambda_j)$ in the definition for aerosol absorbing index, see (1).

$S_i(\lambda)$ The SeaWiFS spectral response function for band i.

$t(\lambda)$ Diffuse transmittance of the atmosphere at the sensor viewing direction.

$t(\lambda_i)$ Atmospheric diffuse transmittance at the instrument viewing direction.

$t_0(\lambda)$ Diffuse transmittance of the atmosphere at the solar direction.

x The abscissa.

y The ordinate.

γ See (16).

ϵ Ratio of the single-scattering aerosol radiances.

$\overline{\epsilon}$ Weighted average of individual ϵ values.

ϵ^+ Aerosol model with the largest ϵ value greater than or equal to $\overline{\epsilon}$.

ϵ^- Aerosol model with the smallest ϵ value greater than $\overline{\epsilon}$.

$\epsilon(\lambda_i, \lambda_j)$ Atmospheric correction parameter defined as the ratio of single-scattered aerosol reflectance between two wavelengths, $\rho_{as}(\lambda_i)/\rho_{as}(\lambda_j)$.

θ Viewing zenith angle measured at the pixel.

θ_0 Solar zenith angle measured at the pixel.

λ Wavelength.

λ_i, λ_j Wavelengths corresponding to sensor spectral bands i and j.

ρ Reflectance.

$\rho_a(\lambda)$ Reflectance measured at the TOA from aerosol scattering alone.

$\rho_{as}(\lambda)$ Single-scattered aerosol reflectance.

$\rho_r(\lambda)$ Reflectance measured at the TOA from Rayleigh scattering alone.

$\rho_{ra}(\lambda)$ Reflectance at the TOA from Rayleigh-aerosol interactive scattering.

$\rho_t(\lambda)$ Reflectance measured at the TOA.

$\rho_w(\lambda)$ Water-leaving reflectance at the sea surface.

σ Standard deviation.

σ' Width of the particle size distribution.

$\tau_a(\lambda)$ Aerosol optical thickness.

$\tau_a^{\rm avg}$ Average $\tau_a(\lambda)$ from each set of measurements.

$\tau_a^{\rm max}$ Maximum $\tau_a(\lambda)$ from each set of measurements.

$\tau_a^{\rm min}$ Minimum $\tau_a(\lambda)$ from each set of measurements.

τ_r Rayleigh optical thickness.

$\omega_a(\lambda)$ Aerosol single scattering albedo.

$\Omega_{\rm tc}$ Total columnar ozone in Dobson units (DU).

References

Ainsworth, E.J., and F.S. Patt, 2000: "Modifications to the TOMS ozone ancillary data interpolation." In: McClain, C.R., E.J. Ainsworth, R.A. Barnes, R.E. Eplee, Jr., F.S. Patt, W.D. Robinson, M. Wang, and S.W. Bailey, SeaWiFS Postlaunch Calibration and Validation Analyses, Part 1. *NASA Tech. Memo. 2000–206892, Vol. 9,* S.B. Hooker and E.R. Firestone, Eds., NASA Goddard Space Flight Center, Greenbelt, Maryland, 69–73.

Bailey, S.W., C.R. McClain, P.J. Werdell, and B.D. Schieber, 2000: "Normalized water-leaving radiance and chlorophyll *a* match-up analyses." In: McClain, C.R., R.A. Barnes, R.E. Eplee, Jr., B.A. Franz, N.C. Hsu, F.S. Patt, C.M. Pietras, W.D. Robinson, B.D. Schieber, G.M. Schmidt, M. Wang, S.W. Bailey, and P.J. Werdell, 2000: SeaWiFS Postlaunch Calibration and Validation Analyses, Part 2. *NASA Tech. Memo. 2000–206892, Vol. 10,* S.B. Hooker and E.R. Firestone, Eds., NASA Goddard Space Flight Center, Greenbelt, Maryland, 45–52.

Barnes, R.A., A.W. Holmes, W.L. Barnes, W.E. Esaias, C.R. McClain, and T. Svitek, 1994: SeaWiFS Prelaunch Radiometric Calibration and Spectral Characterization. *NASA Tech. Memo. 104566, Vol. 23,* S.B. Hooker, E.R. Firestone, and J.G. Acker, Eds., NASA Goddard Space Flight Center, Greenbelt, Maryland, 55 pp.

Charlson, R.J., J.E. Lovelock, M.O. Andreae, and S.G. Warren, 1987: Oceanic phytoplankton, atmospheric sulphur, cloud albedo and climate. *Nature,* **326,** 655–661.

——, S.E. Schwartz, J.M. Hales, R.D. Cess, J.A. Coakley, J.E. Hansen, and D.J. Hofmann, 1992: Climate forcing by anthropogenic aerosols. *Science,* **255,** 423–430.

Clark, D.K., H.R. Gordon, K.J. Voss, Y. Ge, W. Broenkow, and C. Trees, 1997: Validation of atmospheric correction over the oceans. *J. Geophys. Res.,* **102,** 17,209–17,217.

Dave, J.V., 1972: Development of programs for computing characteristics of ultraviolet radiation, *Tech. Rept.,* Vector Case, IBM Corp., Fed. Syst. Div., Gaithersburg, Maryland, 337 pp.

Ding, K., and H.R. Gordon, 1994: Atmospheric correction of ocean-color sensors: effects of the Earth's curvature., *Appl. Opt.,* **33,** 7,096–7,106.

Eplee, R.E., Jr., and F.S. Patt, 2000: "Cloud-top radiance analysis for SeaWiFS bilinear gain knee calibration." In: McClain, C.R., E.J. Ainsworth, R.A. Barnes, R.E. Eplee, Jr., F.S. Patt, W.D. Robinson, M. Wang, and S.W. Bailey, 2000: SeaWiFS Postlaunch Calibration and Validation Analyses, Part 1. *NASA Tech. Memo. 2000–206892, Vol. 9,* S.B. Hooker and E.R. Firestone, Eds., NASA Goddard Space Flight Center, Greenbelt, Maryland, 13–16.

——, and R.A. Barnes, 2000: "Lunar data analysis for SeaWiFS calibration." In: McClain, C.R., E.J. Ainsworth, R.A. Barnes, R.E. Eplee, Jr., F.S. Patt, W.D. Robinson, M. Wang, and S.W. Bailey, SeaWiFS Postlaunch Calibration and Validation Analyses, Part 1. *NASA Tech. Memo. 2000–206892, Vol. 9,* S.B. Hooker and E.R. Firestone, Eds., NASA Goddard Space Flight Center, Greenbelt, Maryland, 17–27.

——, and C.R. McClain, 2000a: "MOBY data analysis for vicarious calibration of SeaWiFS bands 1–6." In: McClain, C.R., E.J. Ainsworth, R.A. Barnes, R.E. Eplee, Jr., F.S. Patt, W.D. Robinson, M. Wang, and S.W. Bailey, SeaWiFS Postlaunch Calibration and Validation Analyses, Part 1. *NASA Tech. Memo. 2000–206892, Vol. 9,* S.B. Hooker and E.R. Firestone, Eds., NASA Goddard Space Flight Center, Greenbelt, Maryland, 43–50.

——, and ——, 2000b: "SeaWiFS global clear-water analysis." In: McClain, C.R., R.A. Barnes, R.E. Eplee, Jr., B.A. Franz, N.C. Hsu, F.S. Patt, C.M. Pietras, W.D. Robinson, B.D. Schieber, G.M. Schmidt, M. Wang, S.W. Bailey, and P.J. Werdell, 2000: SeaWiFS Postlaunch Calibration and Validation Analyses, Part 2. *NASA Tech. Memo. 2000–206892, Vol. 10,* S.B. Hooker and E.R. Firestone, Eds., NASA Goddard Space Flight Center, Greenbelt, Maryland, 29–33.

——, R.A. Barnes, and F.S. Patt, 2000: "Solar data analysis for SeaWiFS calibration." In: McClain, C.R., E.J. Ainsworth, R.A. Barnes, R.E. Eplee, Jr., F.S. Patt, W.D. Robinson, M. Wang, and S.W. Bailey, 2000: SeaWiFS Postlaunch Calibration and Validation Analyses, Part 1. *NASA Tech. Memo. 2000–206892, Vol. 9,* S.B. Hooker and E.R. Firestone, Eds., NASA Goddard Space Flight Center, Greenbelt, Maryland, 28–37.

Frouin, R., M. Schwindling, and P.-Y. Deschamps, 1996: Spectral reflectance of sea foam in the visible and near-infrared: *in situ* measurements and remote sensing implications. *J. Geophys. Res.,* **101,** 14,361–14,371.

Fukushima, H., M. Schmidt, B.J. Sohn, M. Toratani, and I. Uno, 1999: Detection of dust loaded airmass in SeaWiFS Imagery: an empirical dust index in comparison with model-predicted dust distribution over the Pacific in April 1998, *Proc. Int. Symp. Remote Sens. '99,* Korean Society of Remote Sensing, ISSN 1226-9743, 89–94.

Gordon, H.R., 1995: Remote sensing of ocean color: a methodology for dealing with broad spectral bands and significant out-of-band response, *Appl. Opt.,* **34,** 8,363–8,374.

——, and D.K. Clark, 1981: Clear water radiances for atmospheric correction of coastal zone color scanner imagery. *Appl. Opt.,* **20,** 4,175–4,180.

——, O.B. Brown, R.H. Evans, J.W. Brown, R.C. Smith, K.S. Baker, and D.K. Clark, 1988: A semianalytic radiance model of ocean color, *J. Geophys. Res.,* **93,** 10,909–10,924.

——, and M. Wang, 1994a: Retrieval of water-leaving radiance and aerosol optical thickness over the oceans with SeaWiFS: A preliminary algorithm, *Appl. Opt.,* **33,** 443–452.

——, and M. Wang, 1994b: Influence of oceanic whitecaps on atmospheric correction of ocean color sensors. *Appl. Opt.,* **33,** 7,354–7,763.

Herman, J.R., P.K. Bhartia, O. Torres, N.C. Hsu, C.J. Seftor, and E. Celarier, 1997: Global distribution of UV-absorbing aerosols from Nimbus-7/TOMS data, *J. Geophys. Res.,* **102,** 16,911–16,922.

Holben, B.N., T.F. Eck, I. Slutsker, D. Tanre, J.P. Buis, A. Setzer, E. Vermote, J.A. Reagan, Y. Kaufman, T. Nakajima, F. Lavenu, I. Jankowiak, and A. Smirnov, 1998: AERONET—A federated instrument network and data archive for aerosol characterization. *Remote Sens. Environ.,* **66,** 1–16.

Hooker, S.B., W.E. Esaias, G.C. Feldman, W.W. Gregg, and C.R. McClain, 1992: An Overview of SeaWiFS and Ocean Color, *NASA Tech. Memo. 104566, Vol. 1,* S.B. Hooker and E.R. Firestone, Eds., NASA Goddard Space Flight Center, Greenbelt, Maryland, 24 pp.

——, C.R. McClain, J.K. Firestone, T.L. Westphal, E. Yeh, and Y. Ge, 1994: The SeaWiFS Bio-optical Archive and Storage System (SeaBASS), Part 1. *NASA Tech. Memo. 104566, Vol. 20,* S.B. Hooker and E.R. Firestone, Eds., NASA Goddard Space Flight Center, Greenbelt, Maryland, 27 pp.

——, and C.R. McClain, 2000: The calibration and validation of SeaWiFS data. *Prog. Oceanogr.,* **45,** 427–465.

Hsu, N.C., J.R. Herman, P.K. Bhartia, C.J. Seftor, O. Torres, A.M. Thompson, J.F. Gleason, T.F. Eck, and B.N. Holben, 1996: Detection of biomass burning smoke from TOMS measurements, *Geophys. Res. Lett.,* **23,** 745–748.

——, ——, O. Torres, B.N. Holben, D. Tanre, T.F. Eck, A. Smirnov, B. Chatenet, and F. Lavenu, 1999: Comparisons of the TOMS aerosol index with sun photometer aerosol optical thickness: results and applications, *J. Geophys. Res.,* **104,** 6,269–6,279.

——, W.D. Robinson, S.W. Bailey, and P.J. Werdell, 2000: "The description of the SeaWiFS absorbing aerosol index." In: McClain, C.R., R.A. Barnes, R.E. Eplee, Jr., B.A. Franz, N.C. Hsu, F.S. Patt, C.M. Pietras, W.D. Robinson, B.D. Schieber, G.M. Schmidt, M. Wang, S.W. Bailey, and P.J. Werdell, 2000: SeaWiFS Postlaunch Calibration and Validation Analyses, Part 2. *NASA Tech. Memo. 2000–206892, Vol. 10,* S.B. Hooker and E.R. Firestone, Eds., NASA Goddard Space Flight Center, Greenbelt, Maryland, 3–5.

Johnson, B.C., E.A. Early, R.E. Eplee, Jr., R.A. Barnes, and R.T. Caffrey, 1999: The 1997 Prelaunch Radiometric Calibration of SeaWiFS. *NASA Tech. Memo. 1999–206892, Vol. 4,* S.B. Hooker and E.R. Firestone, Eds., NASA Goddard Space Flight Center, Greenbelt, Maryland, 51 pp.

Maritorena, S., and J.E. O'Reilly, 2000: "OC2v2: Update on the initial operational SeaWiFS chlorophyll *a* algorithm." In: O'Reilly, J.E., and 24 Coauthors, 2000: SeaWiFS Postlaunch Calibration and Validation Analyses, Part 3. *NASA Tech. Memo. 2000–206892, Vol. 11,* S.B. Hooker and E.R. Firestone, Eds., NASA Goddard Space Flight Center, Greenbelt, Maryland, 3–8.

McClain, C.R., 2000: "SeaWiFS postlaunch calibration and validation overview." In: McClain, C.R., E.J. Ainsworth, R.A. Barnes, R.E. Eplee, Jr., F.S. Patt, W.D. Robinson, M. Wang, and S.W. Bailey, 2000: SeaWiFS Postlaunch Calibration and Validation Analyses, Part 1. *NASA Tech. Memo. 2000–206892, Vol. 9,* S.B. Hooker and E.R. Firestone, Eds., NASA Goddard Space Flight Center, Greenbelt, Maryland, 4–12.

——, W.E. Esaias, W. Barnes, B. Guenther, D. Endres, S.B. Hooker, B.G. Mitchell, and R. Barnes, 1992: SeaWiFS Calibration and Validation Plan. *NASA Tech. Memo. 104566, Vol. 3,* S.B. Hooker and E.R. Firestone, Eds., NASA Goddard Space Flight Center, Greenbelt, Maryland, 43 pp.

——, R. Evans, J. Brown, and M. Darzi, 1995: "SeaWiFS quality control masks and flags: initial algorithms and implementation strategy." In: McClain, C.R., W.E. Esias, M. Darzi, F.S. Patt, R.H. Evans, J.W. Brown, K.R. Arrigo, C.W. Brown, R.A. Barnes, and L. Kumar: SeaWiFS Algorithms, Part 1. *NASA Tech. Memo. 104566, Vol. 28,* S.B. Hooker, E.R. Firestone, and J.G. Acker, Eds., NASA Goddard Space Flight Center, Greenbelt, Maryland, 3–7.

——, M. Darzi, R.A. Barnes, R.E. Eplee, Jr., J.K. Firestone, F.S. Patt, W.D. Robinson, B.D. Schieber, R.H. Woodward, and E. Yeh, 1996: SeaWiFS Calibration and Validation Quality Control Procedures, *NASA Tech. Memo. 104566, Vol. 38,* S.B. Hooker and E.R. Firestone, Eds., NASA Goddard Space Flight Center, Greenbelt, Maryland, 64 pp.

——, M.L. Cleave, G.C. Feldman, W.W. Gregg, S.B. Hooker, and N. Kuring, 1998: Science quality SeaWiFS data for global biosphere research. *Sea Technol.,* **39,** 10–16.

——, and G. Fargion, 1999: SIMBIOS Project 1998 Annual Report. *NASA Tech. Memo. 1999–208645,* NASA Goddard Space Flight Center, Greenbelt, Maryland, 105 pp.

Moore, K.D., K.J. Voss, and H.R. Gordon, 2000: Spectral reflectance of whitecaps: Their contribution to water-leaving radiance., *J. Geophys. Res.,* **105,** 6,493–6,499.

Morel, A., and B. Gentili, 1996: Diffuse reflectance of oceanic waters. III. Implication of bidirectionality for the remote sensing problem. *Appl. Opt.,* **35,** 4,850–4,862.

Mueller J.L., 2000: "SeaWiFS algorithm for the diffuse attenuation coefficient, $K(490)$, using water-leaving radiances at 490 and 555 nm." In: O'Reilly, J.E., and 24 Coauthors, 2000: SeaWiFS Postlaunch Calibration and Validation Analyses, Part 3. *NASA Tech. Memo. 2000–206892, Vol. 11,* S.B. Hooker and E.R. Firestone, Eds., NASA Goddard Space Flight Center, Greenbelt, Maryland, 24–27.

O'Reilly, J.E., S. Maritorena, B.G. Mitchell, D.A. Siegel, K.L. Carder, S.A. Garver, M. Kahru, and C. McClain, 1998: Ocean color chlorophyll algorithms for SeaWiFS, *J. Geophys. Res.,* **103,** 24,937–24,953.

——, and 21 Coauthors, 2000: "Ocean color chlorophyll *a* algorithms for SeaWiFS, OC2, and OC4: Version 4." In: O'Reilly, J.E., and 24 Coauthors, 2000: SeaWiFS Postlaunch Calibration and Validation Analyses, Part 3. *NASA Tech. Memo. 2000–206892, Vol. 11,* S.B. Hooker and E.R. Firestone, Eds., NASA Goddard Space Flight Center, Greenbelt, Maryland, 9–23.

Remer, L.A., Y.J. Kaufman, and B.N. Holben, 1996: "The size distribution of ambient aerosol particles: smoke vs. urban/industrial aerosol." In: *Biomass Burning and Global Change,* J.S. Levine, Ed., MIT Press, Cambridge, Massachusetts, 519–530.

Robinson, W.D., and M. Wang, 2000: "Vicarious calibration of SeaWiFS band 7." In: McClain, C.R., E.J. Ainsworth, R.A. Barnes, R.E. Eplee, Jr., F.S. Patt, W.D. Robinson, M. Wang, and S.W. Bailey, SeaWiFS Postlaunch Calibration and Validation Analyses, Part 1. *NASA Tech. Memo. 2000–206892, Vol. 9,* S.B. Hooker and E.R. Firestone, Eds., NASA Goddard Space Flight Center, Greenbelt, Maryland, 38–42.

Shettle, E.P., and R.W. Fenn, 1979: Models for the Aerosols of the Lower Atmosphere and the Effects of Humidity Variations on Their Optical Properties. *AFGL-TR-79-0214,* U.S. Air Force Geophysics Laboratory, Hanscom Air Force Base, Massachusetts, 94 pp.

Siegel, D.A., M. Wang, S. Maritorena, and W. Robinson, 2000: Atmospheric correction of satellite ocean color imagery: the black pixel assumption. *Appl. Opt.,* **39,** 3,582–3,591.

Subramaniam, A., R.R. Hood, C.W. Brown, E.J. Carpenter, and D.G. Capone, 2000: A classification algorithm for mapping *Trichodesmium* blooms using SeaWiFS. *Deep-Sea Res.,* (submitted).

Tegen, I., and A.A. Lacis, 1996: Modeling of particle size distribution and its influence on the radiative properties of mineral dust aerosol, *J. Geophys. Res.,* **101,** 19,237–19,244.

Wang, M., 1999a: Atmospheric correction of ocean color sensors: Computing atmospheric diffuse transmittance, *Appl. Opt.,* **38,** 451–455.

——, 1999b: A sensitivity study of the SeaWiFS atmospheric correction algorithm: Effects of spectral band variations. *Remote Sens. Environ.,* **67,** 348–359.

——, 2000: "The SeaWiFS atmospheric correction algorithm updates." In: McClain, C.R., E.J. Ainsworth, R.A. Barnes, R.E. Eplee, Jr., F.S. Patt, W.D. Robinson, M. Wang, and S.W. Bailey, SeaWiFS Postlaunch Calibration and Validation Analyses, Part 1. *NASA Tech. Memo. 2000–206892, Vol. 9,* S.B. Hooker and E.R. Firestone, Eds., NASA Goddard Space Flight Center, Greenbelt, Maryland, 57–63.

——, and H.R. Gordon, 1994: A simple, moderately accurate, atmospheric correction algorithm for SeaWiFS. *Remote Sens. Environ.,* **50,** 231–239.

——, and S.W. Bailey, 2000: "Correction of the sun glint contamination on the SeaWiFS aerosol optical thickness retrievals." In: McClain, C.R., E.J. Ainsworth, R.A. Barnes, R.E. Eplee, Jr., F.S. Patt, W.D. Robinson, M. Wang, and S.W. Bailey, 2000: SeaWiFS Postlaunch Calibration and Validation Analyses, Part 1. *NASA Tech. Memo. 2000–206892, Vol. 9,* S.B. Hooker and E.R. Firestone, Eds., NASA Goddard Space Flight Center, Greenbelt, Maryland, 64–68.

——, B.A. Franz, and R.A. Barnes, 2000: "Analysis of the SeaWiFS spectral band-pass effects." In: McClain, C.R., R.A. Barnes, R.E. Eplee, Jr., B.A. Franz, N.C. Hsu, F.S. Patt, C.M. Pietras, W.D. Robinson, B.D. Schieber, G.M. Schmidt, M. Wang, S.W. Bailey, and P.J. Werdell, 2000: SeaWiFS Postlaunch Calibration and Validation Analyses, Part 2. *NASA Tech. Memo. 2000–206892, Vol. 10,* S.B. Hooker and E.R. Firestone, Eds., NASA Goddard Space Flight Center, Greenbelt, Maryland, 6–11.

Yang, H., and H.R. Gordon, 1997: Remote sensing of ocean color: assessment of water-leaving radiance bidirectional effects on atmospheric diffuse transmittance, *Appl. Opt.,* **36,** 7,887–7,897.

The SeaWiFS Postlaunch Technical Report Series

Vol. 1

Johnson, B.C., J.B. Fowler, and C.L. Cromer, 1998: The SeaWiFS Transfer Radiometer (SXR). *NASA Tech. Memo. 1998–206892, Vol. 1,* S.B. Hooker and E.R. Firestone, Eds., NASA Goddard Space Flight Center, Greenbelt, Maryland, 58 pp.

Vol. 2

Aiken, J., D.G. Cummings, S.W. Gibb, N.W. Rees, R. Woodd-Walker, E.M.S. Woodward, J. Woolfenden, S.B. Hooker, J-F. Berthon, C.D. Dempsey, D.J. Suggett, P. Wood, C. Donlon, N. González-Benítez, I. Huskin, M. Quevedo, R. Barciela-Fernandez, C. de Vargas, and C. McKee, 1998: AMT-5 Cruise Report. *NASA Tech. Memo. 1998–206892, Vol. 2,* S.B. Hooker and E.R. Firestone, Eds., NASA Goddard Space Flight Center, Greenbelt, Maryland, 113 pp.

Vol. 3

Hooker, S.B., G. Zibordi, G. Lazin, and S. McLean, 1999: The SeaBOARR-98 Field Campaign. *NASA Tech. Memo. 1999–206892, Vol. 3,* S.B. Hooker and E.R. Firestone, Eds., NASA Goddard Space Flight Center, Greenbelt, Maryland, 40 pp.

Vol. 4

Johnson, B.C., E.A. Early, R.E. Eplee, Jr., R.A. Barnes, and R.T. Caffrey, 1999: The 1997 Prelaunch Radiometric Calibration of SeaWiFS. *NASA Tech. Memo. 1999–206892, Vol. 4,* S.B. Hooker and E.R. Firestone, Eds., NASA Goddard Space Flight Center, Greenbelt, Maryland, 51 pp.

Vol. 5

Barnes, R.A., R.E. Eplee, Jr., S.F. Biggar, K.J. Thome, E.F. Zalewski, P.N. Slater, and A.W. Holmes 1999: The SeaWiFS Solar Radiation-Based Calibration and the Transfer-to-Orbit Experiment. *NASA Tech. Memo. 1999–206892, Vol. 5,* S.B. Hooker and E.R. Firestone, Eds., NASA Goddard Space Flight Center, 28 pp.

Vol. 6

Firestone, E.R., and S.B. Hooker, 2000: SeaWiFS Postlaunch Technical Report Series Cumulative Index: Volumes 1–5. *NASA Tech. Memo. 2000–206892, Vol. 6,* S.B. Hooker and E.R. Firestone, Eds., NASA Goddard Space Flight Center, Greenbelt, Maryland, 14 pp.

Vol. 7

Johnson, B.C., H.W. Yoon, S.S. Bruce, P-S. Shaw, A. Thompson, S.B. Hooker, R.E. Eplee, Jr., R.A. Barnes, S. Maritorena, and J.L. Mueller, 1999: The Fifth SeaWiFS Intercalibration Round-Robin Experiment (SIRREX-5), July 1996. *NASA Tech. Memo. 1999–206892, Vol. 7,* S.B. Hooker and E.R. Firestone, Eds., NASA Goddard Space Flight Center, 75 pp.

Vol. 8

Hooker, S.B., and G. Lazin, 2000: The SeaBOARR-99 Field Campaign. *NASA Tech. Memo. 2000–206892, Vol. 8,* S.B. Hooker and E.R. Firestone, Eds., NASA Goddard Space Flight Center, 46 pp.

Vol. 9

McClain, C.R., E.J. Ainsworth, R.A. Barnes, R.E. Eplee, Jr., F.S. Patt, W.D. Robinson, M. Wang, and S.W. Bailey, 2000: SeaWiFS Postlaunch Calibration and Validation Analyses, Part 1. *NASA Tech. Memo. 2000–206892, Vol. 9,* S.B. Hooker and E.R. Firestone, Eds., NASA Goddard Space Flight Center, 82 pp.

Vol. 10

McClain, C.R., R.A. Barnes, R.E. Eplee, Jr., B.A. Franz, N.C. Hsu, F.S. Patt, C.M. Pietras, W.D. Robinson, B.D. Schieber, G.M. Schmidt, M. Wang, S.W. Bailey, and P.J. Werdell, 2000: SeaWiFS Postlaunch Calibration and Validation Analyses, Part 2. *NASA Tech. Memo. 2000–206892, Vol. 10,* S.B. Hooker and E.R. Firestone, Eds., NASA Goddard Space Flight Center, 57 pp.